Chemistry and Electronics of the Ge(111) Surface

Thesis by

David Knapp

In Partial Fulfillment of the Requirements

for the Degree of

Doctor of Philosophy

California Institute of Technology

Pasadena, California

2011

(Defended December 1, 2010)

Acknowledgements

Caltech has been an amazing place and I have many people to thank. I would first like to thank my advisor, Prof. Nathan Lewis, for his patience, advice, and for giving me the opportunity to work on interesting projects. I am also grateful to Dr. Bruce Brunschwig for his advice and assistance. I thank my committee members, Professors Jacqueline Barton, Mitchio Okumura, and Harry Atwater, who have been encouraging.

I need to extend my thanks to so many members of the Lewis Group, current and former, for their help in and out of the lab. Thanks to Lauren Webb, Joseph Nemanick, Florian Gstrein, and David Michalak for helping me get started, and for continued advice afterward. My thanks also to Patrick Hurley, Stephen Maldonado, and Erik Johansson, who were great postdocs to work with. Thanks to Brian Sisk and Elizabeth Mayo for the diversions outside the lab. Everyone in the Lewis Group has been kind and helpful; I am leaving off too many names.

Of course, I would not be here without the many years of help from my parents, Bruce Knapp and Ann Therrien.

Abstract

The halogenation/alkylation procedure that has been proven to chemically and electrically passivate the Si(111) surface has been adapted for application to Ge(111). Removal of the Ge(111) surface oxide with 6–9 M HF(aq), followed by exposure to Br_2 vapor, then alkylmagnesium or alkyllithium reagents yields air stable surfaces with surface recombination velocities (SRVs) as low as 40 cm/sec^{-1} at flat-band conditions. Surface charges with a density on the order of 10^{12} cm^{-2} cause a negative surface potential of almost 300 mV in n-type CH_3-Ge(111) samples prepared with this method. The oxidized surface shows a strongly positive surface potential in atmospheric conditions. A negative surface potential is also present in CH_3-Si(111), but the wider bandgap prevents this from causing inversion conditions in extrinsic samples. Ge(111) surfaces alkylated with a larger organic group, such as ethyl or decyl, displayed a weaker surface potential and higher surface recombination velocity as the surface was brought near flat-band. Mercury contacts to alkylated n-type substrates form rectifying junctions with barrier heights of 0.6 ± 0.1 eV. Contacts to p-type substrates or to oxidized n-type substrates show no measurable rectification. X-ray photoelectron spectroscopy (XPS) confirms that the area concentration of surface-bound carbon on CH_3-Ge(111) surfaces is equal to that of CH_3-Si(111) surfaces. Other passivation methods were less successful.

Every atop Ge atom of an ideal CH_3-Ge(111) should be capped and the Ge-C bonds should be directed normal to the surface plane. Infrared absorption spectroscopy (IRAS) of methyl-terminated surfaces prepared from HF-etched precursors did not display distinguishable absorption peaks, but if the Ge substrate is first treated with an anisotropic etch before the HF etch, IRAS confirms the methyl group orientation with the polarization-dependent “umbrella” mode absorption at 1232 cm^{-1} and a polarization-independent rocking mode at 755 cm^{-1}. Well-ordered CH_3-Ge(111) surfaces displayed less surface charging while maintaining the low SRVs, indicating that such surfaces are successfully passivated.

Contents

List of Figures

List of Tables

Chapter 1

Introduction

1.1 Background

1.1.1 Semiconductors

Ever since the development of crystal rectifiers for radar receivers in World War II, semiconductors have played an important role for over half a century in the form of electronics, and are expected to play a critical role in solar power generation.[1,2] Semiconductor theory and technology were established with crystalline semiconductors such as silicon (Si) and germanium (Ge), the latter of which is the focus of this work.

The band structure described in the following sections is a result of electrons moving within a periodic potential, such as that induced by the crystal lattice.[3] The periodicity of the bulk crystal cannot continue out past the physical surface, so there is necessarily a distortion of the crystal potential. Because the surface of the crystal is accessible to contact with other materials, the chemical composition at the surface may be quite different from that of the bulk. For this reason, knowledge and control of the electronics and chemistry of the crystal surface is important for practical use of semiconductor devices.

1.1.2 Surface Potential

When a semiconductor is contacted with a conducting phase, there will be a net transfer of charge until the electrochemical potential of the materials are balanced by the electric potential of the field established at the interface. The conducting phase has a higher density of states than does the semiconductor within the bandgap, so while the charge on the conducting side is located at the interface, the charge in the semiconductor is distributed across a space charge region beneath the surface. The charge density of this region, and hence the width, is determined by the dopant concentration. For a uniform dopant density, it can be approximated that the dopant atoms are uniformly ionized and the carriers depleted to a certain depth. In the case of an n-type semiconductor brought into contact with a metal of lower chemical potential (higher work function), there will be a transfer of electrons to the metal so the metal surface has a negative charge, balanced by the positively charged immobile donor atoms in the semiconductor. This is depicted in Figure 1.1 on page 4. As a conduction band electron is brought to the interface, it is at a greater potential as it approaches the increasingly less-shielded negative charge on the metal. This is described by an approximation in Poisson's equation

$$\frac{\delta^2 V}{\delta x^2} = \frac{\delta E}{\delta x} \approx \frac{q}{\varepsilon_s} N_D \tag{1.1}$$

Integrating and eliminating E yields the relationship between the depletion width W, the dopant density N_D, and the difference in potential between the two phases or built in potential V_{bi}

$$W = \sqrt{\frac{2\varepsilon_s V_{bi}}{qN_D}} \tag{1.2}$$

The current-voltage behavior of the rectifier is dependent upon the concentration of carriers at the surface and available to cross the interface. That surface concentration differs from that of the bulk in a manner governed by the the built-in voltage

$$n_s = n_b \exp\left(\frac{-q(V_{bi} + V)}{kT}\right) \tag{1.3}$$

$$n_b = n_i \exp\left(-\frac{E_F + E_i}{kT}\right) \tag{1.4}$$

where n_s is the surface electron concentration, and n_b is the bulk electron concentration.

The simple model outlined above is complicated by the presence of surface-states. Electrically active surface-states alter the surface carrier concentrations, and the surface potential, by acting as carrier recombination or generation centers. The V_{bi} of a junction is also altered as the surface states accept or donate charge during the initial equilibration. These effects of surface-states are often uncontrolled and undesirable, and the chemical identity of the surface-states is dependent upon the semiconductor material type. For this reason, chemical control of the surface is of critical importance.

Figure 1.1: Band-bending

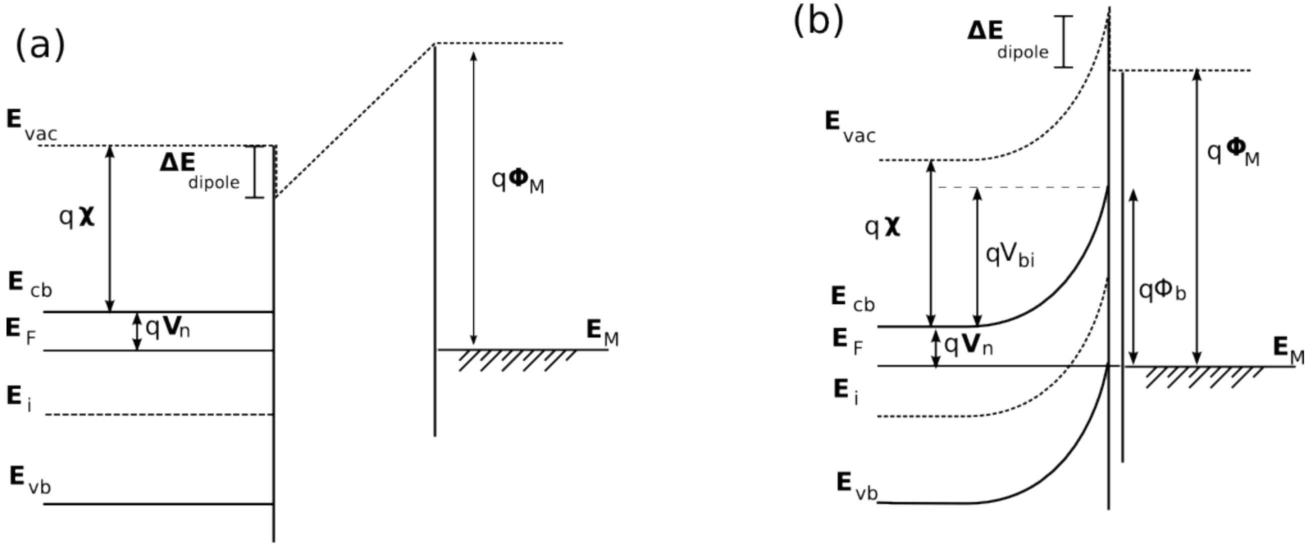

1.2 Silicon & Germanium

Covalent diamond-type semiconductors silicon and germanium are composed of a single element and may be melted and crystallized with a method first discovered by Czochralski for purifying metals.[4,5] For this reason, high purity crystals have long been produced to a degree not easily achievable with compound semiconductors.[6]

Although both Ge and Si have a diamond type crystal structure, reconstructed Si(111) and Ge(111) surfaces prepared in ultra-high vacuum (UHV) have different periodicity of surface atoms, resulting in different chemistries under such conditions. The bare Si(111) surface reconstructs to a 7×7 unit cell.[7] Under vacuum, bare Ge(111) tends to reconstruct to a $c(2 \times 8)$, with two distinct surface atom types, adatoms and restatoms. Adatoms bond to three atoms of the first full atomic layer, occupying 3/4 of the surface bonds of that layer. The restatoms are the remaining 1/4 of the full layer atoms that do not bond to the adatoms.[8,9] As confirmed by STM, charge transfer from the adatoms to the restatoms leads to filled and empty dangling bond types.[9,10] Chemically passivated surfaces on both Si(111) and Ge(111), however, display the 1×1 unit cell. The Ge lattice constant is approximately 4% larger than that of Si, so the distance between neighboring atop atoms of the (111) 1×1 surface is similar for both semiconductors (3.8 Å for Si(111) and 4.0 Å for Ge(111)) so that the two surfaces are geometrically comparable.[11,12]

In the 1950s, Ge and Si were both major components of the developing solid-state electronics field. With the advent of the field effect transistor, however, Si became the dominant material, though Ge has continued to be used in special components for microwave and infrared communications. Silicon oxide is a stable material that may be grown on the crystal surface to form a gate dielectric. Under proper conditions, the crystal/oxide interface can be formed with a minimal electronic defect density.[13] Germanium oxide is water soluble and not stable under most relevant conditions, so that even if a low-defect crystal/oxide interface were to be formed it could not be maintained. For this reason, Si has been useful for technologies using field effect devices while germanium has been largely overshadowed.

In addition to electronics, Si is a dominant material in photovoltaics (PV). The use of crystalline Si for this purpose is in part due to the fact that there existed Si processing capabilities and technology developed for electronics. However, Si has other aspects that ensure that it will be an attractive PV material, even as the PV and electronics technologies diverge and world-wide PV module production outstrips the production of other electronic components. As a practical matter, Si is both non-toxic and abundant, so there is no inherent danger in its widespread use.[14]

1.2.1 Germanium

Electronics

There has been recent interest in Ge for use in field effect transistors. As the number of transistors on an integrated circuit increases, and the power per transistor must necessarily decrease, the gate oxide has decreased to less than 1 nm, and due to both electron tunneling and physical defects in such a thin layer, leakage currents become significant. In order to use a sufficiently thick dielectric that the leakage currents are avoided without sacrificing the electrical performance of the transistor, silicon oxide is replaced with a high-κ material such as hafnium oxide.[13] With the removal of its oxide from the device architecture, Si no longer has this major advantage over Ge.

Ge possesses a hole carrier mobility that is four times that of the hole carrier mobility in Si, an advantage in high-speed circuits and of interest in CMOS technology where the p-channel component has traditionally had poorer performance.[13,15,16] Although the processing of Ge is similar to Si, it can take place at lower temperatures. Ge has a melting point of 937°C versus 1414°C for Si.

Light Absorption

A semiconductor will absorb incident radiation at or above the energy of its bandgap. Photon energy in excess of the bandgap is usually lost as heat. Silicon's 1.12 eV bandgap is also reasonably close to the 1.4 eV gap that would be ideal for efficient collection of sunlight, as represented by the AM 1.5 solar spectrum.[17,18] If the bandgap were larger, much of the incident light would not be absorbed. If the gap were smaller, more would be absorbed but more of the energy wasted as heat rather than producing a voltage. At 0.67 eV, the bandgap of Ge is much too small to efficiently capture solar radiation for useful electricity. However, it can be a component in multijunction solar cells, depicted in Figure 1.2 on page 9, where the higher energy photons are first collected by a wide bandgap absorber. The remaining lower energy photons are collected by a second or third absorber. Multijunction cells are more complicated, and hence more expensive, than single absorber cells. But the similarity in processing to that of Si, and the similarity in lattice parameters to GaAs (1.6 eV gap) indicate that the choice of Ge could mitigate some of the complexity.[3]

1.3 Summary

Ge has much to offer in the fields of electronics and photovoltaics and has enough similarities to Si that comparable passivation techniques may be applied. The research described herein concerns an attempt to passivate the defects through a wet chemical technique similar to that proven to be successful in passivating Si. Elemental analysis of the modified surfaces is performed with x-ray photoelectron Spectroscopy (XPS). Structural analysis is performed with transmission infrared absorption spectroscopy (IRAS). Surface electronics are measured with combined surface recombination velocity (SRV) and low-frequency step-modulated field effect surface conductance measurements. Surface energetics are measured with n-Ge/Hg rectifying soft contacts.

Figure 1.2: Multijunction cell

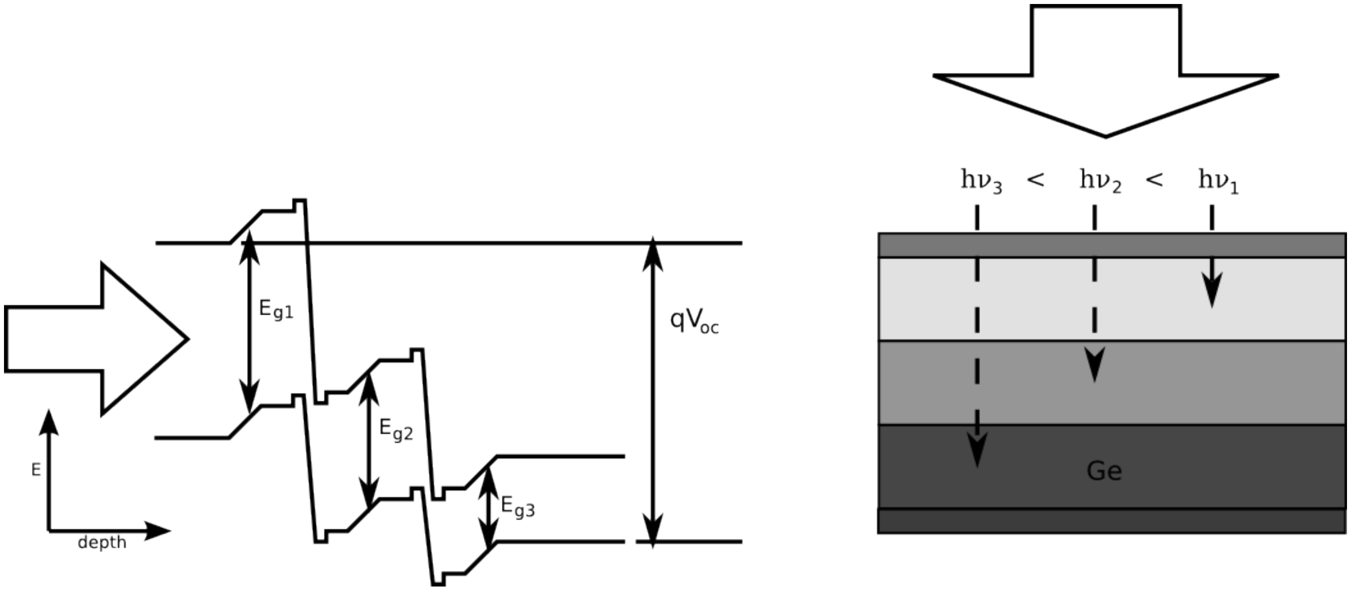

Bibliography

[1] Torrey, H.; Whitmer, C. *Crystal Rectifiers*; McGraw-Hill: New York, 1948.

[2] Riordan, M.; Hoddeson, L.; Herring, C. *Rev. Mod. Phys.* **1999**, *71*, S336–S345.

[3] Pierret, R. *Advanced Semiconductor Fundamentals*; Addison-Wesley Publishing Co.: Reading, Mass., 1989; Vol. 6.

[4] Wagner, R.; Chalmers, B. *J. Appl. Phys.* **1960**, *37*, 581–597.

[5] McCarty, L. *J. Electrochem. Soc.* **1959**, *106*, 1036–1042.

[6] Teal, G.; Little, J. *Phys. Rev.* **1950**, *78*, 647.

[7] Duke, C. *Chem. Rev.* **1996**, *96*, 1237–1259.

[8] Chadi, D.; Chiang, C. *Phys. Rev. B* **1981**, *23*, 1843–1846.

[9] Razado-Colambo, I.; He, J.; Zhang, H.; Hansson, G.; Uhrberg, R. *Phys. Rev. B* **2009**, *79*, 205410.

[10] Becker, R.; Swartzentruber, B.; Vickers, J.; Klitsner, T. *Phys. Rev. B* **1989**, *39*, 1633–1647.

[11] Yu, H.; Webb, L.; Solares, S.; Cao, P.; Goddard, W.; Heath, J.; Lewis, N. *J. Phys. Chem. B* **2006**, *110*, 23898–23903.

[12] Cao, S.; Tang, J.-C.; Shen, S. *J. Phys.: Condens. Matter.* **2003**, *15*, 5261–5268.

[13] Houssa, M.; Chagarov, E.; Kummel, A. *MRS Bull.* **2009**, *34*, 504.

[14] Haxel, G.; Hedrick, J.; Orris, G. *Fact Sheet 087-02 Rare Earth Elements — Critical Resources for High Technology*, `http://pubs.usgs.gov/fs/2002/fs087-02/`.

[15] Frank, M. M.; Koester, S. J.; Copel, M.; Ott, J. A.; Paruchuri, V. K.; Shang, H.; Loesing, R. *Appl. Phys. Lett.* **2006**, *89*, 112905.

[16] Brunco, D. et al. *J. Electrochem. Soc.* **2008**, *155*, H552–H561.

[17] Shockley, W.; Queisser, H. *J. Appl. Phys.* **1961**, *32*, 510.

[18] Sze, S. *Physics of Semiconductor Devices*, 2nd ed.; John Wiley & Sons: New York, 1981.

Chapter 2

Chemical Passivation of Ge(111) Surfaces

2.1 Background

A stable, low defect-density GeO_x/Ge interface that is analogous to the $SiO_x/Si(100)$ interface cannot be formed, so the elimination of surface oxide from Ge would be important to the utilization of Ge as a device material. The original surface passivation through Grignard alkylation of a diamond-type semiconductor had in fact been performed on Ge in 1962.[1] The researchers were successful in eliminating the influence of atmospheric moisture upon the electronic properties of the crystal surface, but still suffered from a large density of surface states, possibly because of an overly aggressive etching procedure. Very little follow-up work on such organic passivation methods was done in the ensuing decades. More recent work has shown that a variation on that early procedure is useful in passivating Si surfaces.[2,3] The alkylated Ge(111) surfaces described in this research were prepared in a similar manner, with some modifications. This chapter is a description of the chemical methods utilized.

Proper cleaning of the substrate is crucial to any successful surface modification.

The well established methods for cleaning Si cannot be directly applied to Ge because the oxide offers no protection. Aqueous acidic oxidizing solutions can easily etch and roughen the surface.[4,5] Repeated etching cycles in aqueous acid etchants and water can remove contaminants such as metal ions, but do still remove crystal material and thus leave open the possibility for further surface roughening.[6–10] Degreasing with organic solvents does not etch the surfaces, but does not remove ionic contaminants, so aqueous etching methods cannot be avoided.

Hydrogen-terminated surfaces may be prepared through the use of aqueous HF solutions. Removal of the oxide is possible, but the well-ordered 1x1 H-Si(111) surface established for Si(111) treated with aqueous NH_4F solution has no reported Ge(111) corollary.[11] Confirmation that the NH_4F solutions do not lead to a flat, hydrogen-terminated surface is easily achieved by noting that the etchant does not produce a hydrophobic Ge surface. There is some disagreement over the stability of the H-Ge(111) surface, but it is generally accepted that it does not posses the stability of the H-Si(111) surface.[8,12,13]

Halogen termination can be achieved in vacuum or in solution.[14,15] The distance between Ge atop atoms is approximately 4 Å, which can accommodate bromine or chlorine on every site.[16,17] While not air-stable over long periods, these surfaces do serve as useful precursor substrates for Grignard alkylation.[1,18]

Sulfide passivation of Ge(100) and Ge(111) in UHV conditions had been reported to successfully remove oxygen through the formation of either 1.0 ML or 0.5 ML sulfur atoms bonded to the surface, depending upon the sulfur source and annealing procedure.[19] Such passivation was then attempted with a more readily accessible wet chemical method involving $(NH_4)_2S$, but an amorphous GeS_x layer was often formed.[12,20,21] Dielectric stacks formed on sulfur-passivated Ge(100) with HfO_2 displayed trap state densities very similar in magnitude to unpassivated stacks.[22] From these results, it appears the sulfide layer formation does not reliably passivate the Ge surface.

Organic passivation can be achieved at relatively low temperatures and could allow further functionalization of the surface. Three methods of attaching long-chain hydrocarbons have been established and are summarized in Figure 2.1. From the hydrogen- or halogen-terminated surface, organic molecules can be attached either through reaction with thiols or with terminal olefins.[12,23–26] The thiol attachment route has the advantage of requiring neither heat nor inert atmosphere, however it has the disadvantage of producing a less chemically robust surface.[23] Hydrogermylation requires only one post-etching step, is completed within a couple of hours, and produces the more chemically inert Ge-C bond at the surface.[25] The Grignard alkylation also produces Ge-C bonds, and is unique in that it allows the attachment of methyl groups to the surface, allowing for the thinnest overlayer and best possible coverage. Larger organic groups, such as ethyl, have a radius of 4.5–5.0 Å, which does not allow for the capping of every atop atom of the Ge(111) surface.[1,27,28]

Because they show the greatest stability and do not require energy-intensive high vacuum techniques, the organic modifications show promise as useful interface passivation methods. This chapter details the experimental procedures for the surface modifications used in the investigations described in the subsequent chapters.

Figure 2.1: Schemes for grafting alkyl monolayers to Ge(111)

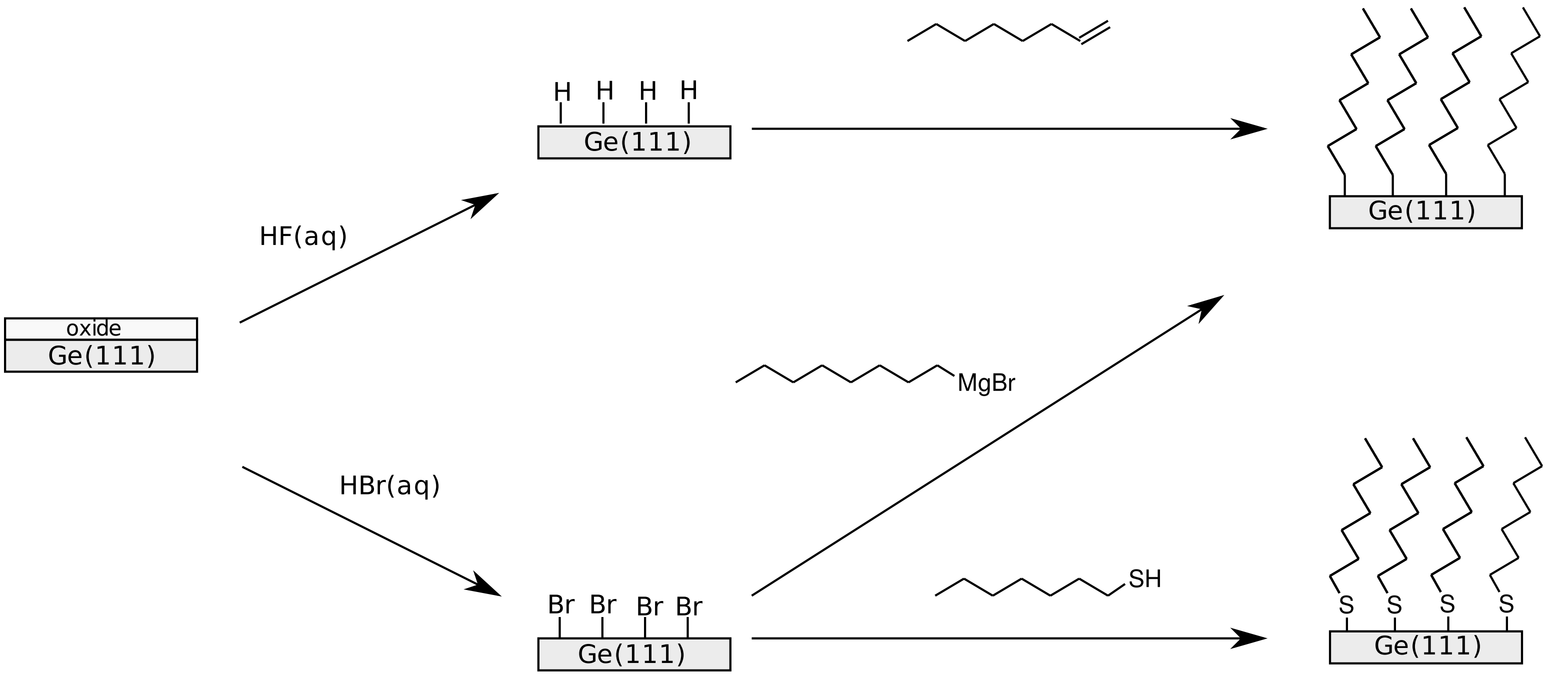

2.1.1 X-Ray Photoelectron Spectroscopy

2.1.1.1 Elemental Analysis

X-ray photoelectron spectroscopy (XPS) is useful for surface sensitive elemental analysis and for obtaining certain chemical information such as oxidation state. The sample under ultra-high vacuum is irradiated with a monochromatic X-ray line of sufficient energy to eject core electrons to vacuum, where they are collected by the analyzer and sorted by kinetic energy. The kinetic energy, KE, is a function of the photo-ionized atom, but also the X-ray energy, hv and the work function, Φ of the specific instrument being used. As a result, the data is usually reported in binding energy, BE

$$BE = hv - KE - \Phi \tag{2.1}$$

which is independent of the X-ray source and instrument.

Figure 2.2 is a survey spectrum of sputter-cleaned Ge. Many of the features visible in the spectrum are either Auger lines or XPS lines compounded with another energy loss pathway. Random scattering of photoelectrons causes the baseline to rise after every strong emission line. A photo-ionized atom may be in an excited state, or a quantized amount of energy may go into bulk plasmons rather than KE so there are often peaks of less intensity located at higher B. eV from the parent XPS line.

Figure 2.2: XPS survey spectrum of clean Ge

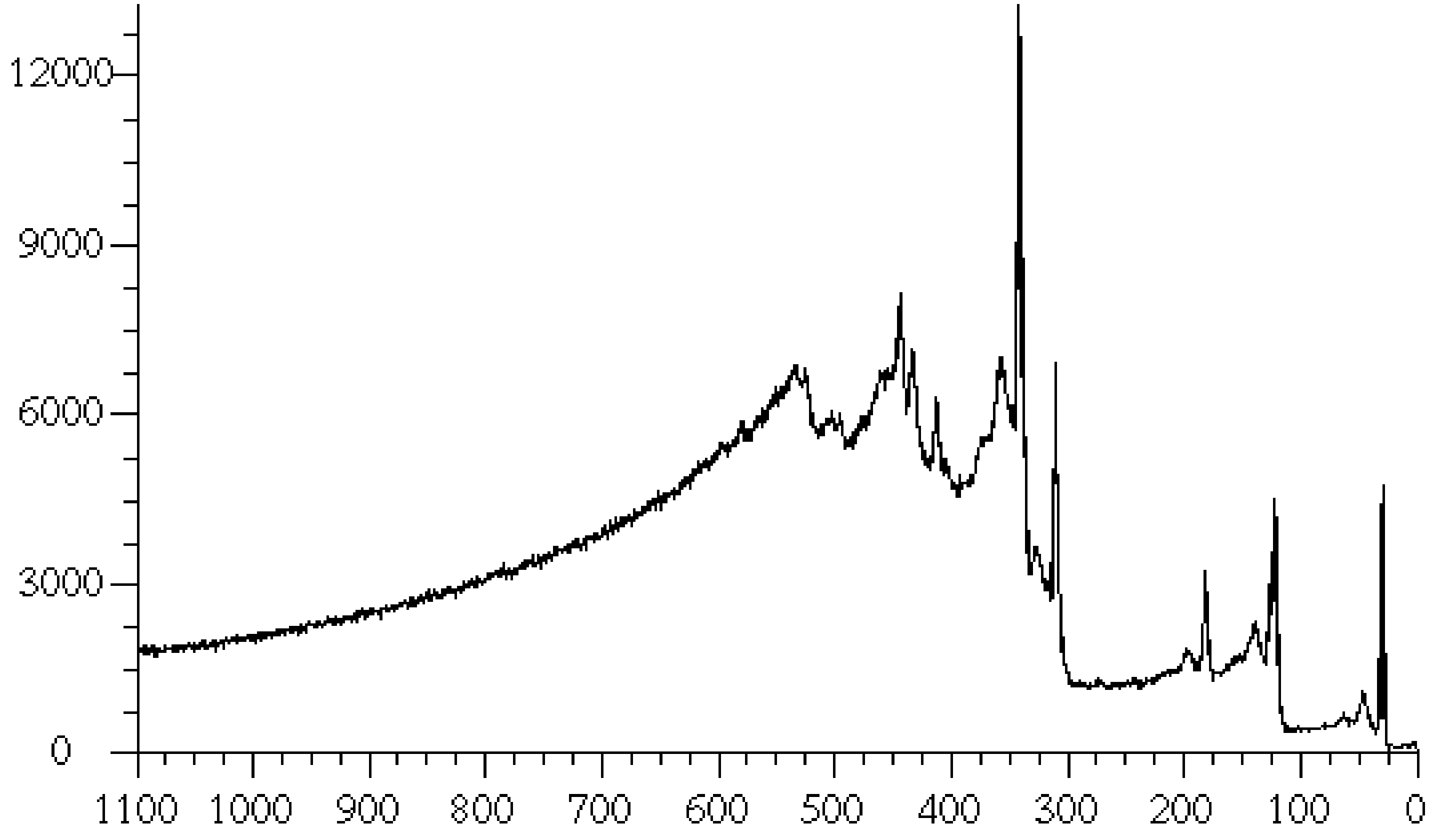

2.1.1.2 Surface Coverage Model

A substrate-overlayer model was used to quantify the composition of the surface region.[29,30] In the following analysis, the X-ray penetration depth far exceeds the photoelectron escape length, λ, so only the escape length affects the XPS line intensity. The escape length is dependent upon the kinetic energy of the photoelectron and the material of the overlayer through which it must travel. This dependence was calculated by the empirical relationship

$$\lambda = 532^{-2} + 0.41a^{1.5}KE^{0.5} \tag{2.2}$$

where a is the atomic diameter.

The spectral peaks of interest in this study are Br 3*d* or C 1*s* of the overlayer atoms and the Ge 3*d* of the crystal surface atoms. Because there will always be hydrocarbon contamination of a surface exposed to air or backstreamed mechanical pump oil, the C 1*s* peak contains a 285 B. eV component arising from carbon bonded to carbon ($\underline{\text{C}}$-C). A core electron of carbon bonded to a less electronegative element such as Ge ($\underline{\text{C}}$-Ge) will have a lower binding energy, so for alkylated samples, there is a C 1*s* component at 284.3 B. eV. The area of that component is a measure of the alkyl groups bonded to the surface.

The Ge 3*d* spectral peak is dominated by emission from the crystal atoms below the surface, which yields a doublet at 29.4 and 30 B. eV. The doublet arises from spin orbit coupling, and has a well established peak intensity ratio. Surface Ge atoms are not readily apparent, but those atoms which are in $+1 - +4$ oxidation states, such as those in an oxide, have a sufficiently higher binding energy to be visible in the 31 – 33 B. eV range, distinguishable from the bulk emission. The intensity of this broad spectral feature is a measure of the chemical oxidation of the Ge surface, as described below.

The thickness of the carbon overlayer is calculated from the C 1s and Ge 3d peak area from

$$\frac{I_{ov}}{I_{Ge}} = \left(\frac{SF_{ov}}{SF_{Ge}}\right)\left(\frac{\rho_{ov}}{\rho_{Ge}}\right)\left[\frac{1-\exp\left(-\frac{d_{ov}}{\lambda_{ov}\sin\theta}\right)}{\exp\left(-\frac{d_{ov}}{\lambda_{Ge}\sin\theta}\right)}\right] \tag{2.3}$$

where is I the peak intensity, ρ is the atomic density, SF is the sensitivity factor, d_{ov} is the overlayer thickness, λ is the photoelectron escape length, and θ is the photoelectron take-off angle determined by the surface orientation relative to the analyzer. The subscript ov signifies an overlayer component, the subscript Ge signifies a Ge component. The Ge 3d spectral peak was chosen over the more surface-sensitive Ge 2p because the 3d photoelectron has a high kinetic energy that is similar to that of the C1s photoelectron, so that $\lambda_{Ge} \approx \lambda_{ov}$ and equation 2.3 may be simplified to

$$d_{ov} = \lambda_{ov}\sin\theta \times \ln\left(1 + \left(\frac{SF_{Ge}}{SF_{ov}}\right)\left(\frac{I_{ov}}{I_{Ge}}\right)\left(\frac{\rho_{Ge}}{\rho_{ov}}\right)\right) \tag{2.4}$$

An alternative formulation that is useful for expressing the fractional monolayer coverage from the 284.3 B. eV C 1s component is

$$\left(\frac{I_{ov}}{I_{Ge}}\right) = \frac{\Phi_{ov}\left(1-\exp\left(\frac{-a_{ov}}{\lambda_{ov}\sin\theta}\right)\right)}{1-\Phi_{ov}\left(1-\exp\left(\frac{-a_{ov}}{\lambda_{Ge}\sin\theta}\right)\right)}\left(\frac{\rho_{ov}}{\rho_{Ge}}\right)\left(\frac{SF_{ov}}{SF_{Ge}}\right) \tag{2.5}$$

where Φ_{ov} is the fractional monolayer coverage, and a_{ov} is the atomic diameter of the overlayer. If Φ_{ov} is not large, and the escape lengths are once again set equal, equation 2.5 can be simplified to

$$\Phi_{ov} = \left[\frac{\lambda_{ov} \sin\theta}{a_{ov}}\right] \left(\frac{\rho_{Ge}}{\rho_{ov}}\right) \left(\frac{SF_{Ge}}{SF_{ov}}\right) \left(\frac{I_{ov}}{I_{Ge}}\right) \tag{2.6}$$

Oxygen incorporation was never intentional for these experiments, so the signal from the 532 B. eV O 1s peak was usually weak and difficult to quantify. The GeO_x layer was instead quantified from the Ge 3d peak. From the intensity ratio of the higher B. eV component to the bulk Ge component, the oxide thickness may be calculated in a manner very similar to that used in equation 2.4.

$$d = \lambda_{ov} \sin\theta \times \left(\ln\left[1 + \left(\frac{I^0_{Ge}}{I^0_{ov}}\right)\left(\frac{I_{ov}}{I_{Ge}}\right)\right]\right) \tag{2.7}$$

where the subscript ov denotes the oxide overlayer. The ratio I^0_{Ge}/I^0_{ov} is an experimentally determined normalization factor obtained from the ratio of pure Ge to pure oxide.[29]

To estimate the fraction of surface atoms that are oxidized, the measured Ge 3d ratio is compared to the expected value for 100% oxidation. Because the kinetic energy of all considered photoelectrons are similar, any scattering and attenuation should be similar and may be ignored. The total intensity, used in the relation of equation 2.8, would have contribution from all photoelectrons able to reach the surface, which would depend upon the atomic density (n_{Ge}), the photoionization cross section (σ_{Ge}), and the take-off angle-dependent escape depth (λ_{Ge}).

$$I_{Ge} \approx n_{Ge}\sigma_{Ge} \int_{0}^{\infty} \exp\left(-\frac{z}{\lambda_{Ge,bulk}\sin\theta}\right) \mathrm{d}z = n_{Ge}\sigma_{Ge}\lambda_{Ge,bulk}\sin\theta \tag{2.8}$$

The surface atoms have the same photoionization cross section, a two-dimensional surface density ($n_{Ge,s}$), but the photoelectrons do not traverse the bulk material, so the surface contribution can be given by

$$I_{Ge,s} \approx n_{Ge,s}\sigma_{Ge} \tag{2.9}$$

If every surface atom is oxidized, the broad oxidized spectral peak would be given by equation 2.9, and the bulk peak component would be $I_{Ge} - I_{Ge,s}$, so a ratio of 0.223 would be obtained from

$$\frac{I_{Ge,s}}{I_{Ge}} = \frac{n_{Ge,s}}{n_{Ge}\lambda_{Ge,bulk}\sin\theta - n_{Ge,s}} \tag{2.10}$$

and division of the measured ratio by equation 2.10 yields the fraction of oxidized surface atoms.

2.2 Experimental

2.2.1 Materials

Unless stated otherwise, all chemicals were purchased from Aldrich or Alfa Aesar and used as received. All water was obtained from a Barnstead Nanopure system and had a resistivity of 18 MΩ-cm. Diethylene glycol dibutyl ether (DEGDBE) was vacuum distilled from $LiAlH_4$ and stored under nitrogen until further use. 1-Decene was vacuum distilled from sodium metal and stored under nitrogen, in the dark, until needed. Br_2(l) was vacuum transferred from phosphorus(V) oxide, subjected to multiple freeze-pump-thaw cycles, and stored in a Schlenk flask until needed. Etching solutions were prepared from dilution (or combination) of 30.7 M (49%) HF, 9.7 M (30%) H_2O_2, 12.0 M (37%) HCl, or 8.8 M (48%) HBr.

Dimethylmagnesium solutions were prepared by adding small portions of 1,4-dioxane to methylmagnesium bromide in diethyl ether until the dioxane•$MgBr_2$ complex no longer precipitated, then the ether solution was filtered through glass wool. Low vapor-pressure organomagnesium and organolithim solutions were prepared from the diethyl ether solutions by addition of an equal volume DEGDBE, then vacuum removal of the diethyl ether to a liquid nitrogen cooled trap.

Two-inch Ge(111) wafers (MTI Corp.) were diced with a diamond scribe to form rectangular fragments of a size appropriate for the experiment, and the edges were ground with carbide paper to prevent shattering. When necessary, regions of the surface were sanded for ohmic contact points. The fragments were then rinsed with water and and either degreased with refluxing isopropanol in an extractor apparatus shown in Figure 2.3 on page 24, or sonicated in a detergent solution (7x cleaning solution, MP BioMedical). To remove any contamination in the oxide layer, the fragments were then rinsed with water, immersed in a 30% hydrogen peroxide for 50 – 70 s, then rinsed again and blown dry with nitrogen.

2.2.2 Surface Modification

2.2.2.1 Grignard Alkylation

Each sample was etched until the etchant solution did not adhere to the surface. The etchant compositions and etching durations are listed in Table 2.1. H-Ge(111) surfaces were prepared by one of two methods. Some samples were very briefly etched with an anisotropic etchant, henceforth referred to as Superoxol etch, composed of a mixture of H_2O, HF, and H_2O_2 in a 4:1:1 volume ratio of their standard concentrations to yield a solution of 1.6 M H_2O_2 and 5.1 M HF(aq). These samples were then thoroughly rinsed and placed in a 6.0–9.0 M HF(aq) solution for 3–6 min, until the surface was cleanly hydrophobic. Samples that were not treated with the Superoxol etch were also etched with 6.0–9.0 M HF(aq), and required longer etching times to become hydrophobic. Cl-Ge(111) samples were produced by etching in 6.0 M HCl(aq) for 20–25 min until hydrophobic. Br-Ge(111) samples were produced by etching in 6.0 M HBr(aq) for 1–3 min.

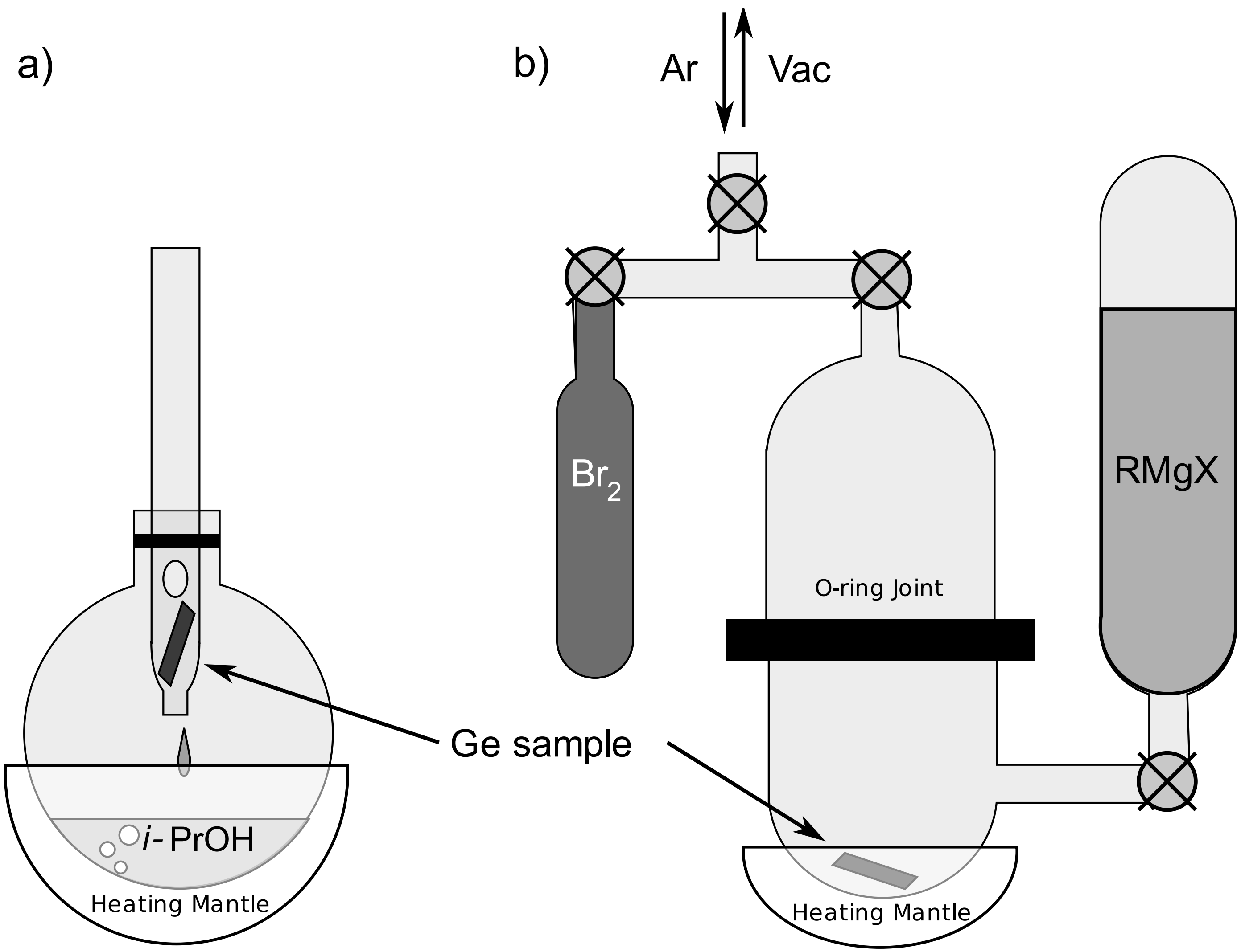

Figure 2.3: Glassware: a. Extractor b. Modified drying chamber

Table 2.1: Procedures of Etching Ge(111)

Etchant Name	step	Composition	duration
HF-6	1	6.0 M HF	20-25 min
HF-12	1	12.0 M HF	8-15 min
HCl-6	1	6.0 M HCl	20-25 min
HCl-9	1	9.0 M HCl	8-10 min
HBr-6	1	6.0 M HBr	1-3 s
HF-NH_4Cl-6	1	6.0 M HF & 6.0 M NH_4Cl	20 min[a]
Superoxol-6	1	1.6 M H_2O_2 & 5.1 M HF	1-3 s
	2	6.0 M HF	3-6 min
Superoxol-6-HCl	1	1.6 M H_2O_2 & 5.1 M HF	1-3 s
	2	6.0 M HCl	>45 min[b]
Superoxol-12	1	1.6 M H_2O_2 & 5.1 M HF	1-3 s
	2	12.0 M HF	30 s

a became coated with hydrocarbons and did not lose hydrophobicity in prolonged contact with water or etchant.
b did not become hydrophobic

Immediately after removal from the etchant, the hydrophobic sample was blown dry with nitrogen and placed in a modified drying chamber, depicted in Figure 2.3b. The chamber was evacuated and backfilled with argon several times. For all but the HBr-etched samples, when the chamber pressure was below 20 mTorr, the vacuum line was closed and the chamber was backfilled with Br_2. After 2–3 minutes, the valve to vacuum was re-opened and the Br_2 captured in a liquid nitrogen trap. Once the pressure was again below 20 mTorr, the low vapor pressure organomagnesium or organolithium solution was added until the sample was completely immersed, and the chamber backfilled with argon. Reactions involving the lithium reagent were not heated, but the organomagnesium solution was heated to 60–70°C and left to react for 3–12 h. In the case of decylmagnesium bromide, the reaction was left for 20–24 h. Once the solution had cooled, the sample was removed and rinsed successively with isopropanol, methanol, water, 1.7 M acetic acid(aq) (to remove magnesium hydroxide), water, methanol, isopropanol, then placed back into the extractor or detergent solution until needed.

2.2.2.2 Hydrogermylation

Samples were etched with 6.0 M HF and placed under vacuum in a drying chamber, as described above. 1-Decene was added to the chamber until the sample was completely immersed, then the chamber backfilled with Ar(g) and heated to reflux for 3 h while under a slight positive argon pressure. Once cooled, the sample was removed and rinsed with hexanes and isopropanol, then placed back into the extractor until further needed.

2.2.2.3 Thiolation

Methanethiol solutions were prepared just prior to use by passing methanethiol vapor through isopropanol. HF etched samples and the thiol solution were placed in a sealed polypropylene container overnight. After removal from the solution, the sample was rinsed with isopropanol and methanol.

2.2.3 Elemental Surface Chemical Analysis

2.2.3.1 Instrumentation

Measurements were performed at vacuum pressures of 10^{-10}–10^{-8} Torr with an M-probe spectrometer interfaced with a computer running ESCA200 Capture software (Service Physics). The monochromatic X-ray line was 1486.6 eV Al Kα directed at 35° to the sample surface. Photoelectrons were collected with a hemispherical analyzer mounted at a 35° angle to the sample surface. The samples were conductive so correction for sample charging was not necessary.

Survey spectra were collected with low resolution settings. Higher resolution scans were collected at settings yielding a full-width at half-maximum of ~0.76 eV.

2.2.3.2 Analysis

Peak fitting of the detailed scans was performed with ESCA2000 Analysis software (Service Physics). Individual peaks of the Ge 3*d* and Br 3*d* doublets were set to have identical asymmetry and Gaussian shape, and a $\frac{5}{2} : \frac{3}{2}$ height ratio of 0.69. All other parameters were allowed to float. Sensitivity factors used for this instrument Br, Ge, Si, and C were 3.16, 1.62, 0.9, and 1.0, respectively.

Atomic diameters were estimated from the inverse cube root of the atomic density,

$$a = \sqrt[3]{A.W./\rho N_A} \tag{2.11}$$

with $A.W.$ being the atomic weight, ρ the density, and $N_A$is Avogadro's number. The sensitivity factors were obtained from the software. Parameters used to calculate the overlayer thicknesses and equivalent monolayer coverages are collected in Table 2.2.

Table 2.2: XPS Analysis Parameters

element	XPS line	SF(a.u.)	λ(nm)	a(nm)	other		
Ge	3d (30 B. eV)	1.62	3.51	0.283	θ	35	degrees
Br	3d (70 B. eV)	3.16	3.46	0.350	$I^0_{Ge}/I^0_{GeO_x}$	1.51	
C	1s (285 B. eV)	1	3.19	0.369	$\lambda_{Ge,bulk}$	2.36	nm
Si	2p (100 B. eV)	0.9	3.42	0.272			

Table 2.3: Hydrocarbon Coverages

Sample Type	$d_{ov}{}^a$ (nm)	d_{ox} (nm)	$\Phi_{ov}{}^b$ (ML)	% oxidized
CH_3-Ge(111)	1.2 ± 0.2	-	1.6 ± 0.2	-
CH_3-Si(111)	1.3 ± 0.2	-	1.7 ± 0.2	-
1-Decene + H-Ge	2.6 ± 0.2	0.20 ± 0.03	-	30 ± 10
$C_{10}H_{21}MgBr$ + Br-Ge	2.2 ± 0.2	0.06 ± 0.06	-	10 ± 10

a. calculated using total C 1*s* signal

b. calculated using 284 B. eV component only

2.3 Results

Table 2.3 summarizes the calculated overlayer coverages.

2.3.1 Inorganic Modification

Although H atoms are not visible in XPS, it can be seen in Figures 2.4 and 2.5 that etching with 9.0 M HF(aq) is effective in removing the oxide. With one hour in lab air, there is significant oxidation. From the integrated area under the low, broad peak in Figure 2.6, the oxide was calculated to be 0.7 ML.

Figure 2.4: Ge 3d region of HF-etched Ge(111)

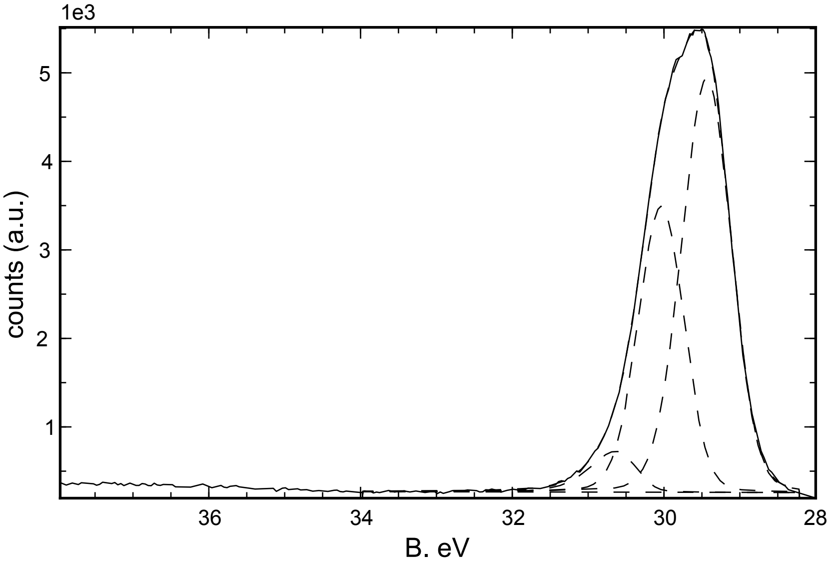

Figure 2.5: Ge 2p region of HF-etched Ge(111)

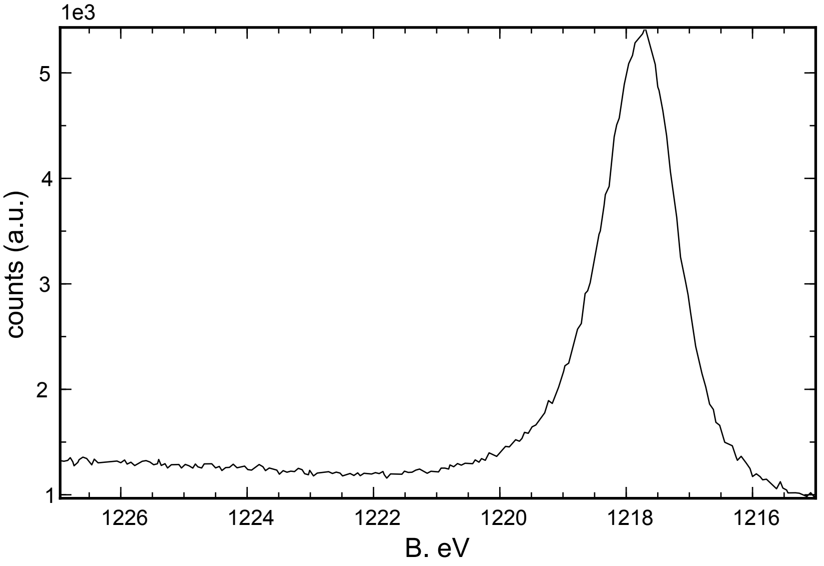

Figure 2.6: Ge 3d region of HF-etched Ge(111) after one hour exposure to air

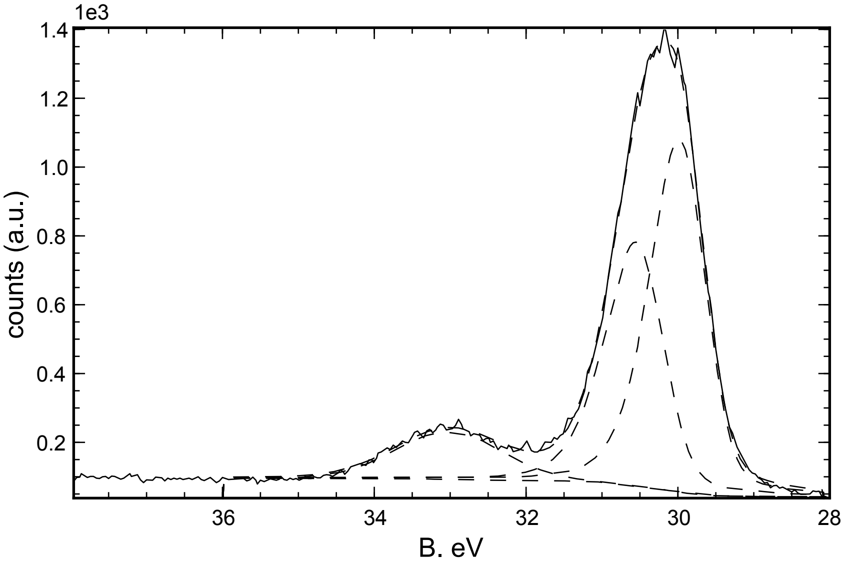

Figure 2.7: Ge 2p region of HF-etched Ge(111) after one hour exposure to air

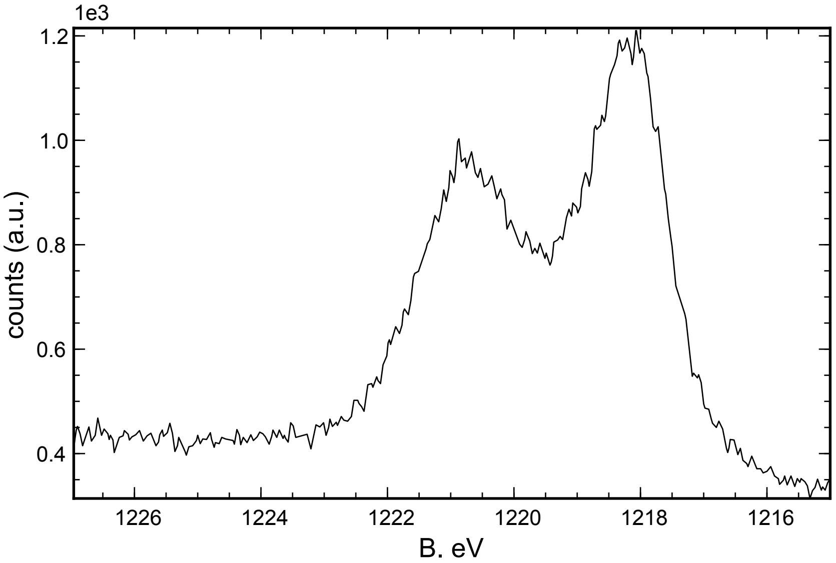

The lack of a significant O 1*s* peak in the survey spectrum Figure 2.8 on page 34, and the lack of noticeable higher B. eV components in the Ge 3*d* or Ge 2*p* spectra, Figures 2.9 and 2.10, show that hydrogen-terminated surfaces immediately treated with Br_2 vapor show little sign of oxidation. From the Br 3*d* peak intensity, shown in Figure 2.11, initial surface coverages are calculated to be 1.0 ± 0.1 ML. Halogenated surfaces show much slower rates of oxidation compared to H-Ge(111), but are not air-stable over the long term. After four days exposure to lab air, there is an appearance of 0.3 ML oxide, and a reduction of the Br 3*d* signal to 0.5 ML. Surfaces that had been etched with 6.0 M HCl(aq) prior to Br_2 exposure displayed 0.5 ML Br, as determined from the ratio of the areas of the Br 3*d* and Ge 3*d* peaks, seen in Figures 2.15 and 2.13. The Ge 2*p* and Ge 3*d*, shown in Figures 2.14 and 2.13, do not display noticeable high B. eV components indicative of oxidized surface species. Evidence for Cl components can be seen from the small peak at 270 B. eV in the survey spectrum of Figure 2.12, but the Cl peaks were not clear in detailed scans and the coverage was not calculated.

Figure 2.8: Survey of Br-Ge(111) from HF-etched precursor

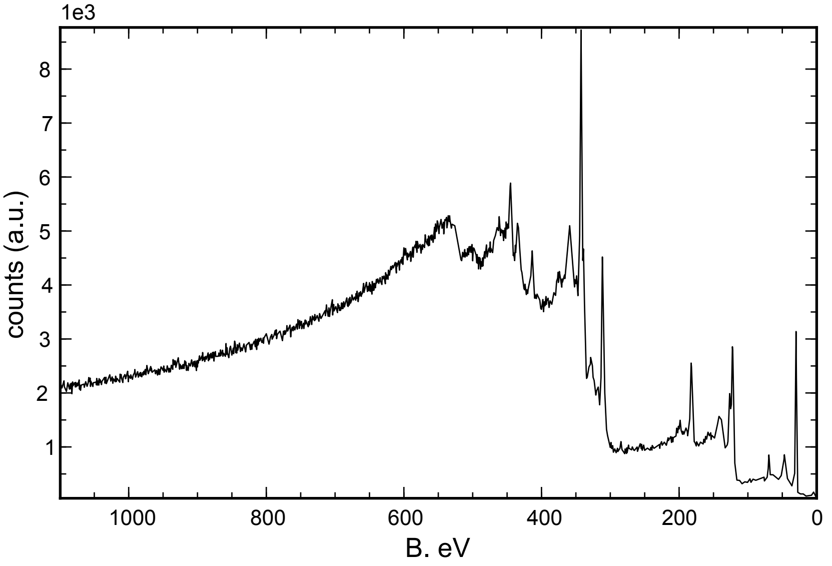

Figure 2.9: Ge 3d region of Br-Ge(111) from HF-etched precursor

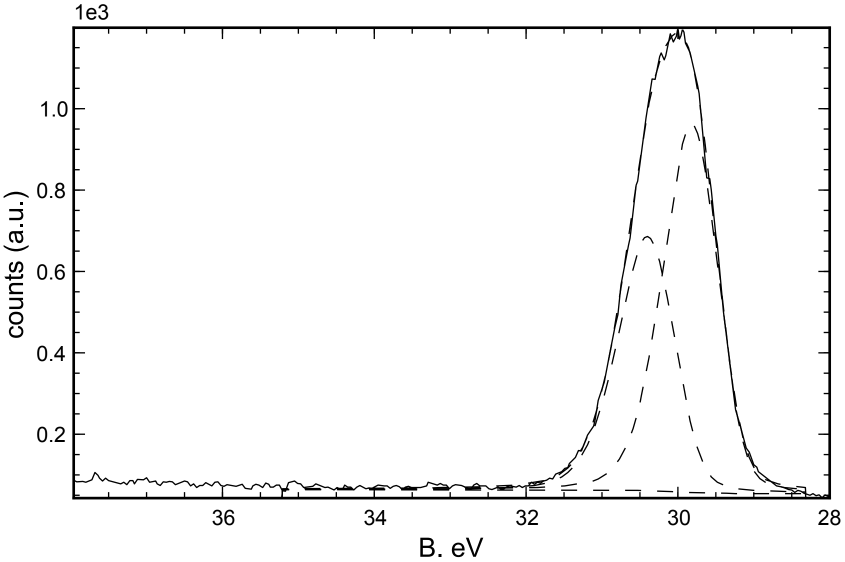

Figure 2.10: Ge 2p region of Br-Ge(111) from HF-etched precursor

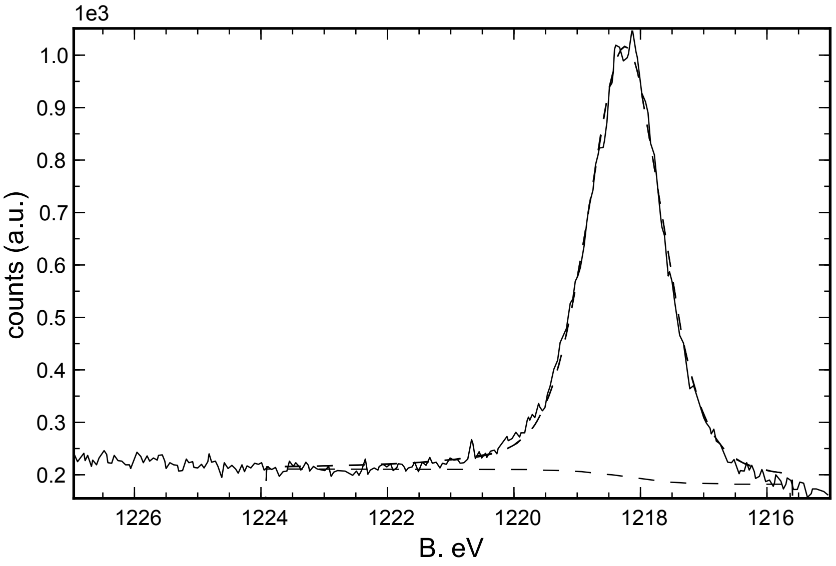

Figure 2.11: Br 3d region of Br-Ge(111) from HF-etched precursor

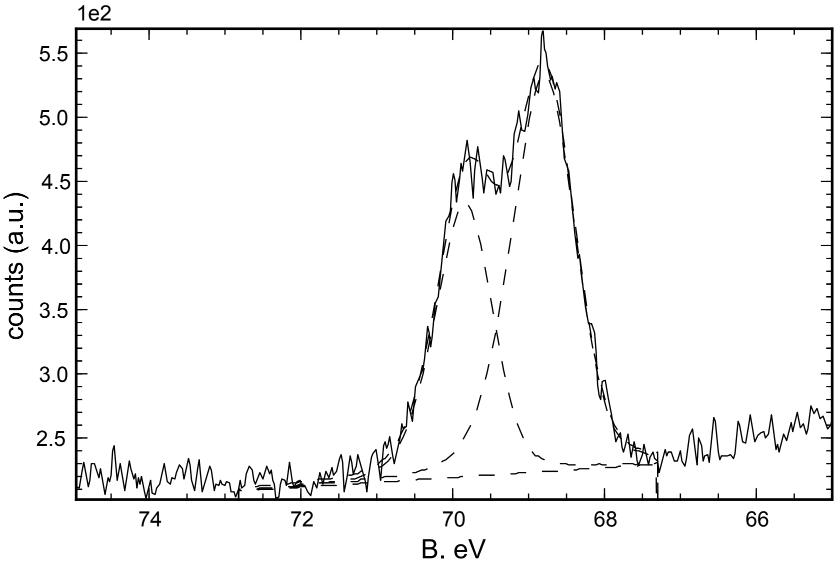

Figure 2.12: Survey of Br-Ge(111) from HCl-etched precursor

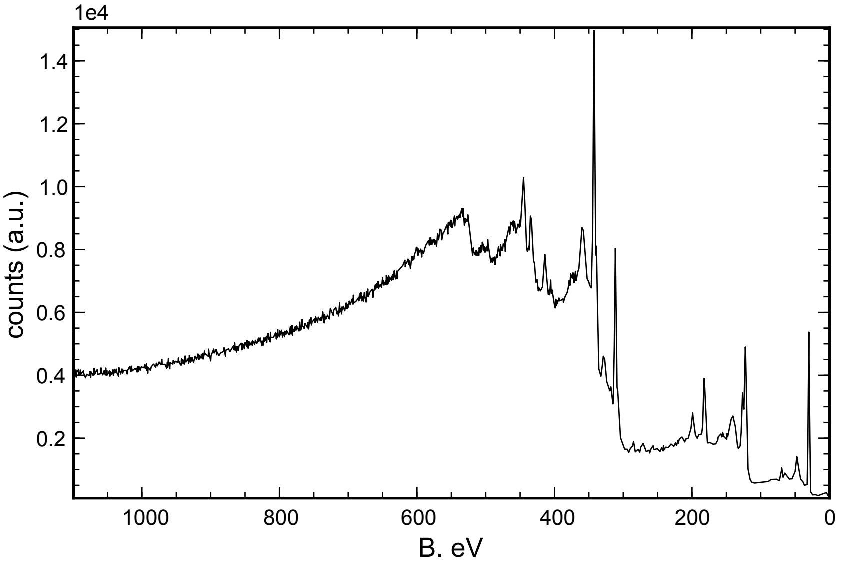

Figure 2.13: Ge 3d of Br-Ge(111) from HCl-etched precursor

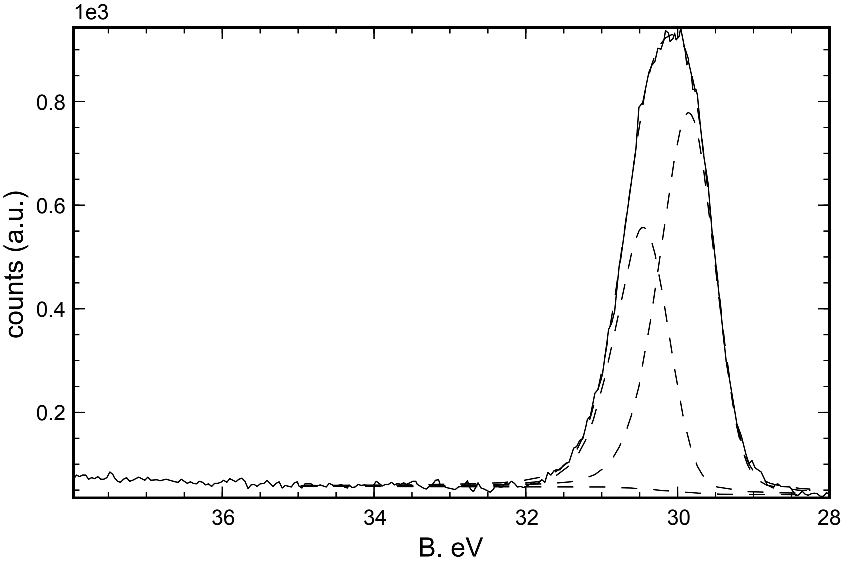

Figure 2.14: Ge 2p of Br-Ge(111) from HCl-etched precursor

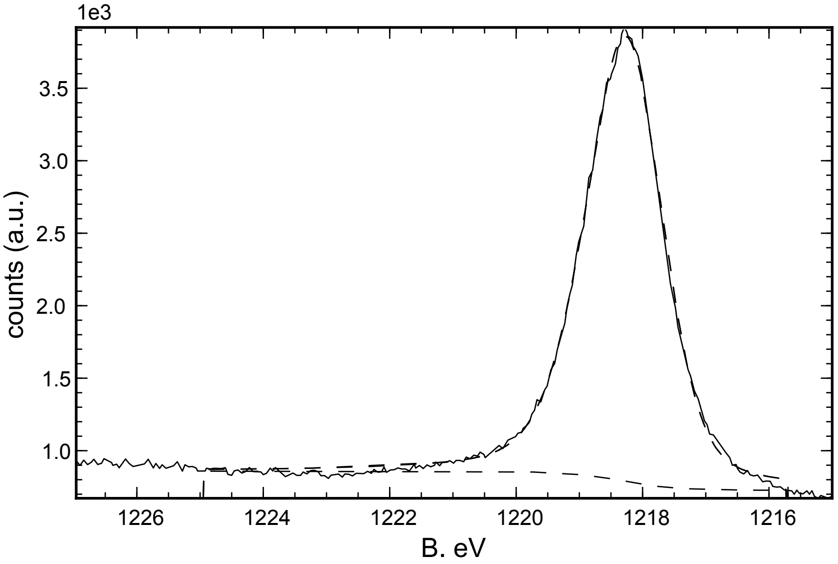

Figure 2.15: Br 3d region of Br-Ge(111) from HCl-etched precursor

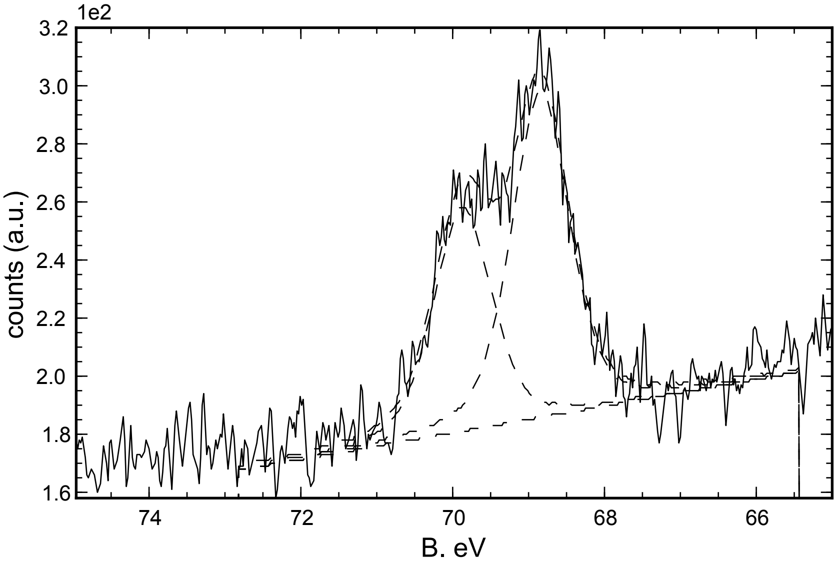

Methanethiol modified surfaces were initially hydrophobic and displayed no detectable oxide. The sensitivity factor of the S 2*p* peak was high enough for the sulfur layer to be detectable, but as can be seen in Figure 2.2 on page 17 the 160 B. eV region does not have a clear background, and obtaining an accurate intensity value for monolayer calculation was not possible. After one day, significant oxidation could be seen in the Ge 3*d* peak displayed shown in Figure 2.19, calculated to be 0.3–0.5 ML, and the S2*p* peak was no longer detectable, as seen in Figure 2.20.

Figure 2.16: Survey of CH_3S-Ge(111)

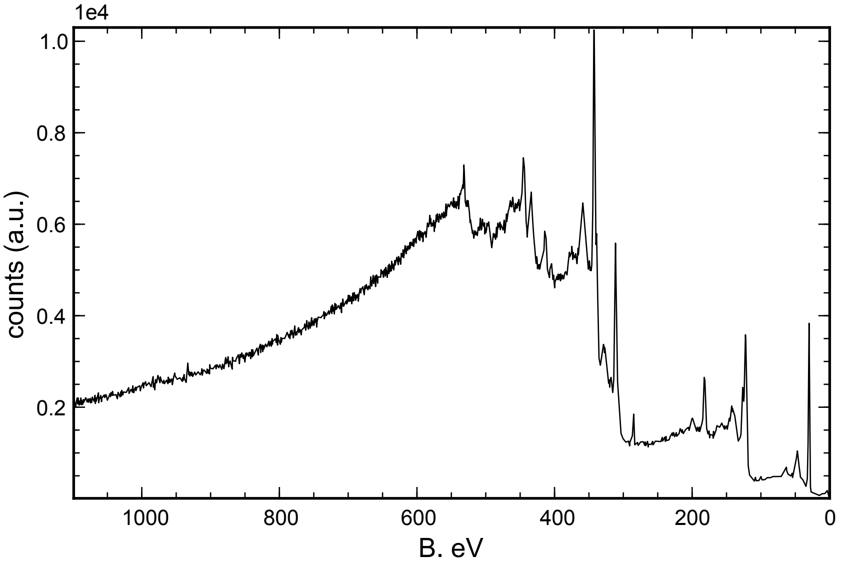

Figure 2.17: S 2p region of CH_3S-Ge(111)

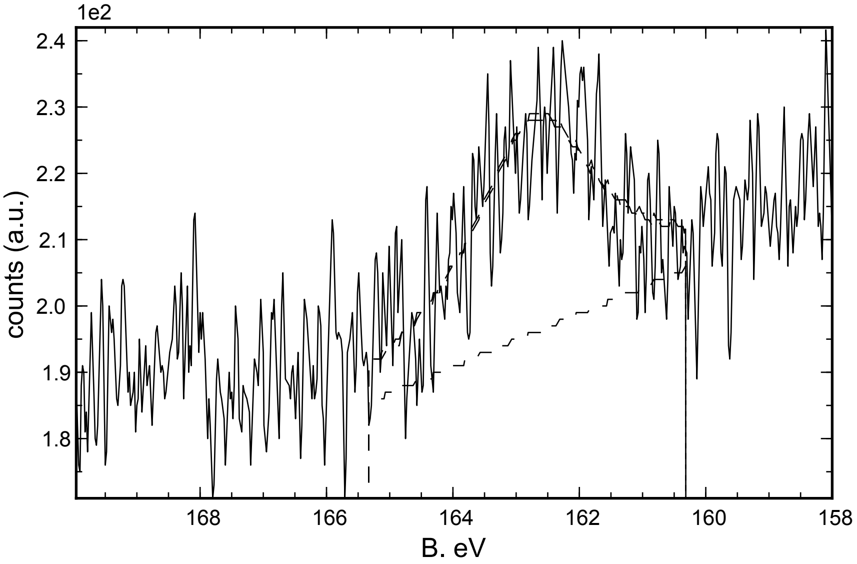

Figure 2.18: Ge 3d region of CH_3S-Ge(111)

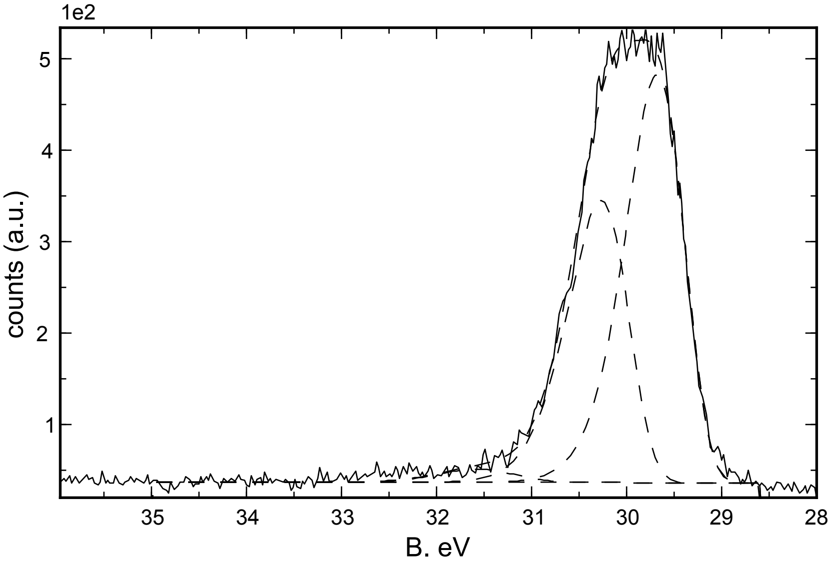

Figure 2.19: Ge 3d region of CH_3S-Ge(111) after 24 hours in air

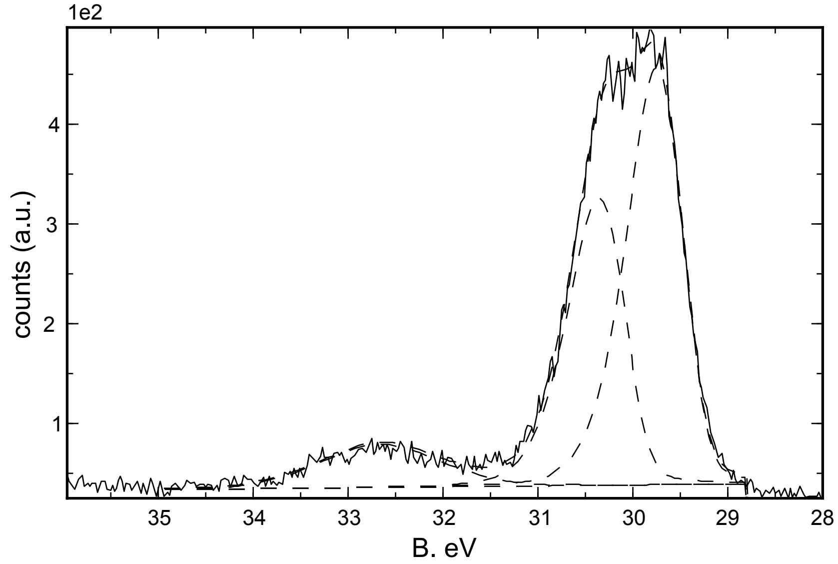

Figure 2.20: S 2p region of CH_3S-Ge(111) after 24 hours in air

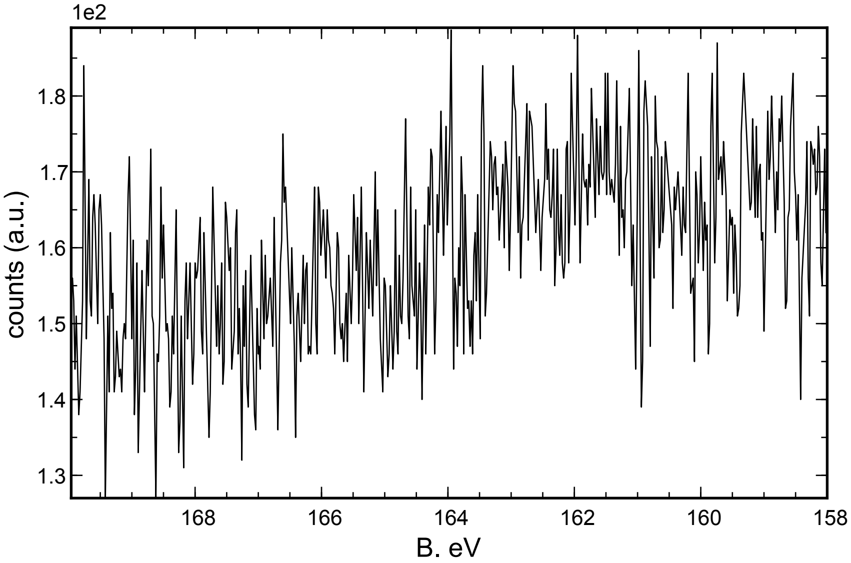

2.3.2 Alkylation

2.3.2.1 Methyl-Terminated Surfaces

Methyl-terminated surfaces showed little sign of oxidation, as seen in Figures 2.21, 2.23, and 2.22, even after the sample had been held in an isopropanol reflux or sonication in detergent solutions for several hours. Such surfaces were stable for at least one week. The lower B eV peak seen in Figure 2.24 is from the surface-capping methyl group. The ratio of the integrated area of the 284.3 B eV peak, I_C, to the integrated area of the Ge 3d peak, I_{bulk}, normalized for element sensitivity, was 0.15 ± 0.02. This is virtually identical to what is observed for CH_3-Si(111) surfaces. Measured by AFM, the surface roughness was 8–13 Å. The value of $I_C : I_{bulk}$ had no strong dependence upon initial etching method.

Figure 2.21: Survey of CH_3-Ge(111)

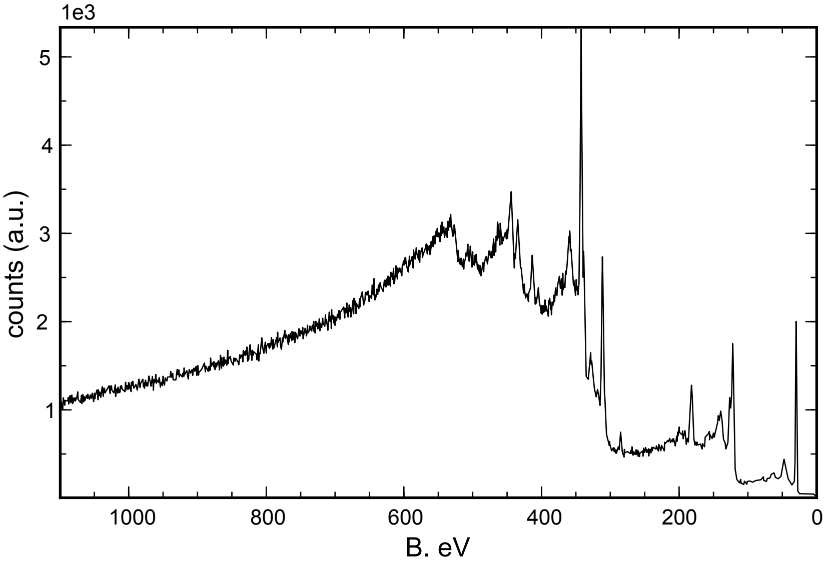

Figure 2.22: Ge 3d region of CH_3-Ge(111)

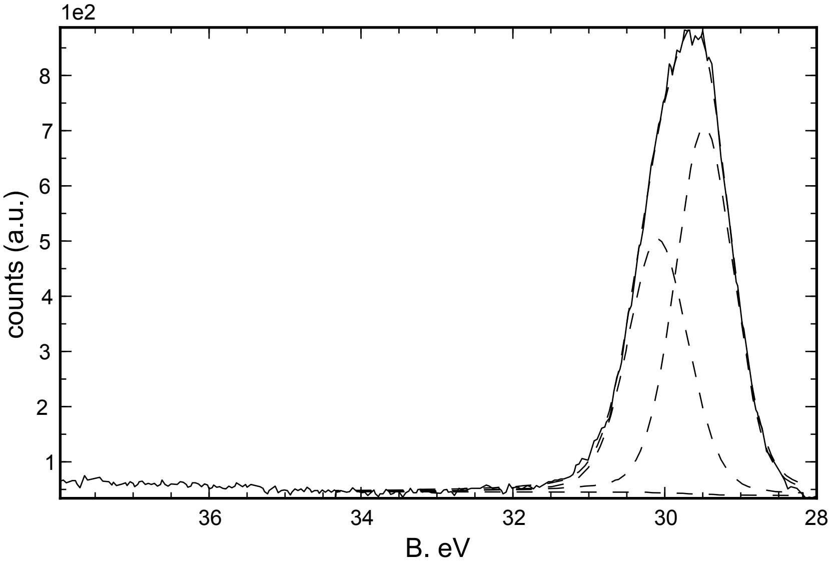

Figure 2.23: Ge 2p region of CH_3-Ge(111)

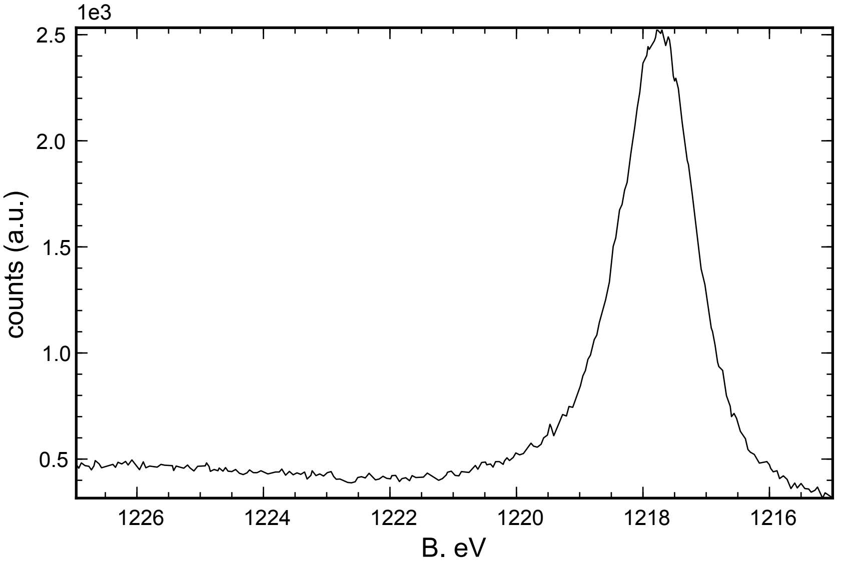

Figure 2.24: C 1s region of CH_3-Ge(111)

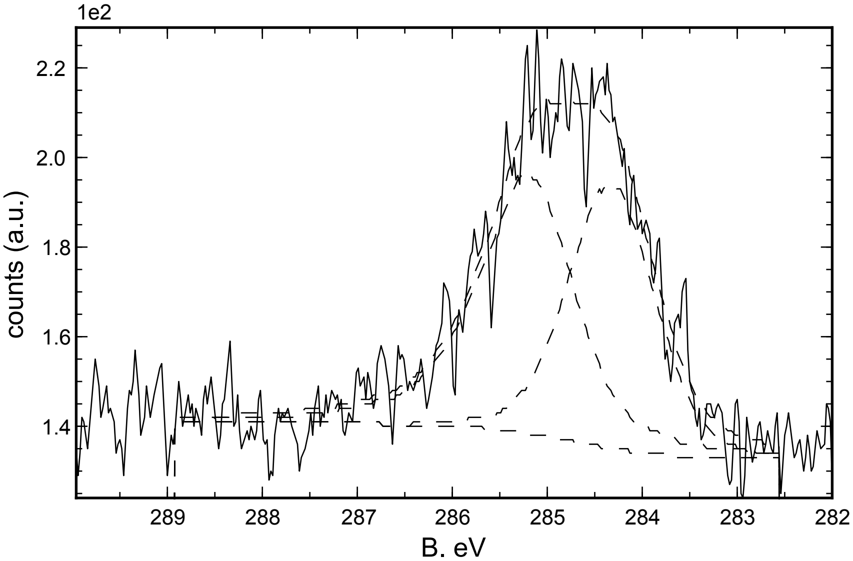

2.3.2.2 Decyl-Terminated Surfaces

Surfaces decyl-terminated through thermal hydrogermylation often showed signs of oxidation of 20–40% of the surface, evident in the higher B eV peaks in Figures 2.28 and 2.29, while similar surfaces prepared through the Grignard alkylation had oxidation levels at or below the 10% detection limit, as evidenced by the lack of a higher B eV component in Figure 2.26 . The long hydrocarbon chain of the decyl groups, in addition to any adventitious hydrocarbon, obscured the C-Ge peak at 284.3 B eV with a large 285 B eV component, as seen in Figure 2.27, so no reliable estimate of the fractional monolayer coverage was possible. The hydrocarbon overlayer thicknesses resulting from both methods were similar, 2.2 ±0.2 nm for the Grignard route, 2.1 ± 0.2 nm for the hydrogermylation.

Figure 2.25: Survey of $C_{10}H_{21}$-Ge(111) prepared from Grignard reagent

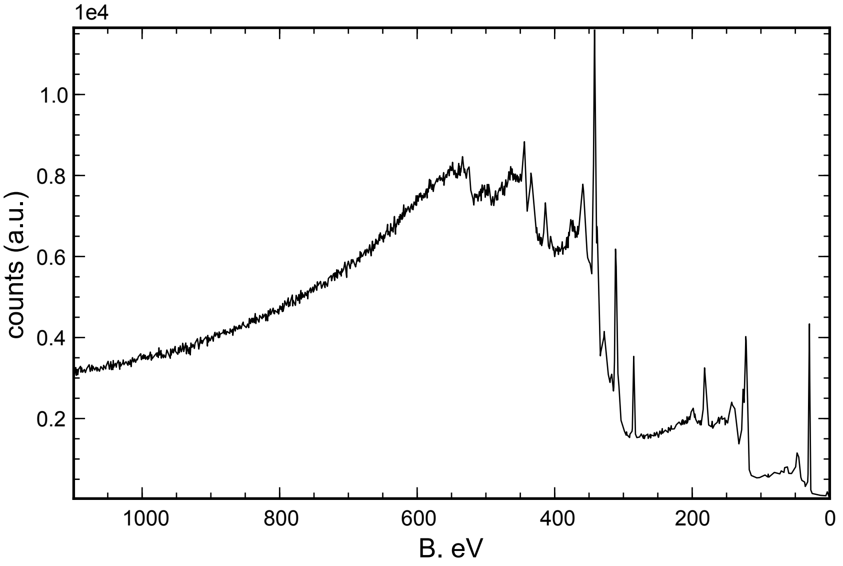

Figure 2.26: Ge 3d region of $C_{10}H_{21}$-Ge(111) prepared from Grignard reagent

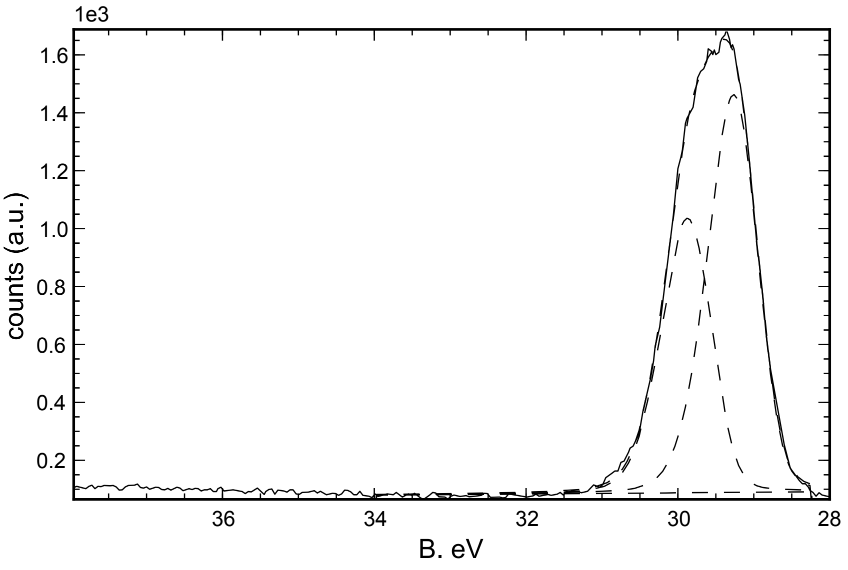

Figure 2.27: C 1s region of $C_{10}H_{21}$-Ge(111) prepared from Grignard reagent

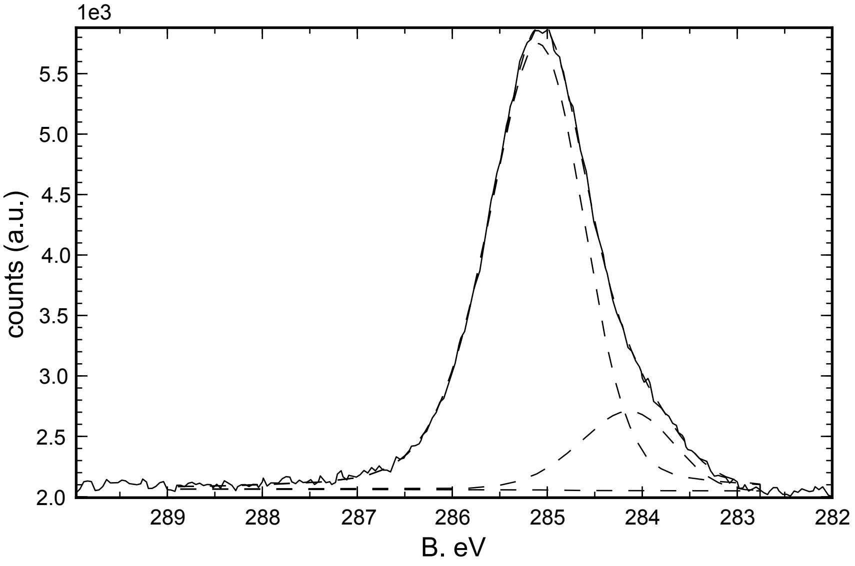

Figure 2.28: Ge 2p region of $C_{10}H_{21}$-Ge(111) prepared from 1-decene

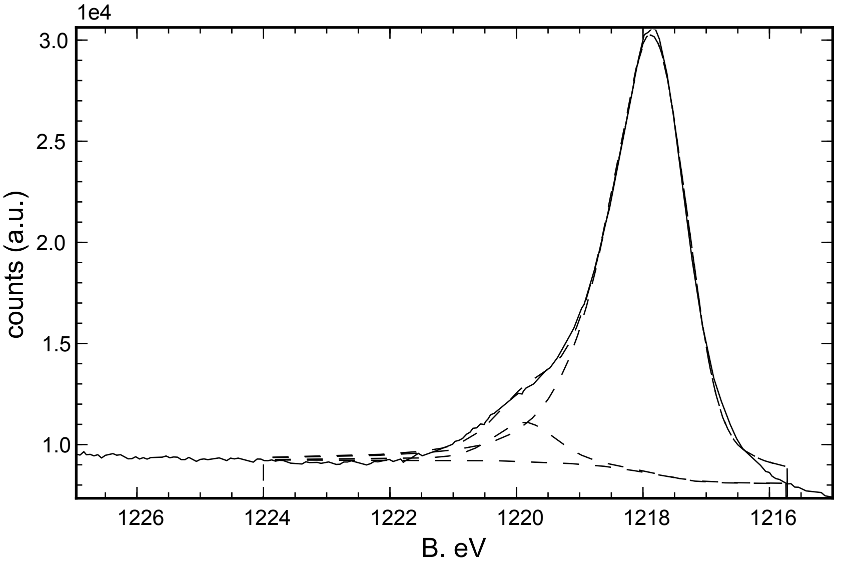

Figure 2.29: Ge 3d region of $C_{10}H_{21}$-Ge(111) prepared from 1-decene

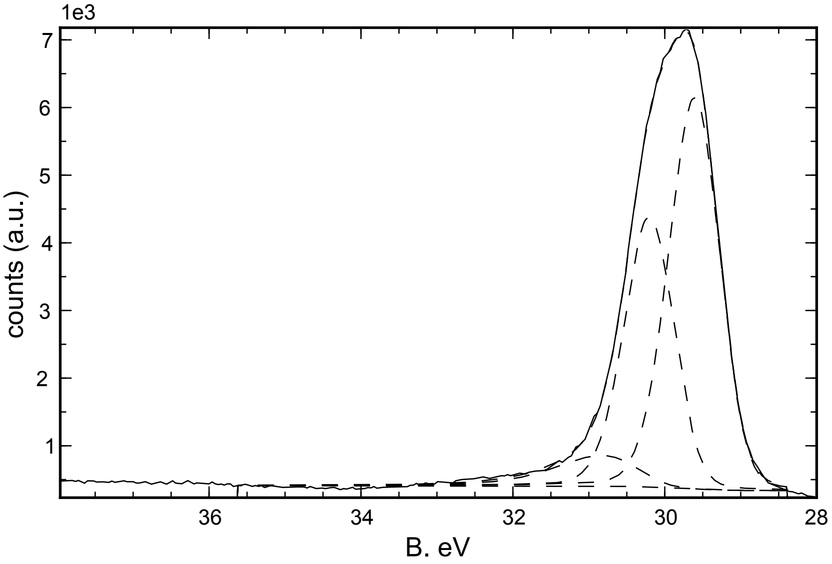

2.4 Discussion

2.4.1 Inorganic Surface Groups

Hydrogen-terminated and halogen-terminated Ge surfaces do not provide chemically stable surfaces, but are useful as intermediates for further processing. The higher reactivity of the H-Ge(111) surface relative to the halogen-terminated surfaces is not simply explained by the bond dissociation energies, for the H-Ge bond is intermediate, at 290 kJ/mol, between Cl-Ge (356 kJ/mol) and Br-Ge (276 kJ/-mol).[31] The chloride-terminated surfaces are believed to be well ordered, but the HF-etched surfaces are not, which would be expected to cause differences in reactivity.[15,16] This atomic roughness could also explain the discrepancy between earlier reports of H-Ge(111) stability and what has been observed more recently, including the work described here.[13,26]

Thiol termination of Ge continues to receive attention because the procedure is simple, the concept is reminiscent of Au-thiol monolayer system, and H-, Cl-, and Br-terminated surfaces are not stable.[6,26] Monolayers attached via a Ge-S bond are not as stable as those attached by a Ge-C bond, but that does not rule out their use as a stable intermediate.[32] In this study, the Ge-S bond was of interest so methanethiol was used, despite the inconvenience of handling, so that the surface was not protected simply by being buried under a thick hydrocarbon layer. The procedure was not optimized, so the presence of oxygen on the surface could have been further minimized. If the Ge-S-C bonding was not stable, the small thiol molecule could be expected to easily desorb. This is confirmed in Figure 2.20 on page 40 by the disappearance of the S 2*p* after one day exposure to air.

2.4.2 Alkyl Groups

2.4.2.1 Methyl

As has been established for CH_3-Si(111), methylation of the Ge(111) surface protects the surface from chemical oxidation by atmospheric conditions. After normalization for differing sensitivity factors, the ratio of surface-bound C 1*s* XPS line to the bulk Ge 3*d* line, $I_{C1s} : I_{Ge3d}$, is nearly identical to the $I_{C1s} : I_{Si2p}$ ratio measured in the CH_3-Si(111) surfaces prepared in this work and in measurements previously reported by others.[33] From this, it can be concluded that there is complete or near complete termination of atop Ge bond sites, and the final surface is comparable to that of Si. The 12±2 Å overlayer thickness (see Table 2.3) is too large for a methyl group with a van der Waals radius of 2.2 Å.[27] However, if the adventitious hydrocarbon peak, which can be seen to comprise just over half the entire C 1*s* signal, is discounted, a measured value of 6 ±2 Å thickness is obtained. Such a value is justifiable if the surface is not atomically smooth over the area of the incident X-ray spot.

A proposed mechanism for the alkylation of the halogenated (or hydrogen-terminated) surface is that alkyl halide impurities are reduced by the Grignard and form radicals, both in solution and on the crystal surface.[34] Evidence of radicals in lithium-halide exchange reactions indicates that the same process is possible for alkyllithium reagents.[35] The report that alkyllithium reagents were ineffective in this type of alkylation raises the question of whether the alkylation mechanism is different for Si and

Ge.[36] In this work however, there were no detectable differences in methylated surfaces prepared from CH_3MgX (X = Cl,Br,I,CH_3) or CH_3Li. This would be consistent with the radical model, which implicates halogenated hydrocarbons as a radical source, because the methyllithium solution was reported by the supplier to contain lithium iodide, and removal of $MgBr_2$ with dioxane, to prepare $(CH_3)_2Mg$ solutions, would have little effect upon halogenated hydrocarbon impurities.

2.4.2.2 Decyl

The long reaction times reported to be necessary for the Grignard alkylation make the quicker one-step hydrogermylation reaction an attractive method of surface passivation. Hydrophobic surfaces with largely non-oxidized surface Ge atoms do indicate that there was surface modification, however it was not as successful as the Grignard reaction route. Both the Grignard alkylation and hydrogermylation routes yielded layer thicknesses that were higher than expected, but if the adventitious hydrocarbon contribution to the C 1*s* signal is assumed to be the same for both the $C_{10}H_{21}$-Ge(111) and CH_3-Ge(111) surfaces and may be similarly subtracted, the resulting 15–16 Å thickness is in better agreement with that seen on Si(111).[37]

The majority of reports on successful hydrogermylation characterize the surfaces by IR, XPS, and contact angle.[24,25,38,39] Of the reports that address the issue, the authors concede that there is some oxidation.[25,38] Considering the higher temperatures necessary in hydrogermylation compared to Grignard alkylation, it is not surprising that there would be degradation of the H-Ge(111). Because the alkyllithium and alkylmagnesium reagents react with water, the reaction conditions for the two-step alkylation are dry, even if there are other oxygen-containing species present. It should be noted that there can be significant variability in the quality of Si(111) surfaces modified by reaction with alkenes, so the occurrence of oxide growth may be eliminated with further optimization of the reaction conditions.[40,41]

2.5 Conclusion

Alkyl monolayers prepared through a milder version of the surface modification technique first attempted almost 50 years ago show initial low oxygen content and long-term resistance to atmospheric oxidation. XPS measurements confirm that the hydrogen-terminated surface is unstable and that the brominated surfaces are slower to oxidize but do not demonstrate long-term stability. The low level of oxidation present in the final alkylated surfaces demonstrates that despite this instability, the hydrogen- and bromine-terminated surfaces are suitable intermediates for the production of stable alkylated surfaces. Methylmagnesium halide, dimethylmagnesium, and methyllithium proved to be effective methylating reagents.

Two other surface passivation techniques were attempted but were not as successful. While it may be possible to prepare low oxygen content monolayers through the use of alkanethiols, the Ge-S bond does not show long term stability. Hydrogermylation does provide a one-step route to a stable overlayer grafted with a stable Ge-C bond, but the initial oxide content was higher than what is seen in the Grignard alkylation method. Furthermore, both thiolation and hydrogermylation reactions are better suited to production of monolayers of larger alkane groups, while the Grignard alkylation method is applicable to methyl groups and larger alkanes.

Bibliography

[1] Cullen, G.; Amick, J.; Gerlich, D. *J. Electrochem. Soc.* **1962**, *109*, 124–127.

[2] Bansal, A.; Li, X.; Lauermann, I.; Lewis, N.; Yi, S.; Weinberg, W. *J. Am. Chem. Soc.* **1996**, *118*, 7225–7226.

[3] Bansal, A.; Lewis, N. *J. Phys. Chem. B* **1998**, *102*, 4058–4060.

[4] Bolts, J. M.; Wrighton, M. S. *J. Am. Chem. Soc.* **1978**, *100*, 5257–5262.

[5] Brunco, D. et al. *J. Electrochem. Soc.* **2008**, *155*, H552–H561.

[6] Ardalan, P.; Musgrave, C.; Bent, S. *Langmuir* **2009**, *25*, 2013–2025.

[7] Kamata, Y.; Ino, T.; Koyama, M.; Nishiyama, A. *Applied Physics Letters* **2008**, *92*, 063512.

[8] Rivillion, S.; Chabal, Y. J.; Amy, F.; Kahn, A. *Appl. Phys. Lett.* **2005**, *87*, 253101.

[9] Maroun, F.; Ozanam, F.; Chazalviel, J.-N. *J. Phys. Chem. B* **1999**, *103*, 5280–5288.

[10] Kosuri, M.; Cone, Q., R. Li; S.M., H.; Bunker, B.; Mayer, T. *Langmuir* **2004**, *20*, 835–840.

[11] Higashi, G.; Chabal, Y.; Trucks, G.; Raghavachari, K. *Appl. Phys. Lett.* **1990**, *56*, 656–658.

[12] Bodlaki, D.; Yamamoto, D.; Waldeck, D.; Borguet, E. *Surf. Sci.* **2003**, *543*, 63–74.

[13] Deegan, T.; Hughes, G. *Appl. Surf. Sci.* **1998**, *123/124*, 66–70.

[14] Fouchier, M.; McEllistrem, M.; Boland, J. *Surf. Sci.* **1997**, *385*, L905–L910.

[15] Lu, Z. *Appl. Phys. Lett.* **1996**, *68*, 1996.

[16] Cao, S.; Tang, J.-C.; Shen, S. *J. Phys.: Condens. Matter.* **2003**, *15*, 5261–5268.

[17] Sun, S.; Sun, Y.; Lee, D.-I.; Pianetta, P. *Appl. Phys. Lett.* **2006**, *89*, 231925.

[18] Wang, D.; Dai, H. *Appl. Phys. A* **2006**, *85*, 217–225.

[19] Newstead, K.; Robinson, A.; Patchett, A.; Prince, N.; McGrath, R.; Whittle, R.; Dudzik, E.; McGovern, J. T. *J. Physics: Cond. Matt.* **1992**, *4*, 8441–8446.

[20] Anderson, G.; Hanf, M.; Norton, P.; Lu, Z.; Graham, M. *Appl. Phys. Lett.* **1995**, *66*, 1123–1125.

[21] Lyman, P.; Sakata, O.; Marasco, D.; Breneman, K.; Keane, D.; Bedzyk, M. *Surf. Sci.* **2000**, *462*, L594–L598.

[22] Frank, M. M.; Koester, S. J.; Copel, M.; Ott, J. A.; Paruchuri, V. K.; Shang, H.; Loesing, R. *Appl. Phys. Lett.* **2006**, *89*, 112905.

[23] Han, S. M.; Ashurst, W. R.; Carraro, C.; Maboudian, R. *J. Am. Chem. Soc.* **2001**, *123*, 2422–2425.

[24] Sharp, I.; Schoell, S.; Hoeb, M.; Brandt, M.; Stutzmann, M. *Appl. Phys. Lett.* **2008**, *92*, 223306.

[25] Choi, K.; Buriak, J. *Langmuir* **2000**, *16*, 7737–7741.

[26] Ardalan, P.; Sun, Y.; Pianetta, P.; Musgrave, C. B.; Bent, S. F. *Langmuir* **2010**, *26*, 8419–8429.

[27] Rivillion, S.; Chabal, Y. *J. Phys. IV* **2006**, *132*, 195–198.

[28] Yu, H.; Webb, L.; Heath, J.; Lewis, N. *Appl. Phys. Lett.* **2006**, *88*, 252111.

[29] Pomykal, K. E.; M., F. A.; Lewis, N. *J. Phys. Chem.* **1995**, *99*, 8302–8310.

[30] Haber, J. A.; Lewis, N. S. *J. Phys. Chem. B* **2002**, *106*, 3639–3656.

[31] *CRC Handbook of Chemistry and Physics*; Lide, D. R., Ed.; CRC Press LLC: Boca Raton, 1999.

[32] S.M., H.; Ashurst, W.; Carraro, C.; Maboudian, R. *J. Am. Chem. Soc.* **2001**, *123*, 2422–2425.

[33] Nemanick, E.; Hurley, P.; Brunschwig, B.; Lewis, N. *J. Phys. Chem. B* **2006**, *110*, 14800–14808.

[34] Fellah, S.; Boukherroub, R.; Ozanam, F.; Chazalviel, J.-N. *Langmuir* **2004**, *20*, 6359–6364.

[35] Seyferth, D. *Organometallics* **2006**, *25*, 2–24.

[36] He, J.; Lu, Z.; Mitchell, S.; Wayner, D. *J. Am. Chem. Soc.* **1998**, *120*, 2660–2661.

[37] Linford, M.; Fenter, P.; Eisenberger, P.; Chidsey, C. *J. Am. Chem. Soc.* **1995**, *117*, 3145–3155.

[38] Hanrath, T.; Korgel, B. *J. Am. Chem. Soc.* **2004**, *126*, 15466–15472.

[39] Chen, R.; Bent, S. *Chem. Mater.* **2006**, *18*, 3733.

[40] Webb, L.; Lewis, N. *J. Phys. Chem. B* **2003**, *107*, 5404–5412.

[41] Aureau, D.; Rappich, J.; Moraillon, A.; Allongue, P.; Ozanam, F.; Chazalviel, J.-N. *J. Electroanal. Chem.* **2010**, *646*, 33–42.

The following chapter contains material adapted in part, with permission, from:

Journal of Physical Chemistry C, 114 (28) 12300–12307, Jun 28 2010

`http://pubs.acs.org/articlesonrequest/AOR-2zUgS72Z5YFJiekWnC5S`

Chapter 3

Electrical Measurements I: Surface Conductance

3.1 Introduction

The electrical defects that are associated with either physical defects or chemical impurities at the surface can have a profound impact upon the electrical characteristics of a semiconductor material. These defects may form electrical states within the bandgap that can capture or emit electronic carriers, which can cause deviations from expected behavior of electrical contacts, as well as provide a relaxation pathway for free carriers. This section outlines the origin of the parameters used to quantify the electronic properties of the the Ge(111) surface as a function of the chemical surface conditions.

3.1.1 Surface Recombination

3.1.1.1 Background

Even for an electrically isolated semiconductor, there must be an eventual relaxation to equilibrium after a perturbation, such as a light pulse in the case considered here. Relaxation through non-radiative, trap-assisted recombination was first modeled by Shockley and Read, and independently by Hall, and is commonly referred to Shockley-Read-Hall (SRH) recombination. The rate of relaxation depends upon the concentration of conduction band electrons (n), valence band holes (h), recombination-generation (R-G) centers, both empty and filled (p_T and n_T, respectively), and proportionality constants describing the rate of electron capture and emission ($c_n$and e_n) and hole capture and emission ($c_p$and e_p). This net recombination is expressed as[1,2]

$$\begin{aligned} r_n &= \frac{\delta n}{\delta t}|_{R-G} = c_n p_T n - e_n n_T \\ r_p &= \frac{\delta p}{\delta t}|_{R-G} = c_p n_T p - e_p p_T \end{aligned} \tag{3.1}$$

Equation 3.1 is generally applicable to any situation involving a non-degenerate semiconductor. If the simplifying assumption is made that the capture and emission coefficients remain constant under both equilibrium ($r_n = r_p = 0$) and non-equilibrium conditions, the emission terms may be rewritten as capture terms dependent upon the R-G center position within the bandgap.

$$e_n = c_n \left(\frac{p_T n}{n_T} \right) = c_n n_1 \tag{3.2a}$$

$$e_p = c_p \left(\frac{n_T p}{p_T} \right) = c_p p_1 \tag{3.2b}$$

where through the relations

$$n_1 \equiv \frac{p_T n}{n_T}$$

$$p_1 \equiv \frac{n_T p}{p_T}$$

$$N_T \equiv n_T + p_T$$

$$n_1 = \left(\frac{N_T}{n_T} - 1 \right) n = \left[\left(1 + \exp \frac{(E_T - E_F)}{kT} \right) - 1 \right] n_i \exp \left[\left(E_F - E_i \right) / kT \right]$$

$$n_1 = n_i \exp \left[\left(E_T - E_i \right) / kT \right] \tag{3.2c}$$

$$p_1 = n_i \exp \left[\left(E_i - E_T \right) / kT \right] \tag{3.2d}$$

Equations 3.1 and 3.2 concern the crystal bulk, but analogous relations can be drawn for surface processes, though the trap and carrier concentrations are in terms of area rather than volume.

$$r_{ns} = c_{ns}\left(p_{Ts}n_s - n_{Ts}n_{1s}\right) \tag{3.3a}$$

$$r_{ps} = c_{ps}\left(n_{Ts}p_s - p_{Ts}p_{1s}\right) \tag{3.3b}$$

For steady-state conditions, $r_{ns} = r_{ps}$ and a general recombination rate can be defined, after rearranging equation 3.3a to replace n_{Ts} & p_{Ts} with N_{Ts}, as

$$R_s = \frac{n_s p_s - n_i^2}{\frac{1}{c_{ps}N_{Ts}}\left(n_s + n_{1s}\right) + \frac{1}{c_{ns}N_{Ts}}\left(p_s + p_{1s}\right)} \tag{3.4}$$

where the factors $(cN_T)^{-1}$have units of velocity, and in the absence of complicating factors such as high-level injection or surface fields, represent the flow of carriers to the surface. Equation 3.4 is valid for the case of a single trap-state level, however real surfaces have a continuum of states so that N_{Ts} is correlated to a density of states, $D_T(E)dE$, integrated over the entire bandgap and R_s becomes

$$R_s = \int\limits_{E_V}^{E_C} \frac{n_s p_s - n_i^2}{\frac{1}{c_{ps}}(n_s + n_{1s}) + \frac{1}{c_{ns}}(p_s + p_{1s})} D_T(E)dE \tag{3.5}$$

For low-level injection ($\Delta n_s = \Delta p_s \ll n_{s0}$), the steady-state carrier concentrations can be related to the equilibrium concentrations through

$$n_s = n_{s0} + \Delta p_s \tag{3.6a}$$

$$p_s = p_{s0} + \Delta p_s \tag{3.6b}$$

$$n_s p_s - n_i^2 = n_{s0} \Delta p_s \tag{3.6c}$$

and $R_s$can be rewritten in terms of the perturbation Δp_s

$$R_s = \left[\int_{E_v}^{E_C} (c_{ps} D_T) \left(1 + \frac{n_{1s}}{n_{s0}} + \frac{c_{ps} p_{1s}}{c_{ns} n_{s0}} \right)^{-1} dE \right] \Delta p_s = s_p \Delta p_s \tag{3.7}$$

The bracketed integral in equation 3.7 depends only upon the surface state distribution, so it is taken as a system parameter, s_p, known as the surface recombination velocity (for n-type samples in this case).

3.1.1.2 Photoconductivity Decay

Recombination center density can be measured, by way of the surface recombination velocity, through photoconductivity decay (PCD) profiles. Excess carriers generated by a rapid light pulse raise the conductivity of the semiconductor. After the pulse, the conductivity will decrease to the original value at a rate defined by the rate of recombination both in the bulk and at the surface. Single-crystal Si and Ge can be prepared with sufficiently high quality that bulk recombination is low and surface recombination dominates. The effective carrier lifetime τ is obtained from the decay constant seen in the PCD profile of conductance as a function of time

$$y(t) = Ae^{-\frac{t}{\tau}} + C \tag{3.8}$$

Because carriers require a finite amount of time to diffuse to the surface, τ is dependent upon the sample geometry. For the case of a wafer with an area that is wide compared to the distance a carrier may traverse, but a thickness that is not, that dependence may be eliminated by converting τ to the surface recombination through

$$\frac{1}{\tau} = \frac{1}{\tau_{bulk}} + \frac{2s}{d} \tag{3.9}$$

where d is the sample thickness, and the factor 2 is due to the sample having two surfaces.

The derivation of s leading to equation 3.7 assumed restrictive conditions of low-level injection and flat bands, but is often extended to arbitrary conditions.[1] For the $\mathrm{SiO}_x/\mathrm{Si}$ interface, the band-bending is not severe and the capture cross-sections of the electrons and holes are similar for the dominant recombination center, so the surface trap density, N_{Ts}, can be fairly approximated by the relation

$$s = \sigma v_{th} N_{Ts} \tag{3.10}$$

where σ is the carrier capture cross-section and v_{th} is the thermal drift velocity.

3.1.2 Surface Charging

Surface states with slow kinetics for one carrier type are not efficient recombination centers, but still interfere with electrical contact formation. While the barrier height of the junction should depend upon the work function of the contacting phase, surface states that accept or donate the charge that would have ideally resided throughout the space-charge region. The resulting insensitivity of the junction properties to the contacting phase is known as *Fermi level pinning.* Fermi level pinning is a well-known feature of metal/Si Schottky diodes. The pinning is believed to arise from formation of silicides during the metal deposition process.[2] Room temperature, solution-phase contacts could be formed without reactive conditions of high temperatures at the silicon surface. More recently, soft contact formation has been explored so that the degree of pinning is not so dependent on contact formation conditions.[3–5]

3.1.2.1 Surface Conductance

The experiment described in this section is designed to measure the charged surface states and associated surface potential. Sample conductance is measured as the surface potential is varied by means of a field plate parallel to the sample surface.[6]

The surface charge associated with the trap states results in carrier concentrations near the surface that are different than those in the bulk. This can be measured as a change in conductance, σ, according to[7]

$$\Delta\sigma = q\left(\mu_n \Delta N + \mu_p \Delta P\right) \tag{3.11}$$

where ΔN and ΔP are the total change in electron and hole concentrations within the near-surface region.

$$\Delta N = \int_{0}^{\infty} (n - n_b) dz \tag{3.12a}$$

$$\Delta P = \int_{0}^{\infty} (p - p_b) dz \tag{3.12b}$$

The factors μ_n and μ_p are surface mobilities, less than or equal to the bulk mobilities, the exact values depend upon the nature of the surface scattering. The deviation from bulk values is greatest in strong inversion or accumulation. Under circumstances closer to flat-band conditions, equation 3.11 is a direct measure of surface potential reflected in the carrier concentrations.

Figure 3.1 on page 67 is a plot of $\Delta\sigma$ as a function of surface potential v_s for a lightly doped n-type sample at room temperature. At flat-band conditions, the excess surface carrier density is zero, so this is taken as the reference point. For positive surface potentials, accumulation conditions exist and the excess electrons raise the total measured surface conductance. Similarly, for sufficiently negative surface potentials, inversion conditions exist and the excess hole concentration is high enough to raise the sample conductance. At less negative potentials, the surface region is depleted of majority carriers, and there is an insufficient concentration of minority carriers to compensate, so the sample conductance is decreased.

For a sample of uniform composition and thickness, the conductance may be related to the measured resistance by

$$\Delta\sigma = \frac{l^2}{A}\left(\frac{1}{R} - \frac{1}{R_0}\right) \tag{3.13}$$

where l is the sample length, $A = l \times w$ is the area of the sample faces. It is difficult to predict $R_o$within the necessary accuracy, but if the semiconductor dopant density is known, the potential at which the surface crosses from depletion to inversion can be calculated, and the point of maximum *resistance* can be used to connect the measured resistance values with the calculated relationship in Figure 3.1 on page 67 by rearranging equation 3.13 to

$$\Delta\sigma - \Delta\sigma_{min} = \frac{l}{2w}\left(\frac{1}{R} - \frac{1}{R_{max}}\right) \tag{3.14}$$

3.1.2.2 Pulsed Fields

If the surface field is varied over a timescale that is fast compared to the recombination processes associated with the surface-states, more information can be gained before steady-state conditions are re-established. If a surface under inversion can be made to rapidly enter accumulation by means of an external field, the excess surface charges responsible for the inversion conditions will be emitted into the near-surface region of the bulk, where they contribute to the carrier concentration, resulting in an initial rise in conductance. The conductance will reach steady-state conditions with a decay constant dependent upon recombination processes, very similar to what is seen for the light pulse response in the PCD measurements. Unlike the PCD, where the magnitude of the response (parameter A) of equation 3.8) is dependent upon the intensity of the light pulse, the magnitude of the pulsed field response is dependent upon the concentration of excess charge in the inversion layer.

In the case of an n-type sample, inversion conditions would arise from the presence of negatively charged acceptor states, and the positive minority carriers associated with the inversion layer that counters the surface states. At the onset of a positive pulse to the surface, the positive charge of the inversion layer is injected into the bulk. Negative charges enter through the ohmic contacts to counter the injected charge. Negative charges also flow to the surface region to counter the positive field plate, but these are accounted for in the steady-state conductance that is eventually reached. The difference between the peak conductance just after the field pulse and the final steady-state conductance is therefore

$$\delta\sigma = q(\mu_n + \mu_p)\Delta P \tag{3.15}$$

where ΔP is the excess positive charge of the inversion layer, and the mobilities have their usual bulk values.

3.2 Experimental

PCD and surface conductance measurements were performed simultaneously with a setup (depicted in Figure 3.3 on page 71) based off of the experiments of Montgomery and Brown.[6] Each sample was an approximately 22 × 12 mm piece of double-side polished wafer. Prior to any chemical treatments, a 1–2 mm region was sanded at

Figure 3.1: Surface conductance vs surface potential

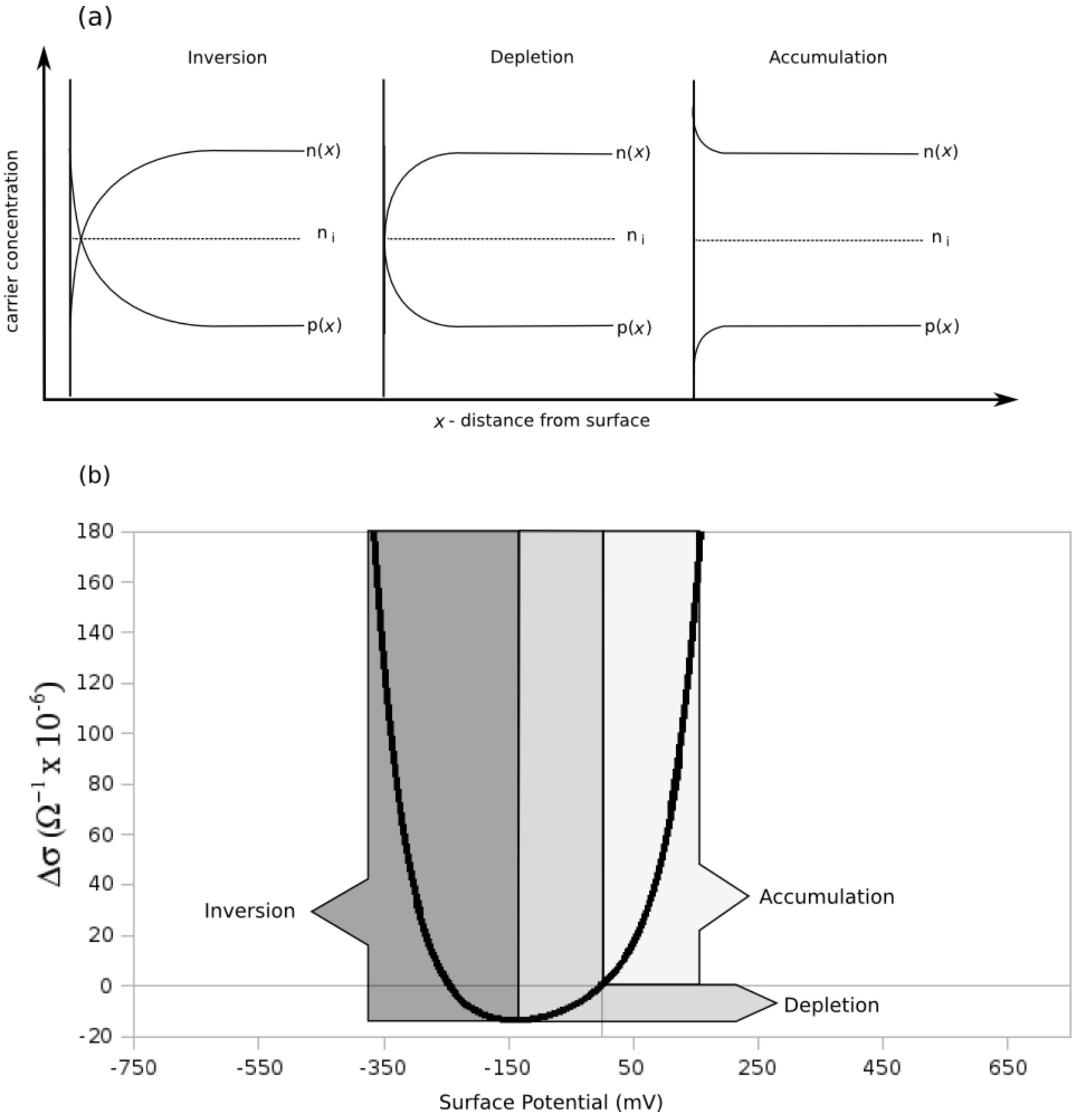

the two shorter edges in order to facilitate ohmic contact formation. After the chemical treatments described in Chapter 2, the ohmic contacts were formed by applying either Ga/In eutectic or Pb/Sn solder.

A gate region was formed on each side of the substrate by clamping the sample between two transparent conductive oxide-coated glass plates. The plates were separated from the Ge surface by a 10–13 micron thick polyvinyl fluoride film (Goodfellow) coated with hydrocarbon oil to exclude air from gaps. The resulting capacitance was approximately 400 pF/cm^2. One end ohmic contact was grounded while the other was connected to a constant-current source. The voltage drop across the sample between the ohmic contacts was continuously monitored with a TDS210 oscilloscope (Tektronix). The gate voltage was supplied by two 2.5 W ±1kV power supplies (Matsusada JB-1N, JB-1P), and controlled by a custom built circuit. The magnitude of the bias was manually adjusted from 0 - ±800 V. The gate bias waveform consisted of 50% duty cycle, 10–20 ms period square wave with pulses of alternating sign.

Photogeneration of carriers for PCD was achieved with a 20–30 ns pulse of 1550 nm light from a laser diode (Laser Components, Inc.), powered by an Electro-Optic Devices ETX-10A laser driver, directed through one of the field plates. The pulse was fired 1–3 ms after the onset of the gate bias. Low-level injection was confirmed from the peak conductance value, which indicated a photogenerated carrier density of $\leq 10^{12}\text{cm}^{-3}$.

For each measured gate voltage, the waveform was signal averaged and stored digitally. The photogenerated transient present in the waveforms were fit to equation 3.8. The voltage at the field-free region was set to zero, and the offset parameter

C was used to determine the change in surface conductance. For each sample, each surface conductance value was recorded, with its corresponding SRV, into a two-column .csv file and converted to surface potential using the Python script in the Appendix. Figure 3.2 is a plot of the correlation calculated with the script and used for the conversion.

3.3 Results

All samples modified through the two-step halogenation which displayed no evidence of oxidation in the XP spectra were found to have a p-type surface (inversion conditions), in agreement with the original ethylation.[8] Surfaces that did display some oxidation were in depletion or accumulation. Hydrogen- and bromine-terminated surfaces were not stable for the conditions or time-scale of the experiment, so they were not measured. Samples that did display oxidation in the XP spectra, including methanethiol-terminated and hydrogermylated samples, showed n-type surfaces (accumulation conditions).

3.3.1 Surface Conductance

Figure 3.12 on page 84 is a plot of the measured surface recombination as a function of surface potential. Samples that displayed very low recombination velocities had no clear maximum. Oxidized samples show low recombination values, but the surface charging is too severe to measure flat-band conditions, so meaningful measurements were not possible. The plotted surface potential values for the oxidized sample were

Figure 3.2: Conductance curves for the Ge (a) and Si (b) substrates used. The solid line is the more heavily doped of the pair.

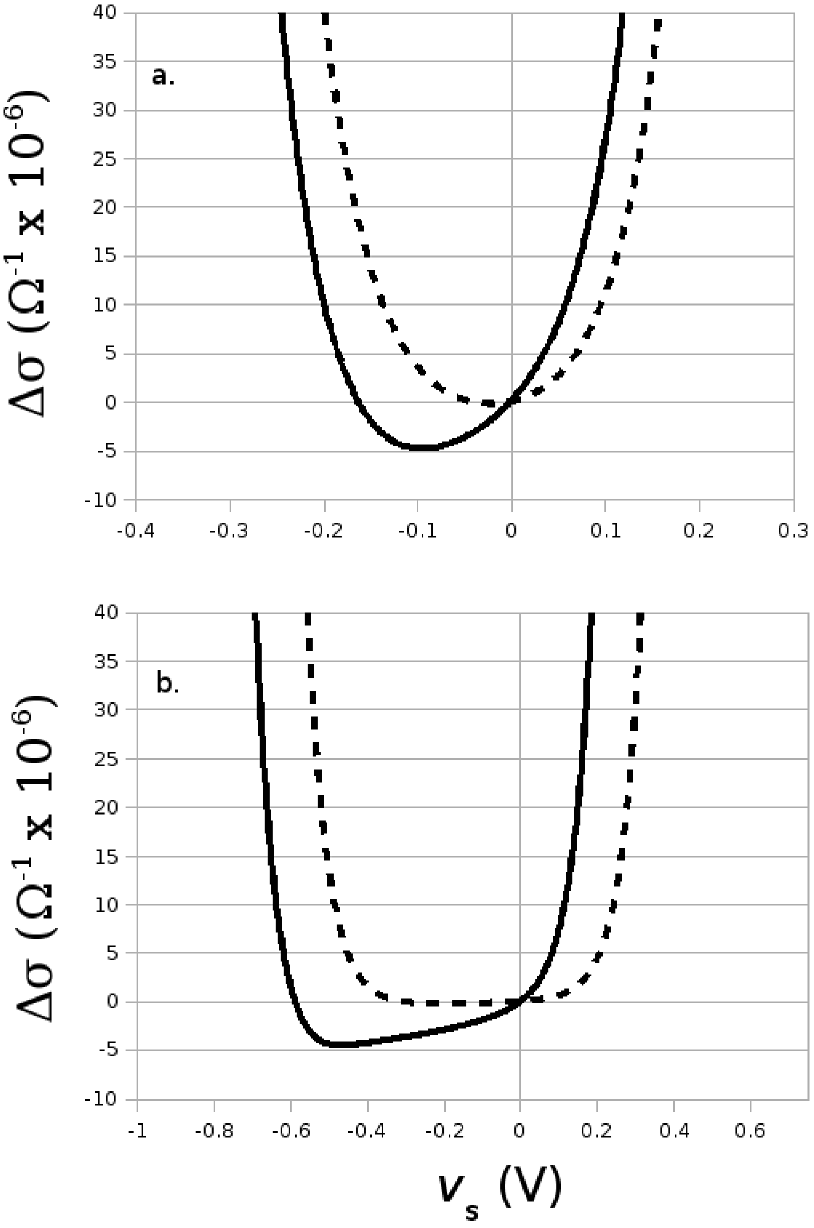

Figure 3.3: Experimental setup

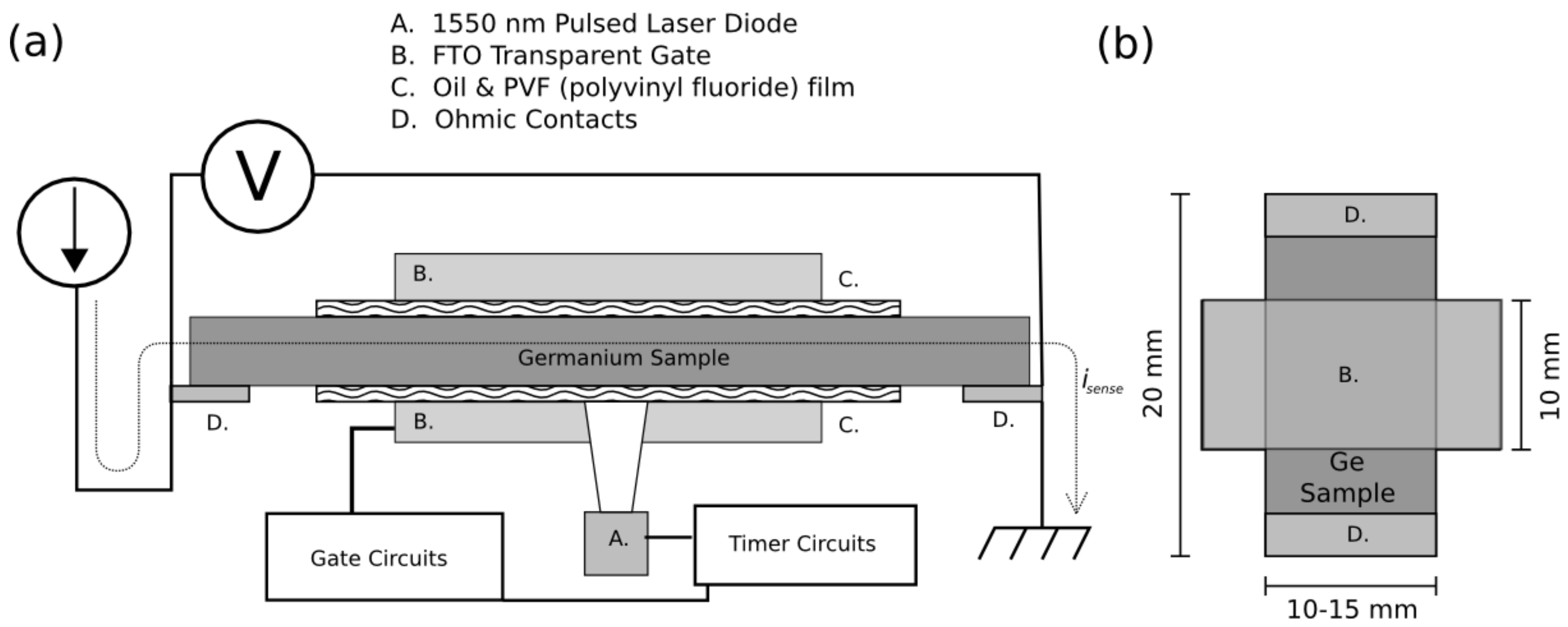

not quantitatively accurate, but serve to illustrate that the oxidized surfaces were under accumulation conditions.

Surface potentials at no applied field and the maximum SRV values of all samples for which the point of minimum conductance and maximum recombination could be reached are collected in Table 3.1. The general trend is that methyl-terminated samples had higher surface charging than the ethyl- and decyl-terminated surfaces, but the surface recombination is lower, even as the surface is brought to flat-band conditions.

3.3.2 Pulsed Fields

Lightly doped n-type methyl- and ethyl-terminated surfaces were under inversion, so the surface charge density could be extracted directly from the transient response to the application of a positive gate bias. Figures 3.4 and 3.5 show the recorded waveforms of the conductance of a methyl-terminated surface in response to a positive and negative gate bias, respectively. The onset of the positive bias in Figure 3.4 coincides with peak 1. The change in conductance from the height of peak 1, to the baseline that follows is dependent upon the excess charge in the inversion layer as given by equation 3.15. Peak 2 is the conductance transient from the optical injection of the laser pulse. The excess charge density was found to be as high as 10^{12} charges per square centimeter for methyl-terminated samples.

The conductance responses of oxidized Ge(111) to a positive and negative gate bias are shown in Figures 3.6 and 3.7, respectively. These waveforms display a different sign in the response to the bias, indicating the surface is not under inversion conditions.

3.3.3 Silicon

CH_3-Si(111) showed similar results to those seen on Ge(111), but it was not possible to span the much larger bandgap by means of the field plate and the point of minimum resistance could not be reached. The experimental configuration was also not well-suited to the high resistance of lightly doped Si, which caused the RC time-constant of the conductance circuit to be of similar magnitude to the time-scales of interest. Qualitative information could still be gained from the sign of the surface conductance response to a gate bias. High resistivity n-type CH_3-Si(111) showed conductance modulations very similar to what is seen in Figures 3.4 through 3.7. Figure 3.8 displays the response of such a surface to a negative gate bias. Due to the RC time-constant, the capacitive spikes at the beginning and end of each gate bias pulse had a noticeably longer duration, but were still useful to confirm that the surface conductance response was of the same sign as that observed in Figure 3.7. Figure 3.9 shows the response of of an native oxide Si(111) surface, from the same wafer, to the same gate bias. The response is opposite that of the methyl-terminated surface and of the same sign as the oxidized Ge(111) surfaces. Moderately doped 70 Ohm-cm n-type Si did not show inversion waveforms. Figures 3.10 and 3.11 show the conductance responses to a negative gate bias of a CH_3-Si(111) and a SiO_x-Si(111), respectively. The capacitive spikes are much narrower because of the lower resistivity of the Si samples. The conductance waveforms do not follow the square wave bias because of relaxation due to surface states associated with carrier recombination or generation, which are in greater number on the oxidized surface and therefore produce a faster relaxation. Despite the relaxation, the signs of the responses can still be seen to be opposite the responses of the higher resistivity Si(111) From Figure 3.2, this would indicate the surface potential of the high-resistivity CH_3-Si(111) is more negative than -200 mV, and that the surface potential of the moderately doped CH_3-Si(111) surface is less negative than -400 mV.

Figure 3.4: Conductance waveform of CH_3-Ge(111) surface in response to positive gate bias

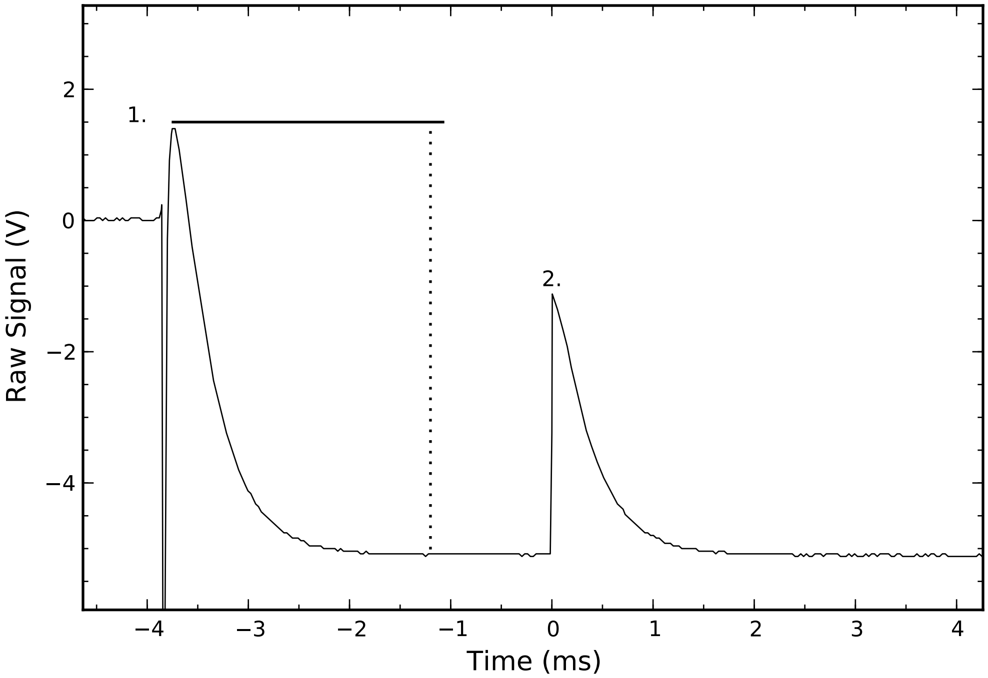

Figure 3.5: Conductance waveform of CH_3-Ge(111) surface in response to negative gate bias

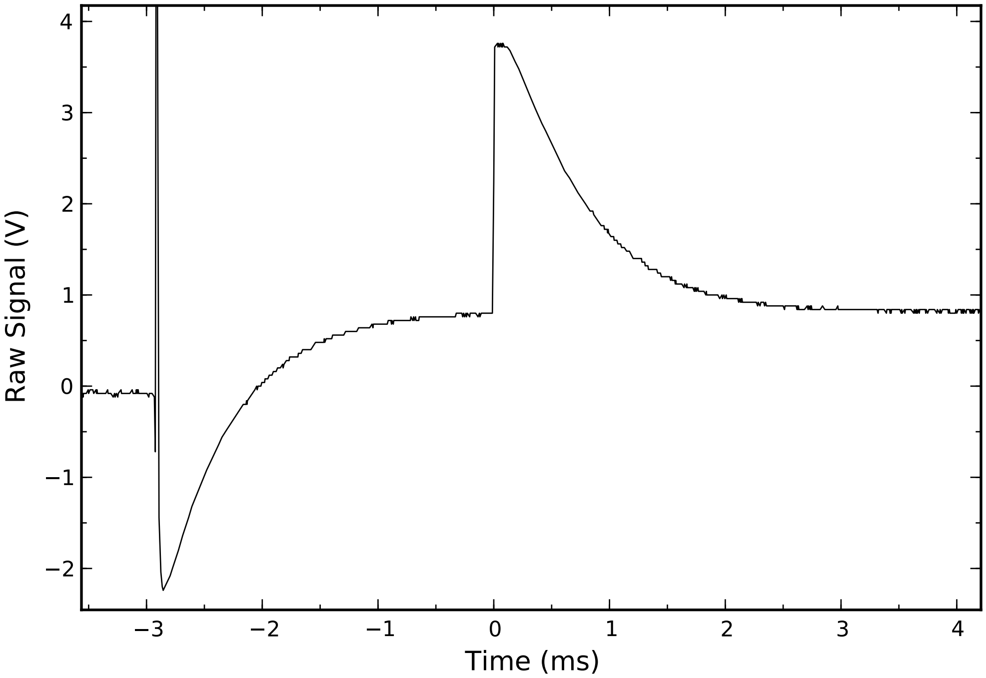

Figure 3.6: Conductance waveform of GeO_x-Ge(111) surface in response to positive gate bias

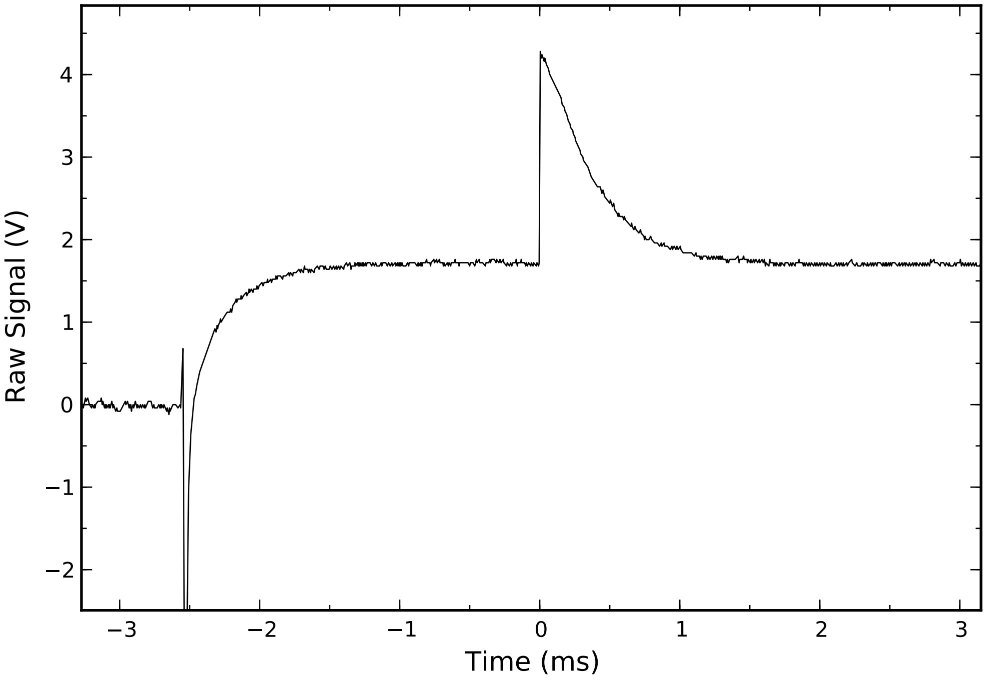

Figure 3.7: Conductance waveform of GeO_x-Ge(111) surface in response to negative gate bias

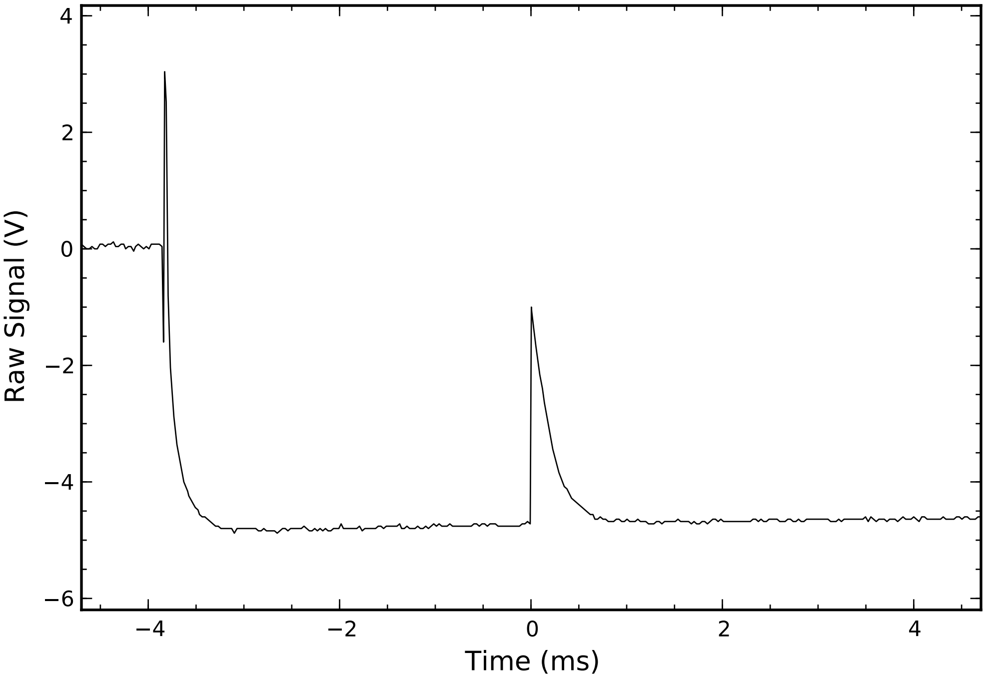

Figure 3.8: Negative gate bias applied to CH_3-Si(111) (N_D=4 × $10^{11}$$cm^{-3}$)

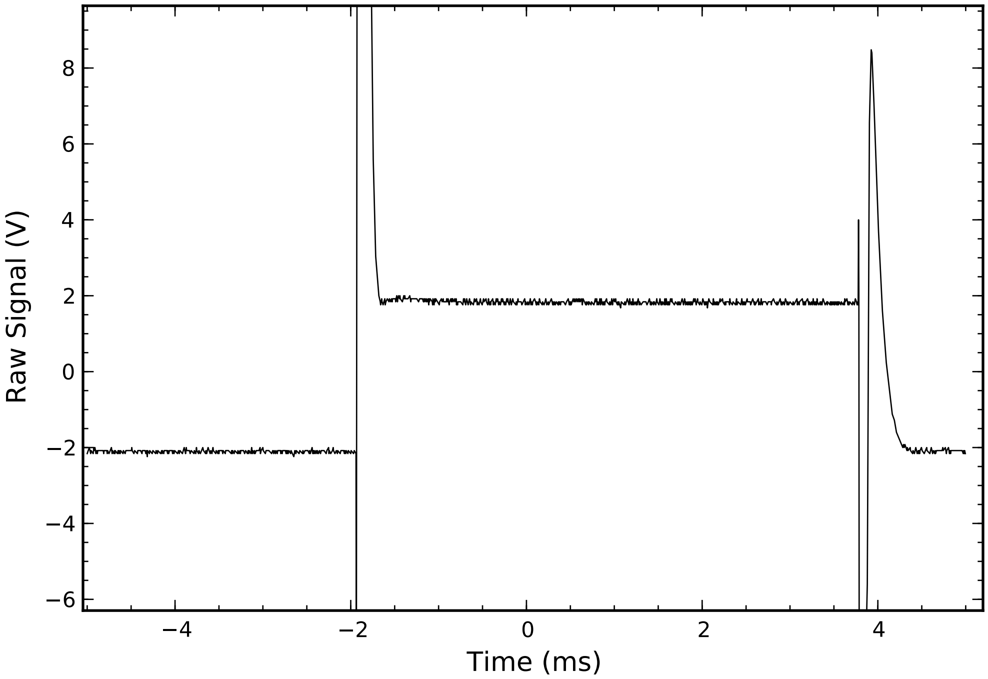

Figure 3.9: Negative gate bias applied to SiO_x-Si(111) (N_D=4×10^{11}cm^{-3})

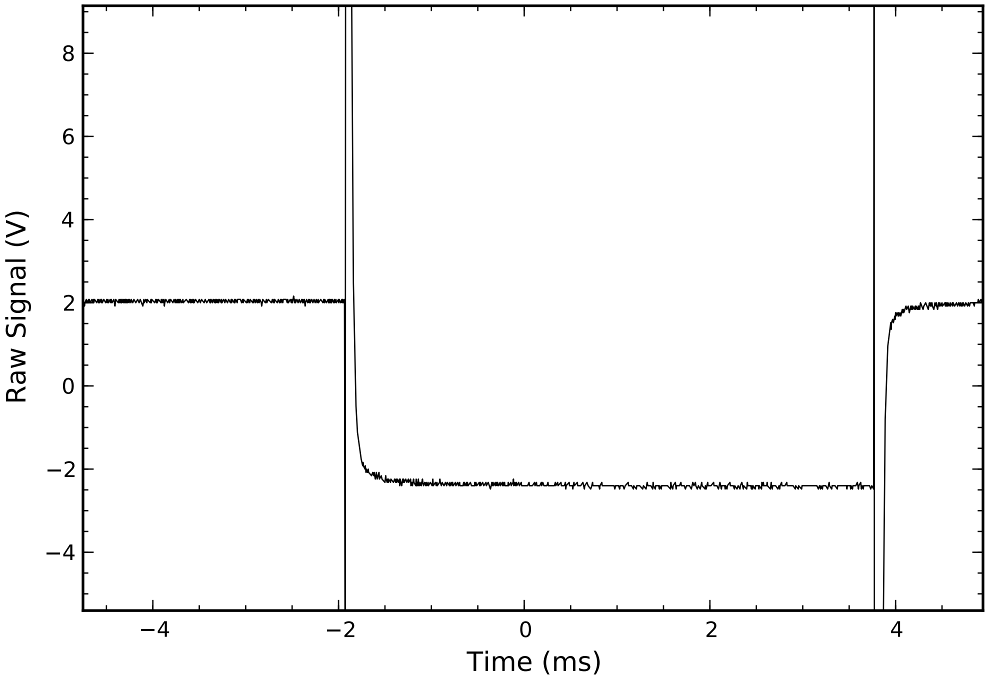

Figure 3.10: Negative gate bias applied to CH_3-Si(111) (N_D=7×10^{13}cm^{-3})

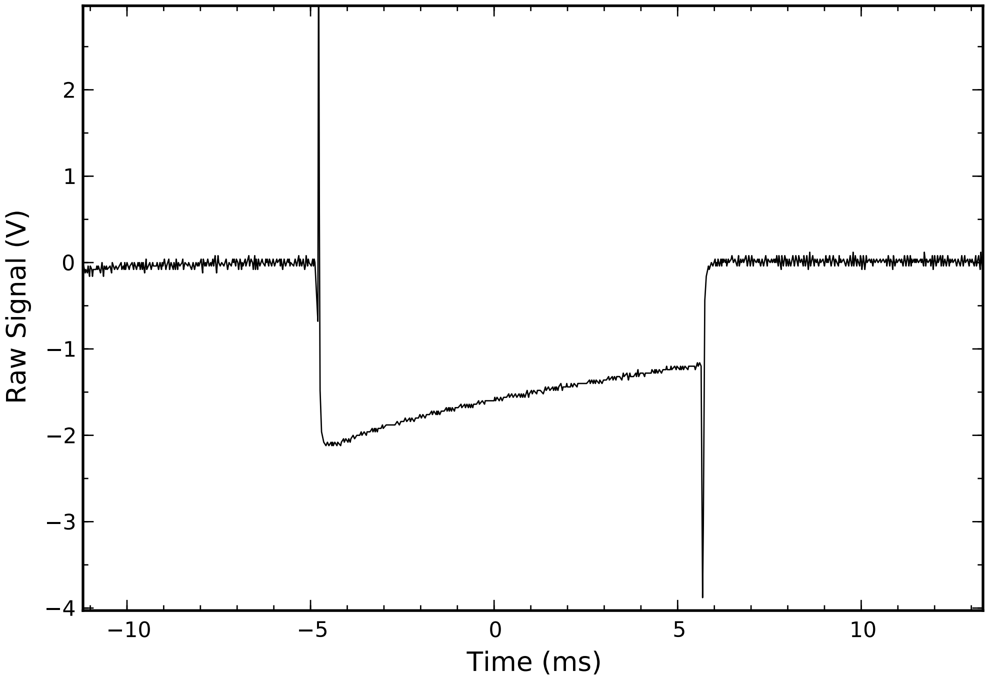

Figure 3.11: Negative gate bias applied to SiO_x-Si(111) (N_D=7×10^{13}cm^{-3})

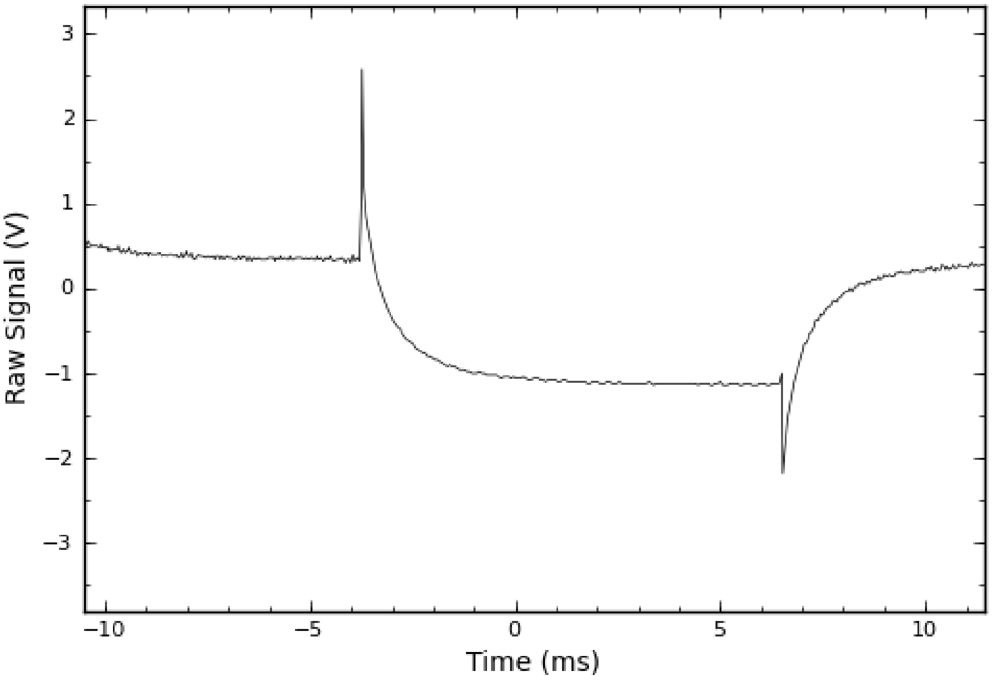

3.4 Discussion

The very low surface recombination measured for methyl- and ethyl-terminated surfaces indicate the halogenation/alkylation method is effective in passivating R-G centers at the surface. The oxidized samples displayed low recombination, but no conclusions can be drawn concerning R-G centers. While the photovoltage generated in high-level injection conditions would have countered the surface potential, the resulting PCD constant would have been a function of both electron and hole lifetimes.[9] If the majority carriers, in this case the electrons, have slower recombination kinetics (a low c_{ns} of equation 3.5) the effective lifetime will be dominated by the slower majority carrier recombination as the surface states are saturated.[10] To keep the measured recombination a function of the sample and not injection level, low-level injection conditions were maintained.

The opposing trends in surface charging and SRV seen in the alkylated surfaces suggest that slight oxidation could be responsible for the less severe band-bending in decyl- and ethyl-terminated surfaces. While relatively recent photoelectron measurements of valence band shifts in oxidizing Ge tend not to support the notion that the oxide is responsible for the positive shift in surface potential for n-type material, it should be noted that such measurements must be performed under UHV conditions.[11–14] It has long been known that water vapor makes an oxidized Ge surface more n-type, and the surface conductance measurements were performed in standard laboratory atmosphere.[6,15] While the sign of the surface potential is consistent with the original ethylation, it is not what would be expected if the methyl groups were

Table 3.1: Equilibrium Surface Potential and Maximum SRV

Sample #	D-1-0	E-1-1	E-1-2	E-1-3	M-1-4	E-2-1	E-2-2	M-2-3
$v_{s,0}$(mV)	-140	-50	-140	-220	-270	-100	-100	-270
SRV_{max} (cm/s)	520	450	210	224	50	230	350	170
Sample #	E-2-4	M-2-5	E-2-6	M-3-1	E-3-2	M-3-3	E-3-4	M-3-5
$v_{s,0}$(mV)	-100	-250	-210	-210	-140	-260	-170	-260
SRV_{max} (cm/s)	480	100	300	140	130	70	150	70

Figure 3.12: Surface recombination vs surface potential

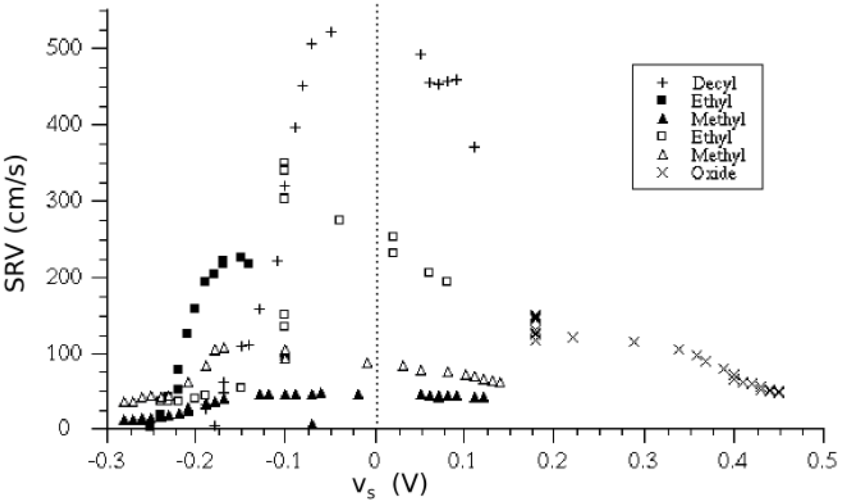

eliminating dangling bonds, based upon theoretical calculations and experimental observations of Ge field effect transistors.[16,17] If the conclusion is that, for methyl-terminated surfaces, the oxide has been eliminated but there still exist dangling bond defects with a density of 10^{12}cm^{-2}, this would imply a deficit in the passivating monolayer on the order of 1%. Such a density is below the detection limit of the available XPS data for these particular surfaces.

A comparison to methyl-terminated silicon is useful because CH_3-Si(111) is a well-studied surface.[18–20] The effective surface passivation by methylation seen in Si(111) has been attributed to the elimination of dangling bonds. Because the molecular geometry for CH_3-Si(111) and CH_3-Ge(111) are so similar, it would be thought that methylation would have a similar effect on dangling bonds of a Ge surface. Conductance experiments performed on CH_3-Si(111) suffered some experimental draw-backs. Intrinsic Si is much more resistive than intrinsic Ge, so time resolution was lost because of the resulting high RC element of the detection circuit. More highly doped material requires stronger fields to span the range of accumulation to inversion conditions. The fields used in this experiment, which were not adequate, were already greater than 200 kV/cm, far exceeding the dielectric strength of the soft hydrocarbon and fluorocarbon spacers necessary to avoid shorting to and damaging the surface. Within the limitations, however, the sign of the conductance response to pulsed fields could still be used to determine which arm of the conductance curve (see Figure 3.2 on page 70) the surface was at. Because the high resistivity material showed inversion conditions, the surface potential had to be more negative than -200 mV. The more highly doped n-type silicon did not show inversion conditions, so the surface potential had to be less negative than -460 mV. This is not in disagreement with photoelectron measurements indicating a negative surface potential of as much as 200 mV.[18,21]

Reports of inversion layers in the chlorinated Si(111) surface raise the question of whether small amounts of halogen atoms are unreacted and causing the negative surface potential.[22] The authors ascribe the observed increase in conductance of Cl-Si(111) relative to H-Si(111) to an inversion layer caused by electron-withdrawing chlorine produced positive holes in the n-type Si. The increased conductance could be caused by an inversion layer, but it could also be caused by an accumulation layer or a surface film. Aside from measuring the decrease in conductance as the chlorine layer degrades in air, the authors did not modify the surface potential, but subsequent UHV STS measurements showed no clear bandgap, which indicated a density of states within the bandgap, which could give rise to an inversion or accumulation layer.[23] The amount of charge in the inversion layer present in the methyl-terminated surface is consistent with 0.1–1% of the Ge(111) surface atoms remaining halogen-terminated. Such a concentration is well below the detection level of the XPS, but is not insignificant. However, the lack of observation of persistent chlorine atoms in similarly prepared methyl-terminated Si(111) samples, for which there is also a shift in surface potential, makes it unlikely that unreacted halogen surface atoms are the cause of the surface charge.[18,20,21,24]

An increase in work function of 1.2-1.5 V was observed for the Cl-Si(111) surface by Lopinski et al., but work function-dependent measurement techniques would be sensitive to the surface dipole, and the authors did not make the distinction.[18,22,25,26] The surface conductance measurements performed here should not be sensitive to surface dipoles because the current used to measure the surface conditions flows parallel to the surface, rather than crossing the interface. Surface fields are applied across the interface, but the magnitude of the bias voltage is never used directly in calculating the surface potential. The band positions would be affected if the semiconductor was in thermal equilibrium with the field-plate conductor, however the 20 micron thick insulator makes the semiconductor insensitive to the conductor work function.

3.5 Conclusion

Alkylated surfaces prepared through the two-step halogenation/alkylation display surface electronics that are quite distinct from the oxidized starting material. Methyl-terminated Ge(111) surfaces show very little surface recombination, but have a surface potential approaching -300 mV. Bulkier alkyl groups are comparable, but show slightly higher SRV and lower surface potential. Oxidized surfaces and all other surfaces, including hydrogermylated surfaces, showed a positive surface potential, but the surface charging was too severe to determine a definite value. The negative surface potential of the methyl-terminated surface is consistent with elimination of states associated with a hydrated oxide, but could be indicative of surface-states located near the valence band.

Silicon surfaces show a similar degree of band-bending, consistent with earlier photoelectron measurements. This is significant because it means that the two-step alkylation is successful for Ge(111) as it is for Si(111), despite the less atomically smooth surface and the unstable H-Ge(111) precursor surface.

Bibliography

[1] Pierret, R. *Advanced Semiconductor Fundamentals*; Addison-Wesley Publishing Co.: Reading, Mass., 1989; Vol. 6.

[2] Sze, S. *Physics of Semiconductor Devices*, 2nd ed.; John Wiley & Sons: New York, 1981.

[3] Maldonado, S.; Plass, K.; Knapp, D.; Lewis, N. *J. Phys. Chem. C* **2007**, *111*, 17690–17699.

[4] Choi, J.; Ahmed, S.; Dimitrova, T.; Chen, J.; Schroder, D. *IEEE Trans. Electron Dev.* **2004**, *51*, 1380–1384.

[5] Sharp, I.; Schoell, S.; Hoeb, M.; Brandt, M.; Stutzmann, M. *Appl. Phys. Lett.* **2008**, *92*, 223306.

[6] Montgomery, H.; Brown, W. *Phys. Rev.* **1956**, *103*, 865–870.

[7] Many, A.; Goldstein, Y.; Grover, N. *Semiconductor Surfaces*; North-Holland Publishing Co.: Amsterdam, 1965.

[8] Gerlich, D.; Cullen, G.; Amick, J. *J. Electrochem. Soc.* **1962**, *109*, 133–138.

[9] Gstrein, F.; Michalak, D.; Royea, W.; Lewis, N. *J. Phys. Chem. B* **2002**, *106*, 2950–2961.

[10] Gaubas, E.; Vanhellemont, J. *Appl. Phys. Lett.* **2006**, *89*, 142106.

[11] Yang, M.; Wu, R.; Q., C.; W.S., D.; Feng, Y.; Chai, J.; Pan, J.; Wang, S. *Appl. Phys. Lett.* **2009**, *94*, 142903.

[12] Hovis, J.; Hamers, R.; Greenlief, C. *Surf. Sci.* **1999**, *440*, L815–L819.

[13] Perego, M.; Scarel, G.; Fanciulli, M.; Fedushkin, I.; Skatova, A. A. *Appl. Phys. Lett.* **2007**, *90*, 162115.

[14] Tabet, N.; Faiz, M.; Hamdan, N.; Hussain, Z. *Surf. Sci.* **2003**, *523*, 68–72.

[15] Kingston, R. *Phys. Rev.* **1955**, *98*, 1766–1775.

[16] Tsipas, P.; Dimoulas, A. *Appl. Phys. Lett.* **2009**, *94*, 012114.

[17] Broqvist, P.; Alkauska, A.; Pasquarello, A. *Phys. Rev. B* **2008**, *78*, 075203.

[18] Hunger, R.; Fritsche, R.; Jaeckel, B.; Jaegermann, W.; Webb, L.; Lewis, N. *Phys. Rev. B* **2005**, *72*, 045317.

[19] Yu, H.; Webb, L.; Ries, R.; Solares, S.; Goddard, W.; Heath, J.; Lewis, N. *J. Phys. Chem. B* **2005**, *109*, 671–674.

[20] Rivillion, S.; Chabal, Y. *J. Phys. IV* **2006**, *132*, 195–198.

[21] Jaeckel, B.; Hunger, R.; Webb, L.; Jaegermann, W.; Lewis, N. *J. Phys. Chem. C* **2007**, *111*, 18204–18213.

[22] Lopinski, G.; Eves, B.; Hul'ko, O.; Mark, C.; Patitsas, N.; Boukherroub, R.; Ward, T. *Phys. Rev. B* **2005**, *71*, 125308.

[23] Cao, P.; Yu, H.; Heath, J. *J. Phys. Chem. B* **2006**, *110*, 2006.

[24] Webb, L.; Rivillon, S.; Michalak, D.; Chabal, Y.; Lewis, N. *J. Phys. Chem. B* **2006**, *110*, 7349–7356.

[25] Bruening, M.; Moons, E.; Yaron-Marcovich, D.; Cahen, D.; Libman, J.; Shanzer, A. *J. Am. Chem. Soc.* **1994**, *116*, 2972–2977.

[26] Maldonado, S.; Lewis, N. *J. Electrochem. Soc.* **2009**, *156*, H123–H128.

The following chapter contains material adapted in part, with permission, from:

Journal of Physical Chemistry C, 114 (28) 12300–12307, Jun 28 2010

`http://pubs.acs.org/articlesonrequest/AOR-2zUgS72Z5YFJiekWnC5S`

Chapter 4

Electrical Measurements II: Mercury Contacts

4.1 Introduction

This chapter describes the electrical characteristics of Ge(111) electrodes in contact with mercury metal, forming a Schottky diode. The barrier height is determined from both the current-voltage behavior and the differential capacitance measurements.

4.1.1 Background

After contact between a metal and semiconductor is established, the Fermi-levels of the two phases will be level at thermal equilibrium. For the case of an ideal n-type semiconductor in contact with a higher work function metal, the difference in potential between the metal work function ($q\phi_m$) and the semiconductor Fermi-level ($\mathrm{E_F}= q(\chi + V_n)$) is dropped across the space-charge region. The energy barrier to electron injection from the metal into the semiconductor conduction band is solely determined by the metal work-function and the semiconductor electron affinity.

$$q\phi_{Bn} = q\left(\phi_M - \chi\right) \tag{4.1}$$

Thermionic emission theory relates the barrier height to the diode current-voltage (J-V) behavior as

$$J_n = J_{ST}\left[\exp\left(\frac{qV}{kT}\right) - 1\right] \tag{4.2}$$

$$J_{ST} = A^{*}T^{2}\exp\left(\frac{-q\phi_{Bn}}{kT}\right) \tag{4.3}$$

by considering the net carrier flux as the sum of the flow from the semiconductor to the metal and from the metal to the semiconductor. A^{*} is the Richardson constant. The first term within the square bracket of equation 4.2 represents the current flowing from the semiconductor to the metal, which is governed by the concentration of electrons with enough energy to surmount the potential barrier of the space-charge region and cross the interface. Under forward bias, the concentration of such electrons increases. The second term of the square bracket represents the barrier to current flow in the opposite direction, which is insensitive to the applied bias. That reverse current is equal in magnitude to the forward current at zero-bias, when the net flow is zero. As can be seen from equation 4.3, the saturation current is governed by the barrier height, a function of the specific materials chosen.

Real Schottky contacts deviate from this behavior because of Fermi level pinning and surface dipoles. A sufficiently large density of surface-states can make the barrier height insensitive to the metal work function, as the potential difference of the two phases is accommodated by the surface-states rather than the space-charge region. Surface dipoles, approximated by a perfect double-layer, introduce a discontinuity in potential, altering the effective electron affinity by an amount $\delta\chi = \sigma M/\varepsilon_0$, where σ is the surface density of the polar molecules that make up the layer, and M is their dipole moment.

4.1.2 Barrier Height Determination

The barrier height can be determined from equations 4.2 and 4.3. The Richardson constant and Schottky barrier lowering are voltage dependent, but can be incorporated into an ideality factor n, so that

$$J \sim \exp\left(-\frac{qV}{nkT}\right) \tag{4.4}$$

and n should be close to 1. The saturation current can then be found by extrapolating to zero bias, and the barrier height is found by rearranging equation 4.3 to

$$\phi_{Bn} = \frac{kT}{q}\ln\left(\frac{A^*T^2}{J_{ST}}\right) \tag{4.5}$$

Fortunately, the barrier height is not very sensitive to the precise value of the A^*, which may not be known.

The flat-band potential, and thus the barrier height, can be determined from the capacitance-voltage behavior. Assuming a uniform ionized dopant density up to the end of the depletion region, the charge Q per unit area A associated with the depletion width W (defined in Chapter 1) can be written as

$$\frac{Q}{A} = qN_DW = \sqrt{2q\varepsilon\varepsilon_0 N_D\left(V_s - \frac{kT}{q}\right)} \tag{4.6}$$

where V_s is the surface potential, the difference between the band-edge positions in the bulk and at the surface. Differentiating the charge with respect to the surface potential yields

$$\frac{1}{A}\frac{\delta Q}{\delta V_s} = \frac{C}{A} = \sqrt{\frac{q\varepsilon\varepsilon_0 N_D}{2\left(V_s - \frac{kT}{q}\right)}} \tag{4.7}$$

The capacitance measured is the ratio of the change in charge at the surface to the change in voltage applied across the semiconductor, also called the differential capacitance. This is physically realized by modulating the surface potential with a small AC voltage applied in addition to the DC bias, V. Rearrangement of equation 4.7 and separation of V_s into its components V_{bi}, the built-in voltage, and V, the DC bias, gives[1]

$$\left(\frac{C_{sc}}{A}\right)^{-2} = \left(\frac{2\left(-V + V_{bi} + \frac{kT}{q}\right)}{q\varepsilon\varepsilon_0 N_D}\right) \tag{4.8}$$

V_{bi} is determined by plotting C^{-2}vs V and extrapolating to the voltage intercept, where $V = V_{bi} + \frac{kT}{q}$. Once V_{bi} is known, Φ is known because $\Phi = V_{bi} + V_n$ and V_n is determined from N_D.

The above treatment does not account for surface-states. The measured differential capacitance is the sum of the space charge region capacitance, C_{SC}, and the surface-state capacitance, C_{SS}. The occupation statistics of the surface-states, and hence C_{SS}, are dependent upon the surface potential. C_{SS} is also dependent upon the capture and emission kinetics of the surface states. The change in observed capacitance due to carrier capture and emission by defect states can be useful for material characterization by techniques such as deep-level transient spectroscopy.[2] However, this will lead to non-linear deviations from the desired $C^{-2} - V$ relationship for the frequencies and surface potentials in which the surface-states are active.[3–5]

4.1.3 Mercury Soft Contacts

Mercury contacts provide a useful test system for probing the effects of surface modification upon diode formation. The high surface tension of the metal allows the contact to avoid being dominated by physically recessed defects such as pinholes. Importantly, the contact is formed at room temperature, so unwanted chemical reactions that often occur during contact formation are avoided.[6–8]

Mercury has been especially useful for testing silicon surfaces because the 4.49 eV work function would ideally put contacted Si of either dopant type into rectifying depletion conditions. Ge has a very similar electron affinity to silicon, so n-type Ge would be expected to form rectifying Hg contacts, but the valence band position is very close to the Hg work function and p-Ge would not be expected to form clearly rectifying contacts.

Synchrotron experiments performed on CH_3-Si(111) and H-Si(111) show the effective electron affinity (χ_{eff}) deviates significantly from the bulk affinity of 4.05 eV to values of 3.67 eV and 4.17 eV, respectively.[9] These shifts were confirmed with Hg/Si contacts, where n-type CH_3-Si(111) and p-type H-Si(111) were strongly rectifying but the n-type H-Si(111) and p-type CH_3-Si(111) were not.[8] Hg/Ge contacts have not been studied as thoroughly, but experiments conducted on Ge electrodes have demonstrated that alkane modified surfaces can allow rectifying contacts to be formed on n-type and intrinsic substrates.[10] The research presented here examines Hg contacts on CH_3-, C_2H_5-, and $C_{10}H_{21}$-Ge(111) surfaces. Unlike the field effect experiments of the previous chapter, the semiconductor surface is in thermal equilibrium with a conducting phase, so the surface energetics are affected by the surface dipole.

4.2 Experimental

Single-side polished samples with an area of approximately 1 cm^2 were alkylated as described in Chapter 2. Ga/In eutectic was spread across the rough surface to form an ohmic contact. The sample was placed rough side down on a copper plate and a Teflon tube was lowered to press an o-ring against the polished surface. Electronic grade mercury (Alfa Aesar) was poured into the Teflon barrel to contact the area of the sample surface within the o-ring. A platinum wire was immersed into the top of the mercury column to allow electrical connection. Connections were made to a 1286 Solartron Potentiostat and Schlumberger SI 1260 Frequency Response Analyzer in a two-electrode configuration with the copper plate as the working electrode and the platinum wire as the counter electrode. The area of the mercury contact was verified by contacting the mercury column to a gold-coated glass slide and measuring

Figure 4.1: Equivalent circuit

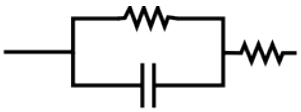

the resulting hole in the gold layer.

$I-V$ curves were measured in the range -0.4 to 0.6 V, or up to 200 mA. Impedance analysis was performed under reverse bias conditions (0–0.6 V) with 10 mV AC modulation. The AC frequency was varied from 10^2–10^6 Hz. Curve fitting of the Bode and Nyquist plots to the model circuit in Figure 4.1 was accomplished with the Z-plot package.

4.3 Results

Results for methyl-, ethyl-, and decyl-terminated surfaces of on substrates of different dopant density (denoted **I-V**) are collected in Table 4.1. Wafer **I** was undoped, wafers **II-V** were antimony doped. Junctions that could not be fitted to the simple cell in Figure 4.1, for example requiring replacement of the parallel capacitance with a constant phase element, are not included, with the exception of those from wafer **I** because no undoped samples were obtained that showed the desired behavior. P-type samples, oxidized samples, and samples prepared by thermal hydrogermylation with 1-decene did not show rectification necessary to calculate a barrier height. Figure 4.2 shows J-V curves of three Hg/Ge(111) Schottky junctions. The solid line is from a $C_{10}H_{21}$-Ge(111) surface derived from modification of an n-type substrate with decylmagnesium bromide. The dot-dashed curve is from a CH_3-Ge(111) surface, derived from the modification of an undoped substrate (wafer **I**) with methylmagnesium bromide. The dashed curve is of $C_{10}H_{21}$-Ge(111) surface derived from the thermal hydrogermylation reaction with H-Ge(111). The dashed curve showed very little rectification, so no differential capacitance date could be collected.

The sample represented by the solid line of Figure 4.2 showed a greater degree of rectification, and more ideal behavior, as displayed in Figures 4.3 and 4.4. The impedance increased linearly with a slope of 1, over a frequency range of almost two decades, and the phase angle of the AC current approached 90°, indicating the parallel capacitance of the space-charge region dominated the system impedance over those frequencies. The differential capacitance values obtained by fitting the frequency response data to the circuit in Figure 4.1 were used to construct the Mott-Schottky plots in Figure 4.5. The CH_3-Ge(111) and $C_{10}H_{21}$-Ge(111) samples were from the same wafer and ideally would have had the same slope. Such variations, possibly due to differences in contact area, are reflected in the dopant density values in Table 4.1.

The undoped samples, represented by the center curve of Figure 4.2, displayed rectification, but as can be seen from Figures 4.6, 4.7, and 4.8, a single capacitance was not the dominant element over any frequency range, so the equivalent circuit was not a useful model and a straightforward Mott-Schottky analysis was not possible.

Table 4.1: Junction Properties of Hg/Ge(111)

	$C^{-2}-V$ measurements		$J-V$ measurements	
sample type	$N_{\mathrm{D}}(\mathrm{cm}^{-3})^{a}$	$\Phi_{\mathrm{Bn},C^{-2}-V}(\mathrm{V})$	quality factor n	$\Phi_{\mathrm{Bn},J-V}(\mathrm{V})$
CH_3-Ge **I**	N/A[b]	N/A[b]	2.0 ± 0.2	0.53 ± 0.05
$C_{10}H_{21}$-Ge **I**	N/A[b]	N/A[b]	2.15 ± 0.08	0.52 ± 0.01
CH_3-Ge **II**	$1.3 \pm 0.2 \times 10^{15}$	0.44 ± 0.12	1.6 ± 0.2	0.55 ± 0.05
C_2H_5-Ge **II**	$3.6 \pm 0.4 \times 10^{14}$	0.67 ± 0.07	1.6 ± 0.2	0.55 ± 0.05
$C_{10}H_{21}$-Ge **II**	$3.7 \pm 0.4 \times 10^{14}$	0.56 ± 0.06	1.68 ± 0.2	0.57 ± 0.05
CH_3-Ge **III**	$7.9 \pm 0.3 \times 10^{16}$	0.43 ± 0.03	1.45 ± 0.28	0.65 ± 0.03
C_2H_5-Ge **III**	$7.9 \pm 1 \times 10^{16}$	0.61 ± 0.09	1.07 ± 0.02	0.67 ± 0.02
$C_{10}H_{21}$-Ge **III**	$4.6 \pm 0.4 \times 10^{16}$	0.63 ± 0.05	1.21 ± 0.04	0.61 ± 0.01
CH_3-Ge **IV**	$6.7 \pm 0.6 \times 10^{15}$	0.52 ± 0.07	1.34 ± 0.11	0.60 ± 0.03
$C_{10}H_{21}$-Ge **IV**	$4.2 \pm 0.5 \times 10^{15}$	0.61 ± 0.04	1.15 ± 0.05	0.69 ± 0.01
CH_3-Ge **V**	$1.1 \pm 0.4 \times 10^{17}$	0.47 ± 0.1	1.6 ± 0.2	0.65 ± 0.05
$C_{10}H_{21}$-Ge **V**	$0.9 \pm 0.4 \times 10^{17}$	0.8 ± 0.2	1.4 ± 0.3	0.63 ± 0.05

a Donor density as determined by the slope. *b* Not available, data could not be fit to equivalent circuit model in Figure 4.1.

Figure 4.2: Representative *J*-*V* curves of alkylated Ge(111)/Hg Schottky contacts. Solid line is for n-type Ge(111) surface derived from decylmagnesium bromide, dashed line is undoped Ge(111) surface derived from methylmagnesium bromide, dotted line is from n-type Ge(111) derived from 1-decene.

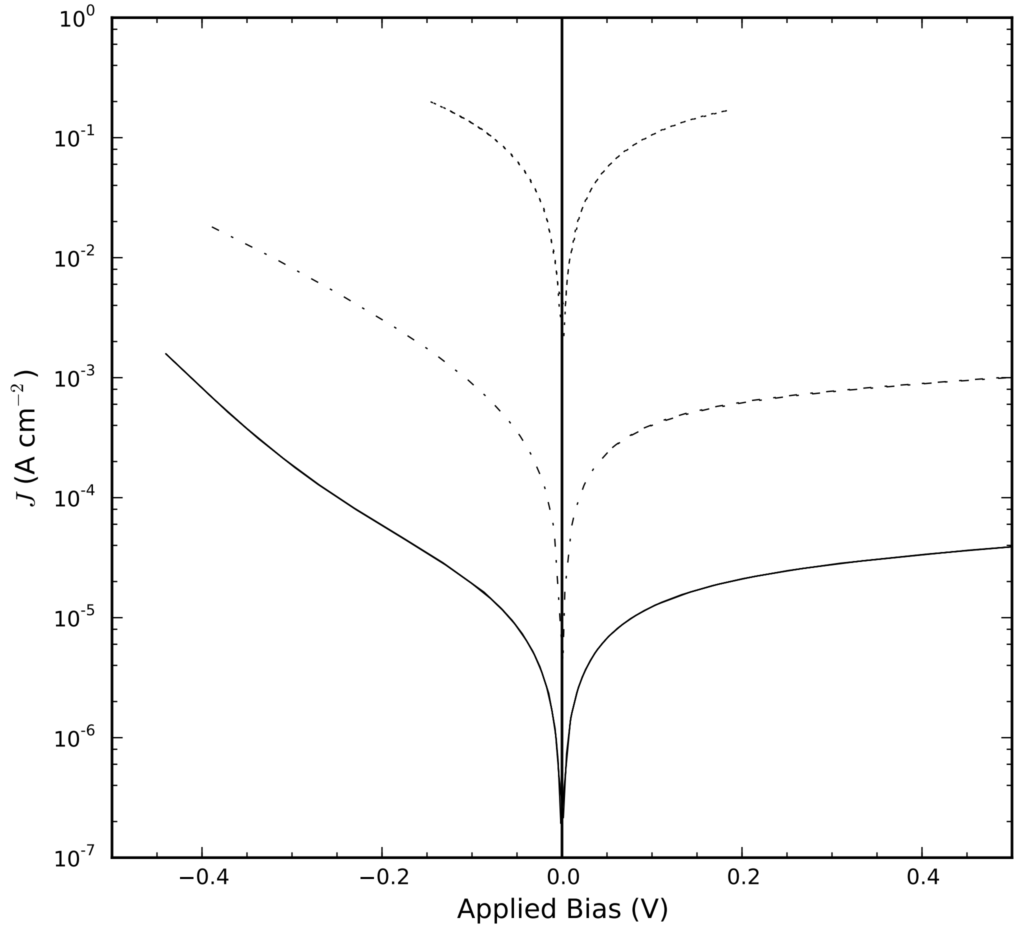

Figure 4.3: Hg/$C_{10}H_{21}$-Ge(111) junction (wafer **III**)

(a)

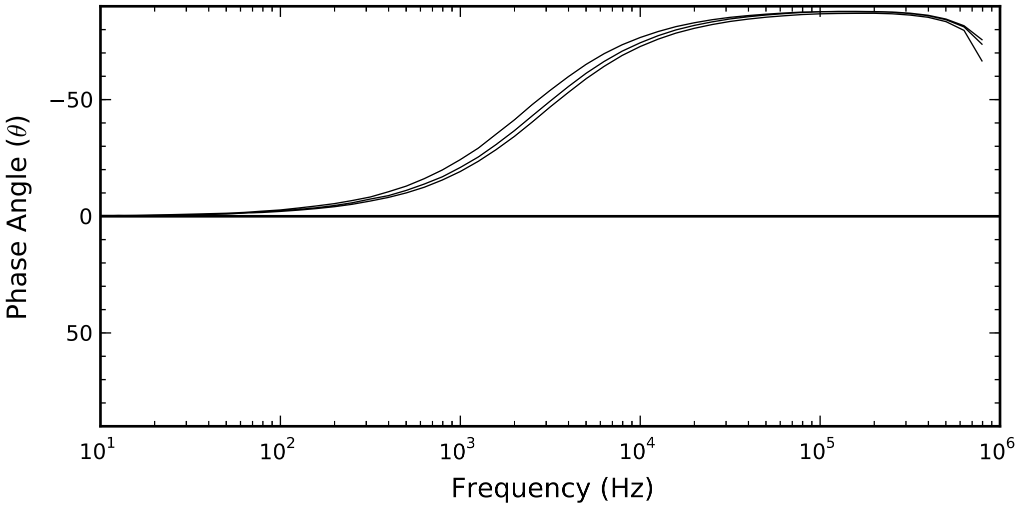

(b)

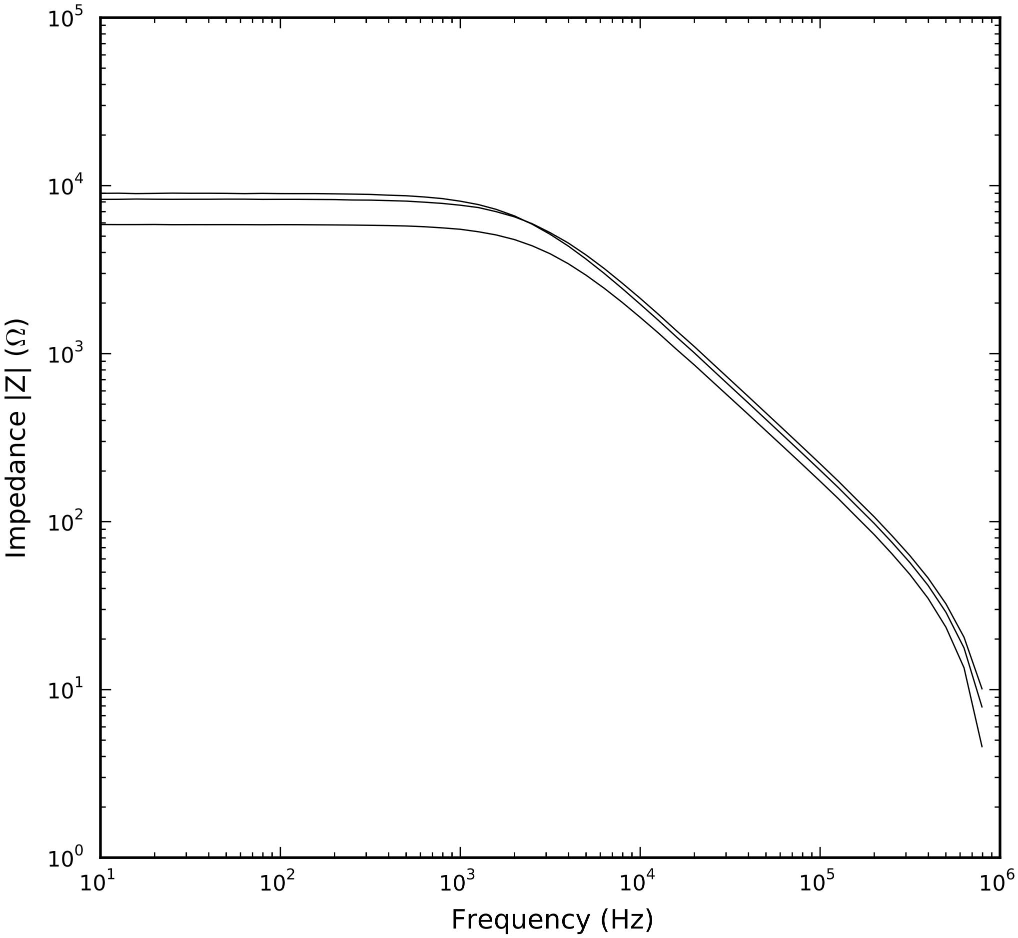

Figure 4.4: Hg/CH$_3$-Ge(111) junction (wafer **III**)

(a)

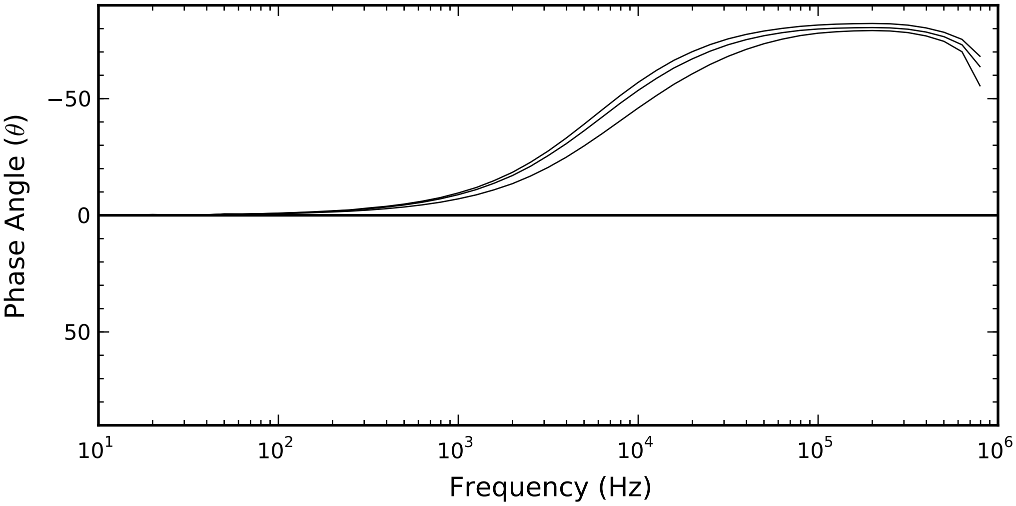

(b)

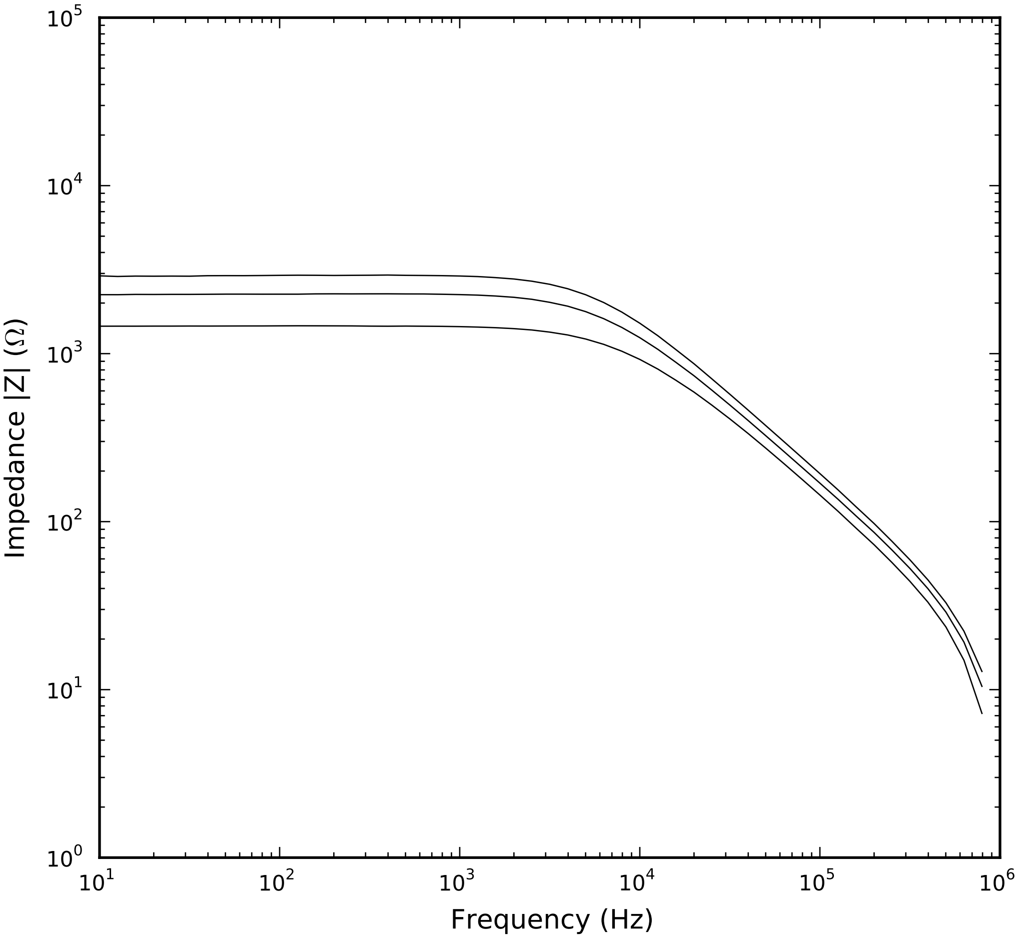

Figure 4.5: Mott-Schottky plots for Hg/CH_3- and $C_{10}H_{21}$-Ge(111) junction (wafer **III**)

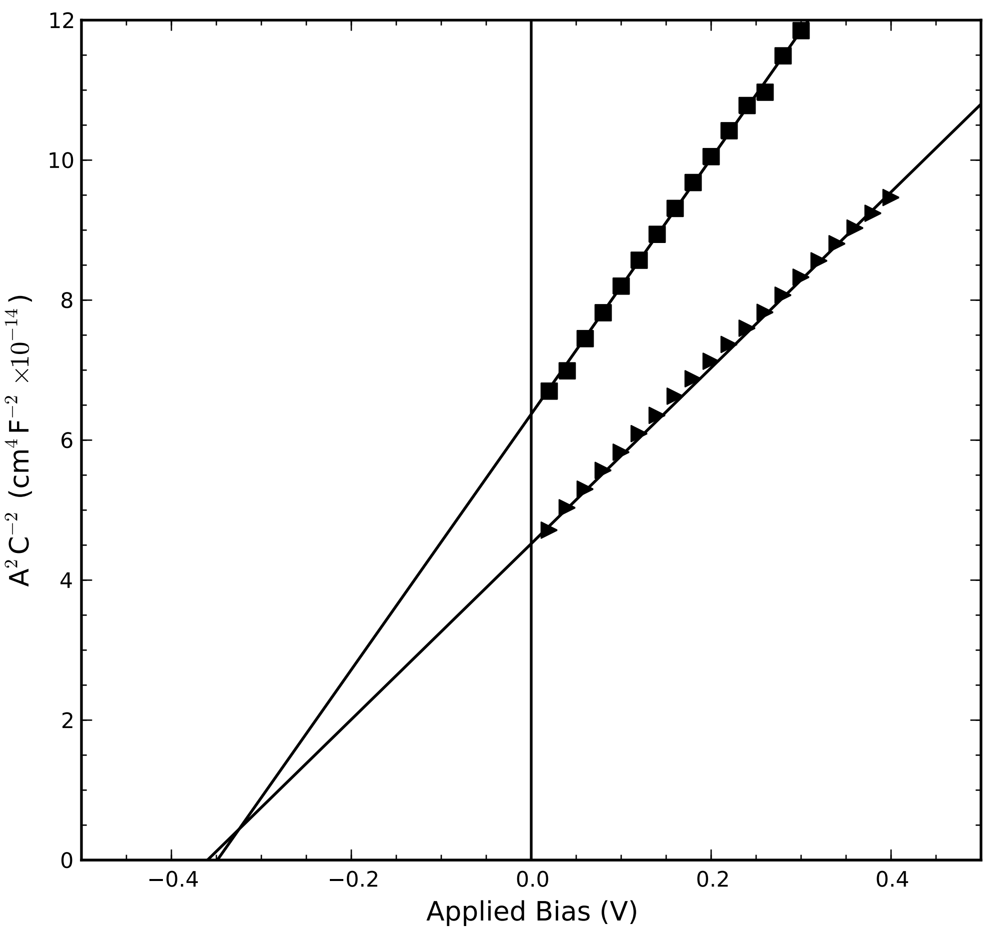

Figure 4.6: Hg/$C_{10}H_{21}$-Ge(111) junctions (wafer **I**)

(a)

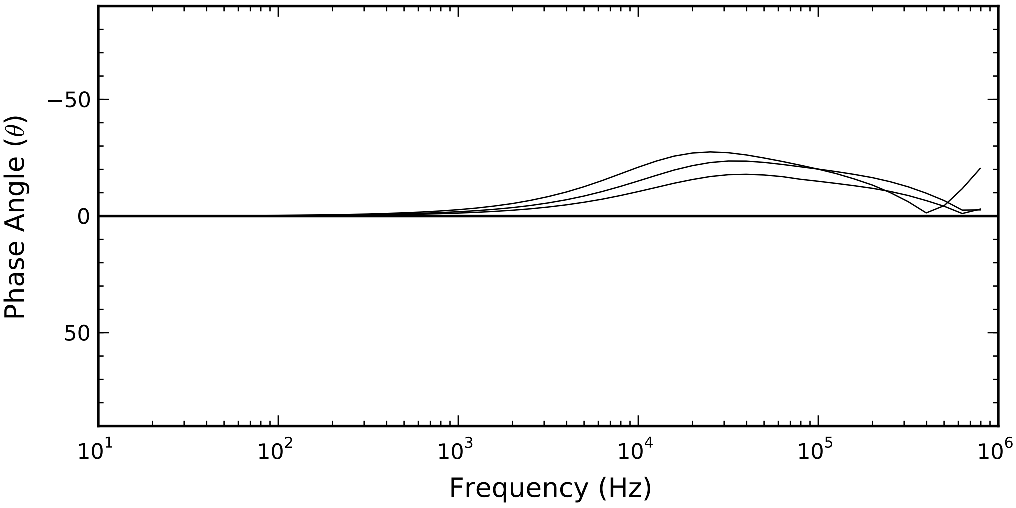

(b)

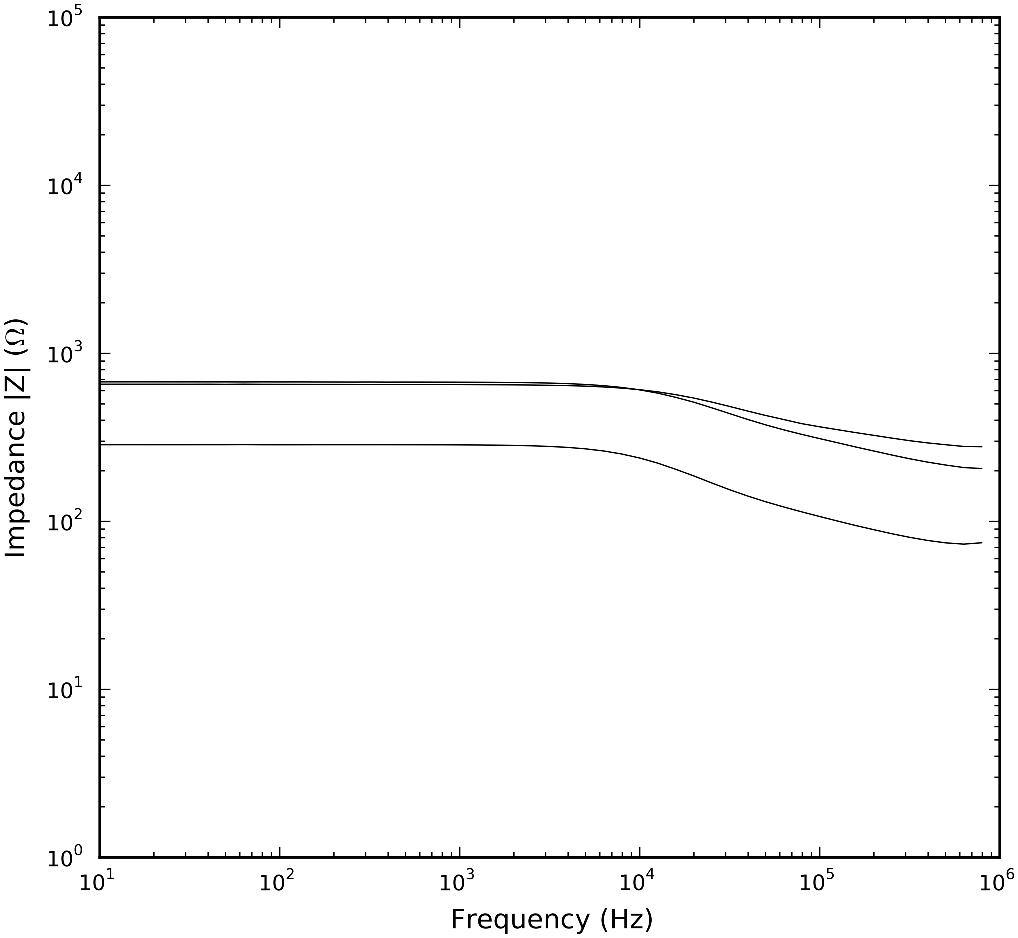

Figure 4.7: Hg/CH_3-Ge(111) junctions (wafer **I**)

(a)

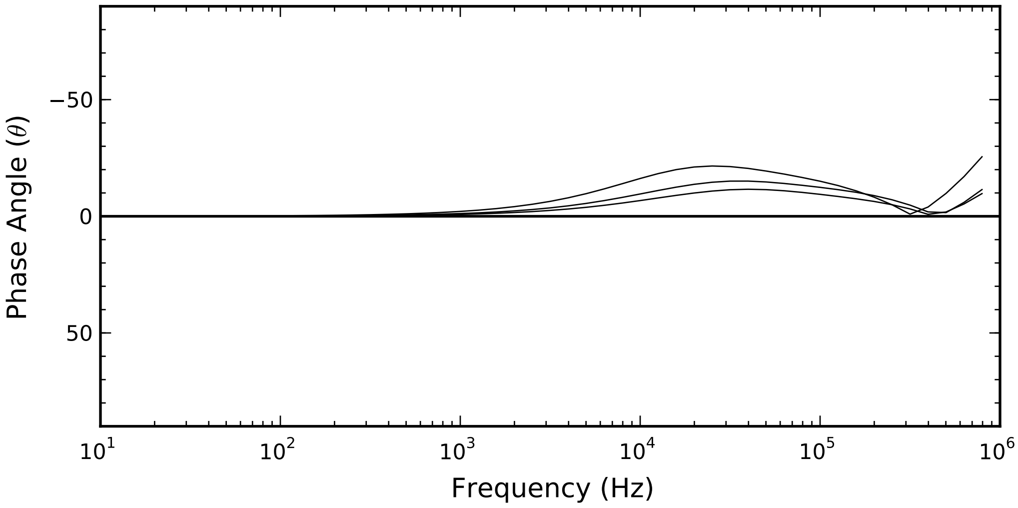

(b)

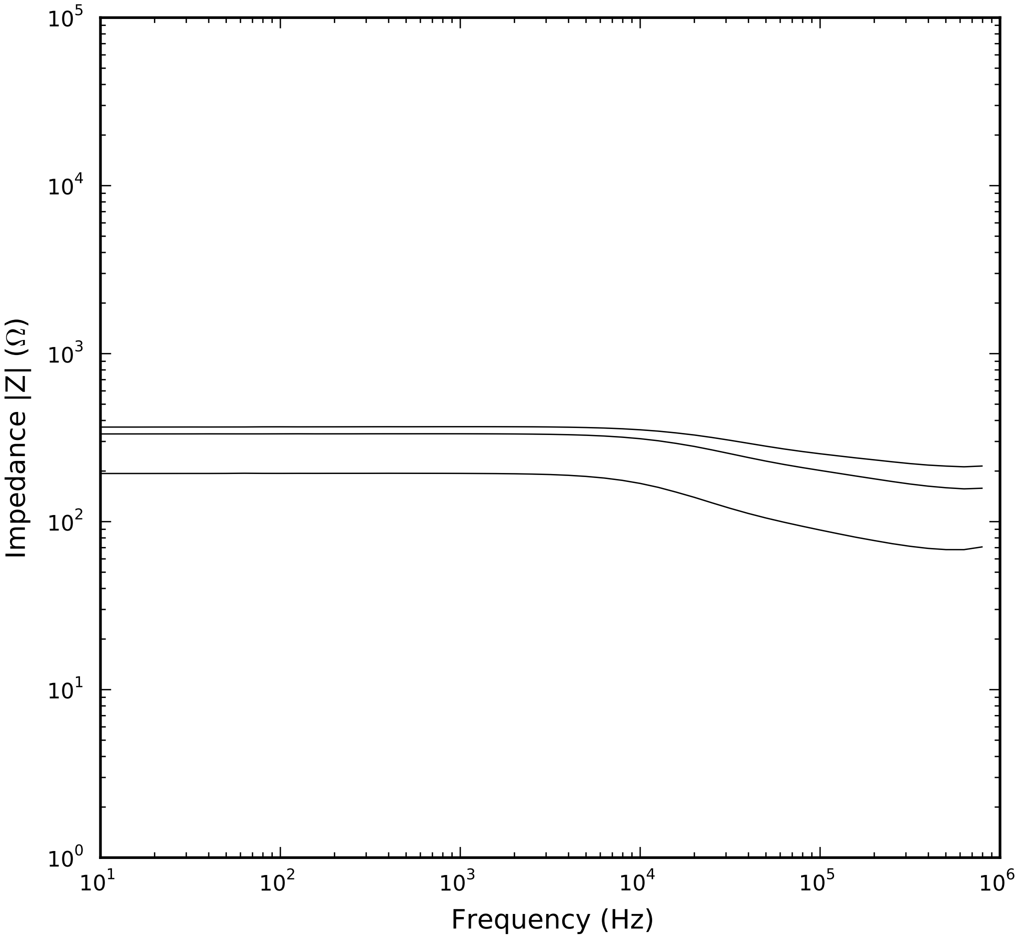

Figure 4.8: Mott-Schottky plots for Hg/CH_3-Ge(111) junction (wafer **I**)

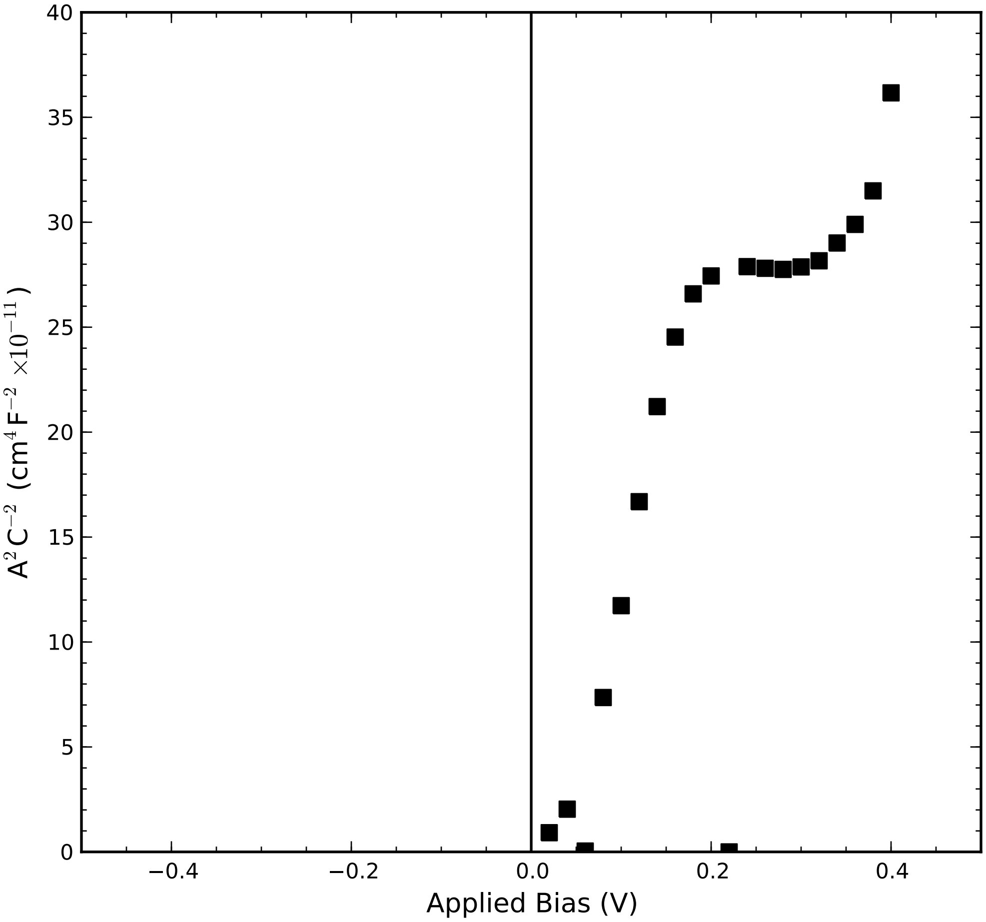

4.4 Discussion

Of the samples studied, rectifying contacts with sufficient uniformity to allow flat-band measurements could only be formed with those prepared through the halogenation/alkylation method. This is in agreement with the conductance data of Chapter 3, which indicated all other surfaces were under n-type accumulation conditions. Sharp et al. were able to measure rectifying contacts with surfaces treated with 1-octadecene, and reported a barrier height of 0.41 V for n-type Ge(100) samples.[10] The contacts were not ideal however, because the reported ideality factors were greater than 2, indicating deviations from the thermionic emission process. A significant shift in barrier height due to a surface dipole would not be expected for a (100) surface because the arrangement and density of surface bonds do not allow as high a density of alkane moieties with the necessary orientation.[11] Hydrocarbon moieties with two or more carbons do not result in as high a surface dipole as do methyl groups.[12] Therefore, a lower barrier height for large alkanes on a (100) surface, relative to that seen on the (111) surface, could be expected if surface dipoles influenced the conditions at the junction.

Within error, the barrier heights from $C^{-2} - V$ and $J - V$ data were in agreement with a barrier height of 0.6 V, over 100 mV higher than predicted simply from the bulk electron affinity and Hg work function. This is smaller than the approximately 400 mV shift in the χ_{eff} of CH_3-Si(111) seen in photoelectron measurements and Hg junctions.[8,9] Because the electronegativity of Ge is very similar to that of Si (2.01 versus 1.90), the surface atomic density is similar (7.84×10^{14} (Si) vs 7×10^{14}(Ge)), and the C-H bonds have the same orientation, the dipole responsible for the shift should be similar. However, the bandgap of Ge is only 0.67 eV, so the possible barrier height is limited and differences in surface dipoles cannot be determined from the measured Hg/n-Ge(111) junction barrier heights.

The lack of rectification for Hg contacts to p-type substrates is consistent with the high barrier heights that were observed for n-type Ge(111) samples treated with the halogenation/alkylation procedure. While the measured Hg/n-Ge(111) barrier heights do not distinguish between ideal behavior or the pinning traditionally seen in solid-state Schottky contacts to n-Ge, they do confirm the lack of pinning at a positive surface potential associated with a surface oxide.

4.5 Conclusion

N-type Ge(111) surfaces modified through the halogenation/alkylation process exhibited barrier heights of 0.6 ± 0.1 V. The differential capacitance versus voltage behavior of such junctions indicated near-ideal behavior, in contrast to substrates that were either left unprotected or modified with 1-decene, which showed little detectable rectification. Differences in barrier height due to Fermi level pinning or due to surface dipole effects of methyl groups versus ethyl or decyl groups could not be resolved because of the narrow bandgap of Ge and the instability of H-Ge(111).

Bibliography

[1] Sze, S. *Physics of Semiconductor Devices*, 2nd ed.; John Wiley & Sons: New York, 1981.

[2] Lang, D. *J. Appl. Phys.* **1974**, *45*, 3023–3032.

[3] Dewald, J. *Bell Syst. Tech. J.* **1960**, *39*, 615.

[4] Hens, Z.; Gomes, W. *Phys. Chem. Chem. Phys.* **1999**, *1*, 3607–3615.

[5] Huygens, I.; Strubbe, K. *J. Electrochem. Soc.* **2008**, *144*, F49–F54.

[6] Choi, J.; Ahmed, S.; Dimitrova, T.; Chen, J.; Schroder, D. *IEEE Trans. Electron Dev.* **2004**, *51*, 1380–1384.

[7] Hunger, R.; Fritsche, R.; Jaeckel, B.; Webb, L.; Jaegermann, W.; Lewis, N. *Surf. Sci.* **2007**, *601*, 2896–2907.

[8] Maldonado, S.; Plass, K.; Knapp, D.; Lewis, N. *J. Phys. Chem. C* **2007**, *111*, 17690–17699.

[9] Hunger, R.; Fritsche, R.; Jaeckel, B.; Jaegermann, W.; Webb, L.; Lewis, N. *Phys. Rev. B* **2005**, *72*, 045317.

[10] Sharp, I.; Schoell, S.; Hoeb, M.; Brandt, M.; Stutzmann, M. *Appl. Phys. Lett.* **2008**, *92*, 223306.

[11] Zandvlient, H. *Phys. Rep.* **2003**, *388*, 1–40.

[12] Jaeckel, B.; Hunger, R.; Webb, L.; Jaegermann, W.; Lewis, N. *J. Phys. Chem. C* **2007**, *111*, 18204–18213.

The following chapter contains material submitted for publication in *Journal of Physical Chemistry C*. It will not be publicly available until one year after publication. A link will be provided when available.

Chapter 5

Transmission Infrared Absorption Spectroscopy

5.1 Introduction

As has been described in the preceding chapters, the Ge(111) surface can be alkyl-terminated in a method very similar to the thoroughly investigated Si(111) surface. However, while the process does produce alkyl-terminated surfaces with electrical properties superior to those of the oxide, the lack of a mild, anisotropic etchant analogous to NH_4F, is a drawback to the production of a surface as well ordered as that of alkyl-terminated Si(111). The methyl-terminated Si(111) surface prepared though the halogenation/alkylation procedure has been well characterized by infrared absorption spectroscopy (IRAS) and scanning tunneling microscopy (STM) to show that every top silicon atom may be capped by a methyl group, with the Si-C bond directed normal to the surface plane.[1–4] While longer chain hydrocarbons groups, such as octadecyl, have been grafted to crystalline Ge and shown to display a crystallinity indicative of a well-ordered overlayer, evidence of a similar level of order at the Ge-C bond has not yet been reported.[5–7]. The work described in this chapter characterizes the alkyl-terminated Ge(111) surface through transmission IRAS to indicate that the methyl-terminated Ge(111) surface can be well ordered, with the Ge-C bond directed normal to the surface, as depicted in Figure 5.1.

Figure 5.1: Methyl group oriented normal to the Ge(111) surface

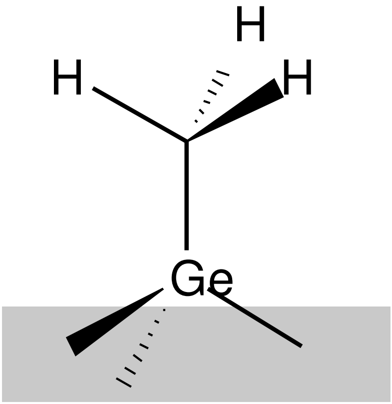

5.1.1 Background

Transmission

Germanium transmits light of wavelengths between 2 and 14 μm, so it is a commonly used infrared optical material often used in internal reflection experiments.[8] Silicon may also be used as an infrared optical material, however multiphonon absorption limits the useful spectral range to 1 – 6.7 μm.[9] Transmission IR absorption spectroscopy experiments (TIRAS), in the arrangement depicted in Figure 5.2, have been used for the study of monolayers on silicon wafers because the optical path within the crystal bulk is a single pass through a 500 μm wafer rather than the centimeter or greater in a multiple internal reflection configuration, so that the spectral range is no longer confined by bulk absorption.

While the phonon absorption of Ge does not limit the spectral range to the degree observed in Si, there are other reasons to use TIRAS. ATR requires specially crafted multiple internal reflection elements (IRE), which limits the sample availability. Comparison between different samples is also complicated because of the integral role the IRE has in the optical path, so that the precision of alignment required is difficult to achieve. TIRAS requires only standard semiconductor wafers and has a simplified optical path, so that comparisons between samples is more easily achieved.

Orientation of vibrational modes relative to the surface plane can be measured by controlling the angle of incidence of the IR on the wafer. At the Brewster angle, the reflected beam path is parallel to the electric field of the transmitted p-polarized light. There can be no emission from the surface as a result, so the reflected beam intensity is zero and all p-polarized light is transmitted, while s-polarized light is largely reflected, as indicated in Figure 5.2. The electric field vector of the transmitted light is at an angle to the wafer surface, with components both perpendicular and parallel to the surface. Vibrational modes that are perpendicular to the surface may absorb energy from the component of the p-polarized light in the same orientation, and surface parallel vibrational modes similarly absorb the parallel component, so that all modes are visible in the collected absorption spectrum. If the angle of incidence is changed to be closer to normal incidence, the component of the transmitted p-polarized light that may be absorbed by the vibrational mode perpendicular to the surface is reduced relative to the parallel component because the electric field vector is more parallel to the surface. In addition, the transmission ratio of s-polarized light to p-polarized light is increased, and electric field vector is parallel to the surface. As a result, the surface parallel vibrational modes are observed in the absorption spectra while the perpendicular modes are not.

External Reflection

In contrast to the ATR technique, external reflection measurements involve the light reflected off the surface of the higher refractive index material. While external reflection spectroscopy has traditionally been used to study adsorbed layers on metals, it may also be used for semiconducting and dielectric materials such as silicon of germanium.[10–12] Unfortunately, the same reflection/transmission properties that make TIRAS possible lead to a reflected beam that has very low power, resulting in a very low signal-to-noise ratio. However, the method does possess some desirable aspects: it does not require the special substrate geometries necessary for the more commonly used ATR technique; and the absorption spectra are highly polarization dependent, so that detailed structural information may be obtained. The overlap of the electric field vector of incident p-polarized light with the transition dipole moment vector of vibrations both parallel and perpendicular to the surface in the X-Y plane leads to two absorption components, A^x and A^z, respectively. One of the corresponding electric field components of the reflected beam must be out of phase while the other is in phase (see Figure 5.3), so that A^x and A^z will have opposite signs. Below the Brewster's angle, the reflected p-polarized light is in phase with the incident light and the A^z bands are positive while the A^x bands are negative (greater reflected power at that energy). The signs of the absorption components change as the angle of incidence is greater than the Brewster's angle. While the opposing signs of the absorption components can lead to complicated spectra for vibrational modes at an acute angle off the surface normal and would require simulations for interpretation, the simple geometry of the methyl groups as depicted in Figure 5.1 on page 114 would lead to distinct absorption bands composed wholly of either A^x or A^z.[13,14]

Figure 5.2: IR beam and sample wafer geometry for TIRAS

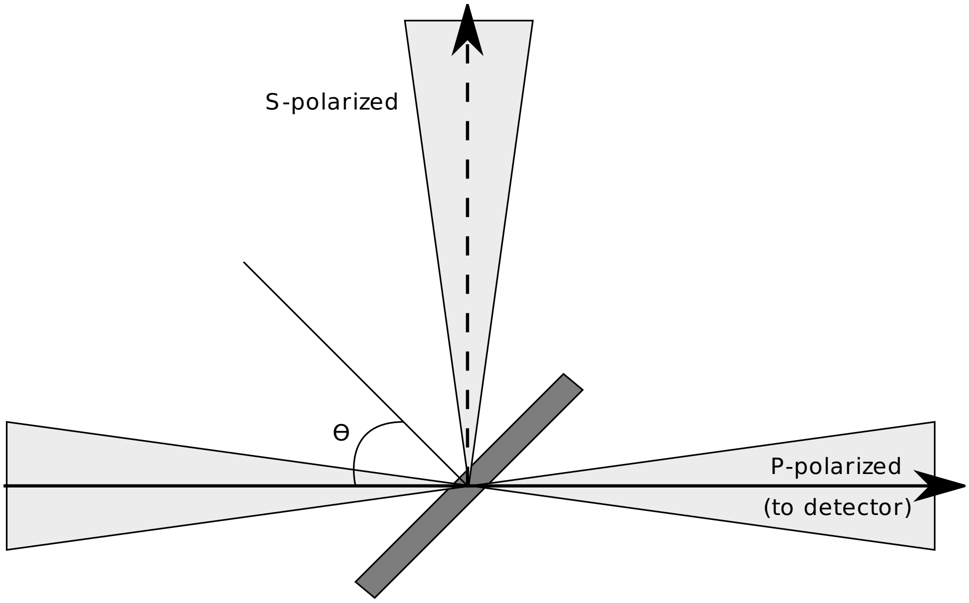

Figure 5.3: Beam and polarization geometry of IR radiation encountering dielectric surface

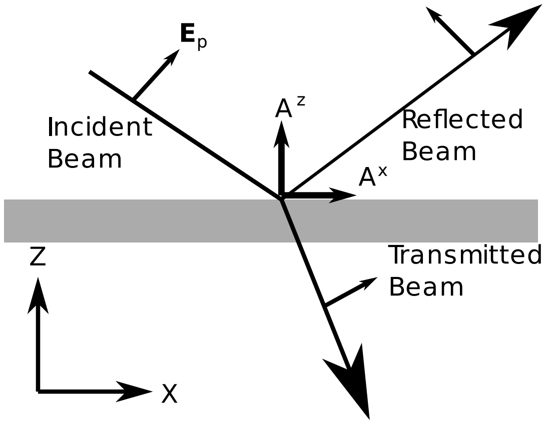

5.2 Experimental

Transmission infrared absorption spectroscopy was performed with a Nicolet 6700 FTIR, equipped with a custom-built accessory that held the sample upright on one edge, with the surface normal at a fixed angle, θ, of either 30° or 74° with respect to the path of the incident beam. For each stable sample, 3–5 single beam spectra of 1000 scans each were collected with a thermoelectrically cooled deuterated triglycine sulfate (DTGS) detector at a resolution of 4 cm^{-1}, a resolution which minimized the interference pattern produced by internal reflections. For less chemically stable surfaces, single-beam spectra of only 500 or 200 hundred scans were collected for etched surfaces. All spectra were converted to absorption spectra using other spectra collected the same day as background. The elapsed time between the sample and background spectra was minimized to avoid baseline distortion and imperfect subtraction of optical component absorptions due to spectrometer drift. Absorbance spectra were corrected for atmospheric CO_2 and H_2O absorption peaks. Because the background and sample spectra could not usually be collected from the same wafer within an allowable time-span, weak, broad signals below approximately 1000 cm^{-1} were difficult to distinguish from bulk absorptions or the artifacts previously mentioned.

External reflectance spectroscopy was performed with a variable angle reflectance accessory (Seagull, Harrick Scientific) and a polarizer to linearly polarize the incident beam parallel to the plane of incidence. In order to suppress multiple reflections, the sample wafers were single-side polished. So that no reflection from a supporting surface would interfere with the measurement, the samples were held by the edges and unsupported on the bottom. The low throughput of the setup required the collection of 5,000 scans for a single-beam spectrum.

5.3 Results

5.3.1 Methyl-Terminated Ge(111) Surfaces

Figure 5.4 displays a CD_3-Ge(111) sample against a CH_3-Ge(111) background. Both surfaces had been prepared through the bromination/methylation of HF-etched surfaces that had been pre-treated with the H_2O_2 anisotropic etch. The negative peaks at 1232 cm^{-1} and 755 cm^{-1} are due to the CH_3 groups of the background sample, the positive peaks at 2121 cm^{-1}, 951 cm^{-1}, and 577 cm^{-1} are due to the $\nu_s(CD_3)$, $\sigma_s(CD_3)$, and $\rho(CD_3)$ modes, respectively, of CD_3 groups. The higher energy modes in both sample and background disappear as θ is changed from 74° (lower spectrum) to 30° (upper spectrum), indicating those vibrational modes are normal to the surface plane, as would be expected for a methyl group bonded to the Ge(111) 1×1 surface.

Figure 5.4: CD_3-Ge(111) vs CH_3-Ge(111)

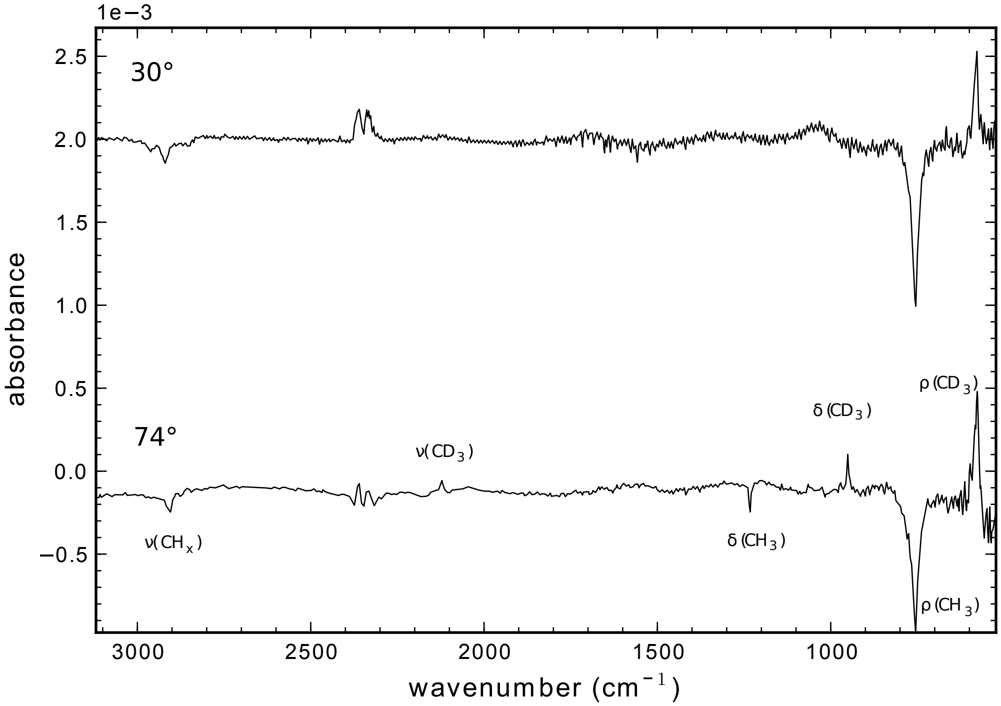

Further confirmation of the sensitivity of the absorption bands to the orientation of the electric field of the incident radiation can be seen in the external reflectance spectra of Figure 5.5, collected at $\theta = 67°$ off normal incidence. Because the angle of incidence is below the Brewster angle for both Si and Ge, a positive absorption is due to vibrational modes that are either perpendicular to the surface and present in the sample, or parallel to the surface and present in the background.[12] The inverse is true for the negative peaks. The upper spectrum is of a CH_3-Si(111) surface with H-Si(111) as background. The positive peak at 627 cm^{-1} is attributable to the Si-H bending mode of the background, while the positive peak at 1257 cm^{-1} and the negative peak at 757 cm^{-1} are attributable to the CH_3 umbrella mode and rocking mode, respectively.[1] The lower spectrum is of CH_3-Ge(111) with a rinsed oxide as background, so while there is no peak analogous to the H-Si(111) mode, the two CH_3 modes are present. The signs of the CH_3 absorption bands indicate that for both CH_3-Si(111) and CH_3-Ge(111), the methyl groups are oriented normal to the surface.

Figure 5.5: External reflectance spectra of CH_3-Si(111) and CH_3-Ge(111)

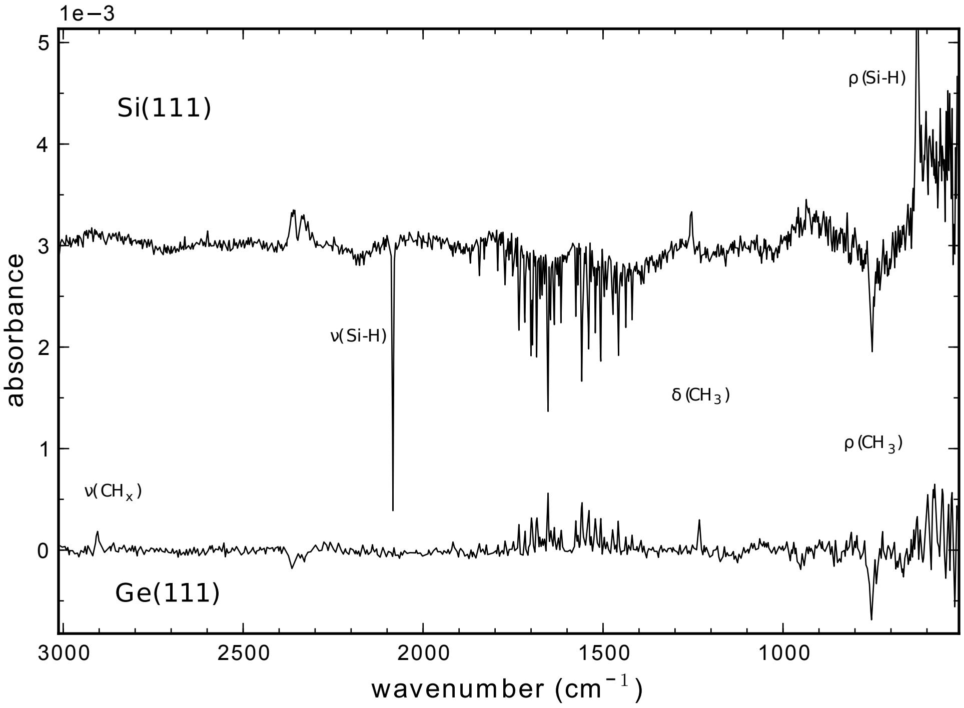

The halogenation/alkylation procedure reliably produces hydrophobic surfaces with little or no oxide, but the quality of the monolayer can depend strongly upon the initial etching method. The spectra presented in Figure 5.6 on page 125 are representative of the variation. The upper spectrum is of a sample that had been prepared by exposure of a Cl-Ge(111) surface, generated by etching with 6.0 M HCl, to a CD_3MgI solution. There is some evidence of the deuterated methyl group in the form of the $\nu_s(CD_3)$ mode at 2121 cm^{-1}, but the dominant peaks are not related to the desired monolayer and the spectrum does not give evidence of a methyl monolayer. The lower spectrum is of a surface prepared by etching with 6.0 M HBr, then exposure to CH_3MgI solution. The $\sigma_s(CH_3)$ mode at 1232 cm^{-1} and the $\rho(CH_3)$ mode at 755 cm^{-1} are clearly apparent, indicative of a methyl-terminated Ge surface.

If the samples are prepared from HF-etched surfaces, but are not pre-treated with the anisotropic etchant, the spectra resemble the upper spectrum of Figure 5.6 in that there is no clear evidence of the methyl vibrational modes. Conversely, if the HCl-etched surfaces are exposed to Br_2 vapor prior to methylation, the IR spectra of the resulting surfaces indicate well-ordered methyl monolayers, as seen in Figure 5.7. A mixture of 6.0 M NH_4Cl and 6.0 M HF could, after exposure to Br_2 vapor, also be used to produce well ordered CH_3-Ge(111) surfaces, which are shown in Figure 5.8. The variations on the general halogenation/alkylation procedure that were attempted, and their success as determined by TIRAS, are summarized in Table 5.1 on page 129. Increasing the concentration of the HF etchant to 12.0 M reduced the etching time required for the production of a hydrophobic surface, but gave results otherwise similar to the procedures involving 6.0 M HF(aq).

The absorption peak positions observed for CH_3- and CD_3-terminated surfaces are collected in Table 5.2. As can be seen both in the table and in Figure 5.9, the absorption peaks are shifted to a lower energy on Ge(111) compared to Si(111), but are otherwise similar.

Figure 5.6: CH_3-Ge(111) derived from surfaces etched with 6.0 M HCl or HBr, but not exposed to Br_2 vapor

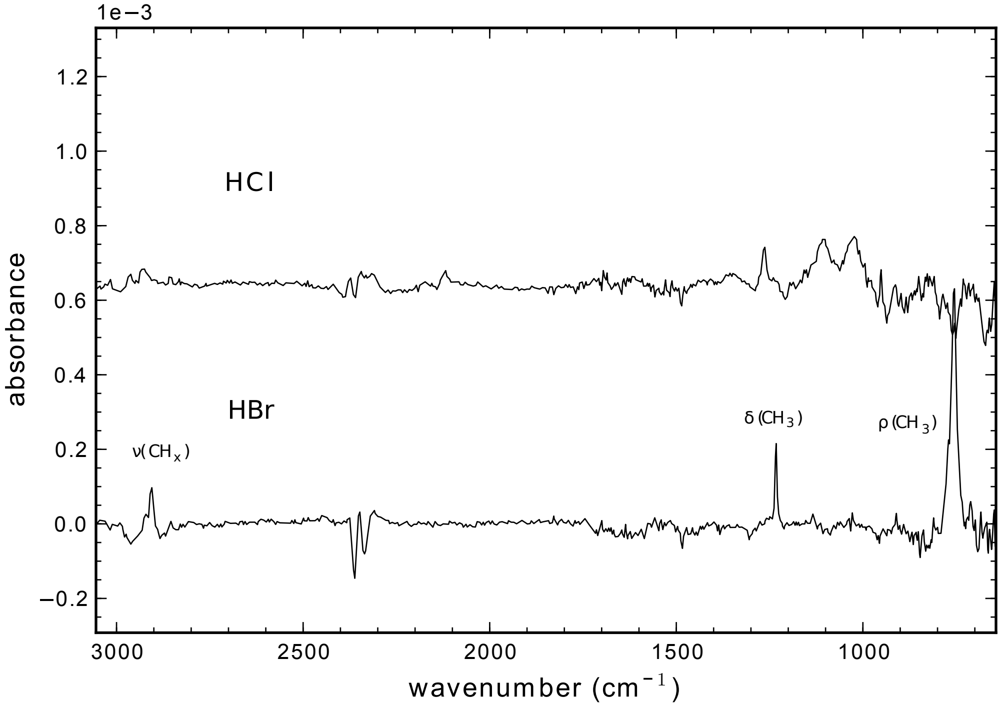

Figure 5.7: CH_3-Ge(111) derived from surfaces etched with 6.0 M HCl then exposed to Br_2 vapor

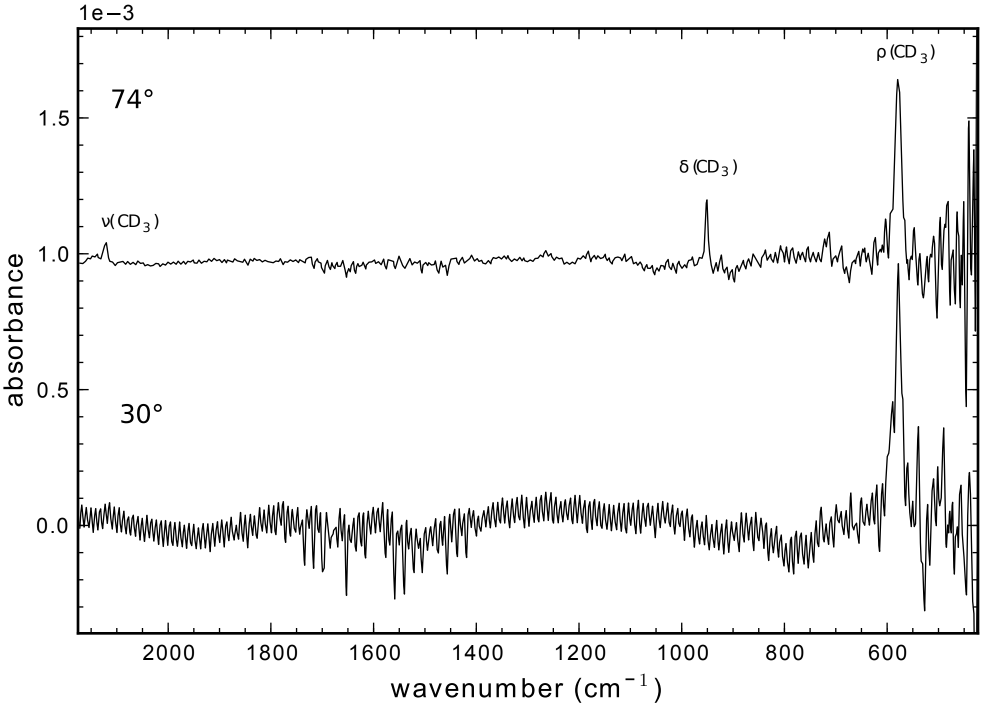

Figure 5.8: CH_3-Ge(111) derived from surfaces etched with $NH_4Cl{-}HF$ mixture then exposed to Br_2 vapor

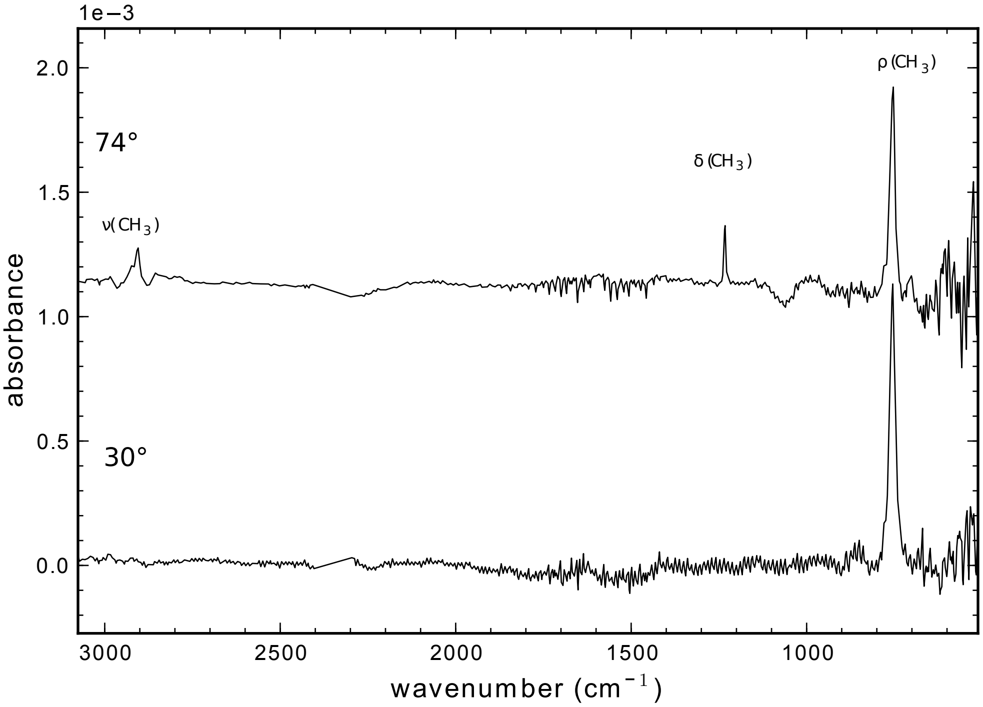

Figure 5.9: CD_3-Si(111) and CD_3-Ge(111)

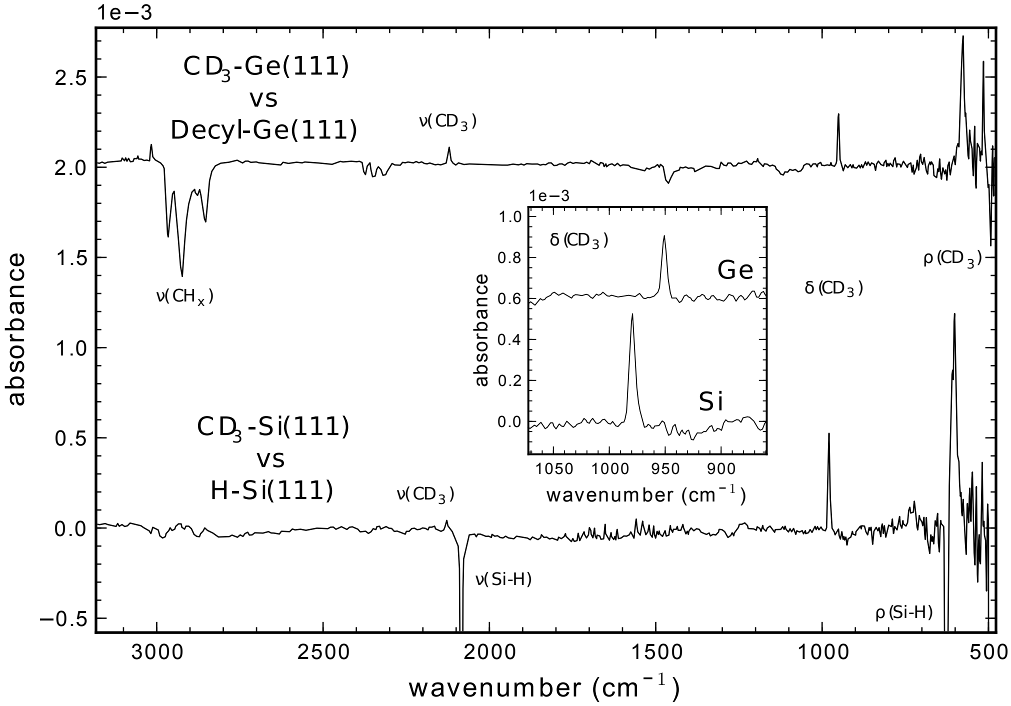

Table 5.1: Methylation Procedures

step number	process	surface type	success[a]
1	1-3 s Superoxol etch	GeO_x	
2	3-6 min 6.0 M HF	H-Ge(111)	
3	15-30 s Br_2 exposure	Br-Ge(111)	
4	3-12 h CH_3MgX (ether)	CH_3-Ge(111)	Y
1	20-25 min 6.0 M HF	H-Ge(111)	
2	15-30 s Br_2 exposure	Br-Ge(111)	
3	3-12 h CH_3MgX (ether)	CH_3-Ge(111)	N
1	20-25 min 6.0 M HCl	Cl-Ge(111)	
2	15-30 s Br_2 exposure	Br-Ge(111)	
3	3-12 h CH_3MgX (ether)	CH_3-Ge(111)	Y
1	20-25 min 6.0 M HCl	Cl-Ge(111)	
2	3-12 h CH_3MgX (ether)	CH_3-Ge(111)	N
1	1-3 s 6.0 M HBr	Br-Ge(111)	
2	3-12 h CH_3MgX (ether)	CH_3-Ge(111)	Y

a as determined by the presence of clear IR absorption peaks

5.3.2 Etched Surfaces

Samples that were not uniformly hydrophobic after etching did not become hydrophobic upon the completion of the alkylation procedure, and were seen with XPS to have varying but significant amounts of oxide. Samples that were etched for longer than was required to become hydrophobic became less hydrophobic as judged by the adhesion of the etching solution to the wafer surface. This is in general agreement with what has been observed on HF(aq) etching of Ge(100).[6] This effect was particularly noticeable in the case of surfaces treated with the Superoxol etchant. The etching times noted in Table 5.1 were adjusted to maximize the hydrophobicity as observed by the wetting of the surface by the etchant. The use of a H_2O_2 & HF-based etchant has some similarity to the sequential H_2O_2 then HF(aq) treatment used by others, however the sequential method resulted in surfaces indistinguishable from HF-only method.[15] The use of 3.3 M HCl(aq) is cited in the literature, but it required etching times greater then 30 min, and the etchant adhered to the surface non-uniformly.[16] Pretreatment of the sample with Superoxol etch prior to 3.3 M HCl(aq) resulted in a surface that remained uniformly hydrophilic for at least 45 min.

Hydrofluoric etchant

The unstable nature of the H-Ge(111) surface made it difficult to collect quantitative spectra, however absorptions attributable to Ge-H stretching modes were usually observed for HF-etched surfaces, with the notable exception of surfaces that were etched with the H_2O_2-based etchant prior to etching with 6.0 M HF(aq), a procedure henceforth referred to as Superoxol-6. This is demonstrated in Figure 5.10, which shows spectra of two 6.0 M HF(aq) etched surfaces, the upper of which had been treated with the H_2O_2-based etch just prior and shows no meaningful absorption bands. The lower spectrum shows a clear peak at 2040 cm^{-1}, attributable to the ν(Ge-H) stretch.[17–19] If the HF concentration is increased to 12.0 M, the Ge-H stretching is observed for surfaces both treated and not treated with Superoxol etch. In addition to the stretching mode absorption, there is another absorption at 560 cm^{-1}, shown in Figure 5.11, that is more noticeable in the sample that had been treated with Superoxol etch, but may be present in the HF-only sample as well.

The 560 cm^{-1} peak is less stable than the ν(Ge-H), and is entirely gone within ten minutes. If the peak at 560 cm^{-1} is initially present on the surface treated with the anisotropic etchant and then 6.0 M HF(aq), but is simply too air-sensitive to be measured, a hydrocarbon film may help protect it from moisture to extend the lifetime. The results of adding 2,4-dimethylpentane to the 6.0 M HF(aq) etchant are shown in Figure 5.12. Both spectra are of the same sample, but the background of the upper spectrum is the sample after it had been allowed to sit undisturbed in the spectrometer for 50 min. The background of the lower spectrum is the sample after sonication in detergent to restore a cleanly hydrophilic surface. The peak at 560 cm^{-1} does not coincide with the (C-H) modes in the lower spectrum. This peak is tentatively assigned to the rocking mode, ρ(Ge-H), analogous to that seen in H-Si(111)[20–22]

Hydrochloric and Hydrobromic Etchants

Surfaces treated with HCl(aq) or HBr(aq) did not show any absorption bands within the available spectral window, aside from adventitious hydrocarbon C-H stretching modes near 3000 cm^{-1}, which varied in intensity between samples. XP spectra confirmed the presence of the halogen at the surface, but the vibrational modes were too low in energy for the instrumentation used.

Ge(111) surfaces that had been treated with HCl(aq) or HBr(aq) did not show any infrared absorption bands within the available spectral window, aside from adventitious hydrocarbon C-H stretching modes near 3000 cm^{-1}, which varied in intensity between samples. XP spectra of surfaces etched with 6.0 M HCl(aq) and exposed to Br_2 showed evidence of both Cl and Br, but the Cl peaks were not intense enough to be quantified. After Br_2 exposure, the fractional monolayer coverage of Br was calculated from the XP spectra to be 1.0±0.1 for the surfaces etched with only 6.0 M HF(aq), 1.1±0.1 for the surfaces etched with Superoxol-6, and 0.5±0.1 for the surfaces etched with 6.0 M HCl(aq).

Figure 5.10: 6.0 M HF(aq)-etched Ge(111) at 74° incidence

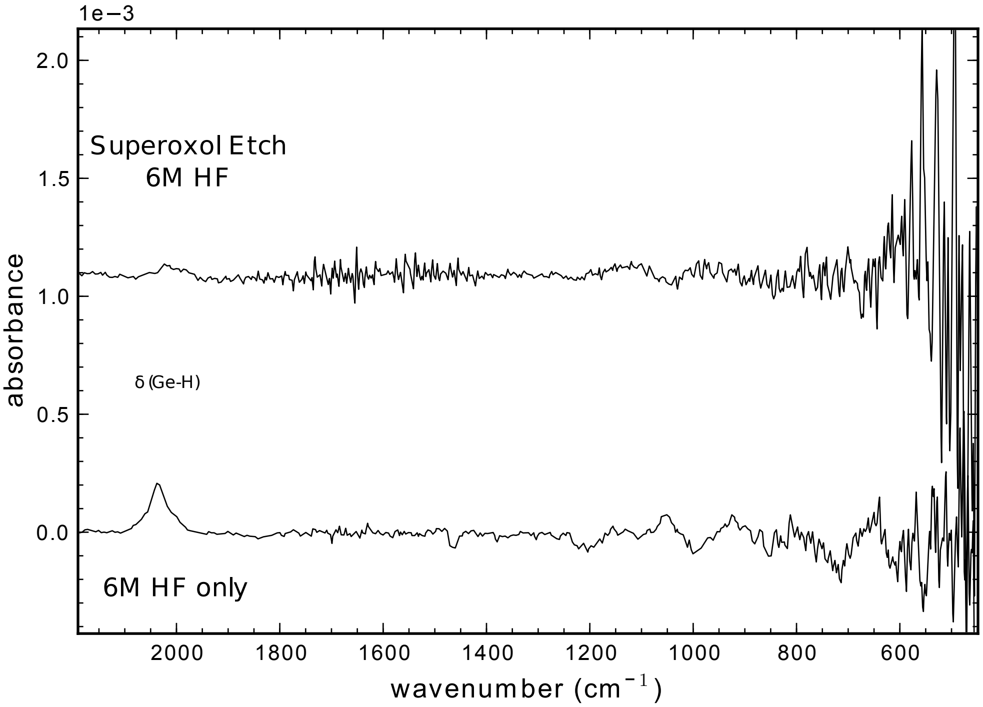

Figure 5.11: 12.0 M HF(aq)-etched Ge(111) at 74° incidence

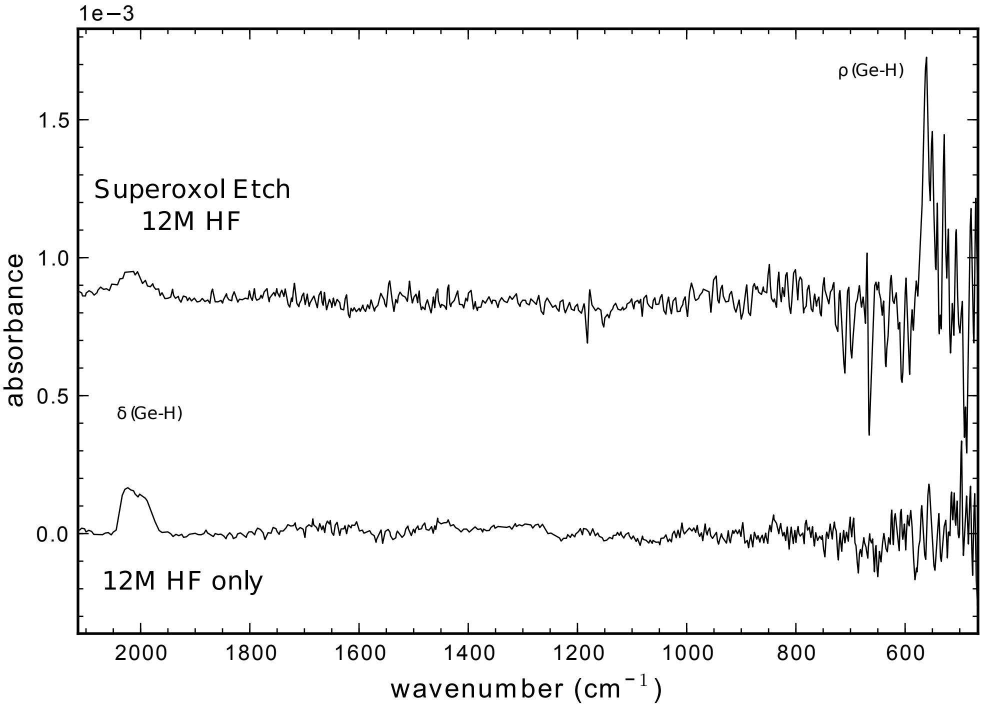

Figure 5.12: Effect of hydrocarbon in 6.0 M HF etchant

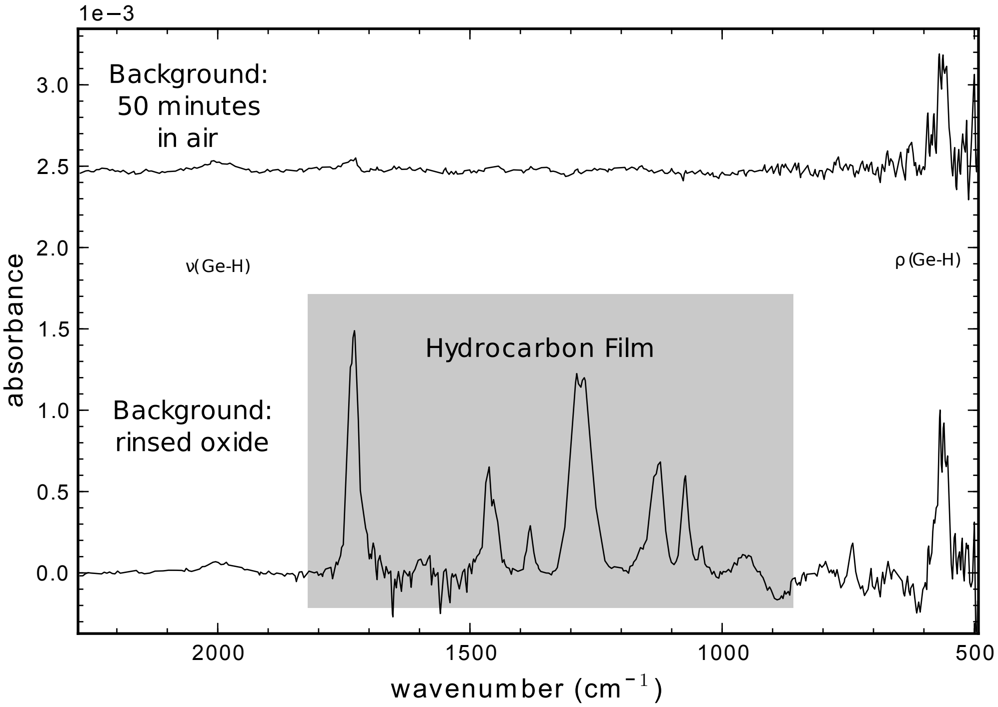

5.3.3 Decyl-Terminated Surfaces

The C-H stretching region of two $C_{10}H_{21}$-Ge(111) samples measured at 74° incidence is shown in 5.14. The top spectrum was prepared from a surface etched with the H_2O_2-based anisotropic etchant and the lower spectrum was prepared from a surface etched with 6.0 M HF only. The absorption peak positions and intensities match what has been established for similar monolayers on Au or Si surfaces, so the peaks at at 2854 cm^{-1} and 2924 cm^{-1} may be assigned to symmetric and antisymmetric methylene stretching modes, $\nu_s(\text{CH}_2)$ and $\nu_{as}(\text{CH}_2)$.[12,23,24] The peaks at 2879 cm^{-1} and 2966 cm^{-1} may be assigned to the symmetric and antisymmetric methyl stretching modes, $\nu_s(\text{CH}_3)$ and $\nu_{as}(\text{CH}_3)$. Figure 5.13 displays the same samples, measured at 30° incidence. There is a noticeable reduction in the $\nu(\text{CH}_3)$ modes. The features above 3000 cm^{-1} are artifacts due to atmospheric methane, and do not have any relation to the surface.

Figure 5.13: ν(C-H) region of $C_{10}H_{21}$-Ge(111) at 30° incidence

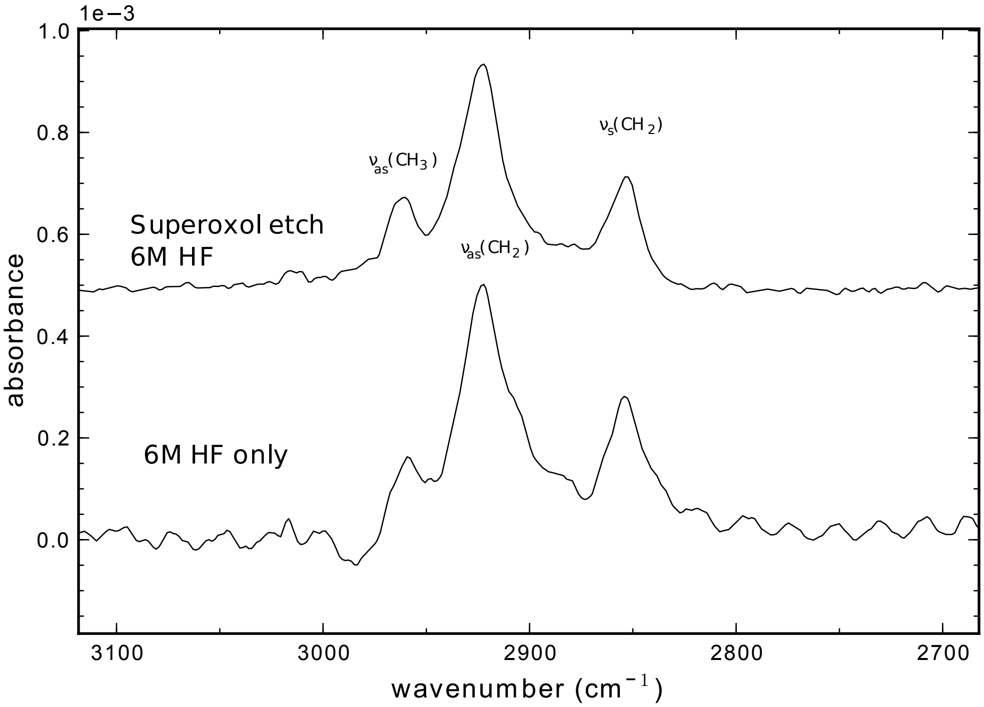

Figure 5.14: ν(C-H) region of $C_{10}H_{21}$-Ge(111) at 74° incidence

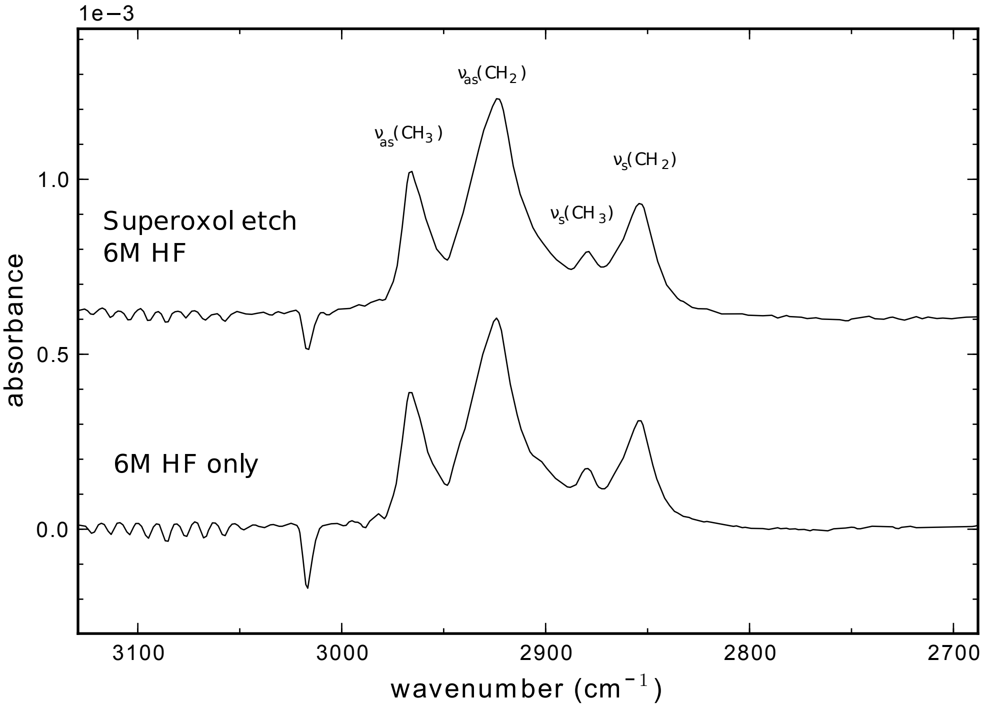

Table 5.2: Position and Full-Width at Half-Maximum[a] of Alkyl Monolayer Infrared Absorption Modes

Surface Type	Vibrational Mode	position (cm^{-1})	FWHM (cm^{-1})	orientation[b]
CH_3-Ge(111)				
	$\nu_s(CH_3)$	2906	4	$\perp$
	$\delta_s(CH_3)$	1232.5	6	$\perp$
	$\rho(CH_3)$	755	15-17	$\parallel$
CD_3-Ge(111)				
	$\nu_s(CD_3)$	2121	7	$\perp$
	$\delta_s(CD_3)$	951	5-6	$\perp$
	$\rho(CD_3)$	577	15-20	$\parallel$
$C_{10}H_{21}$-Ge(111)				
	$\nu_s(CH_3)$	2879	N/A[c]	
	$\nu_{as}(CH_3)$	2966	N/A[c]	
	$\nu_s(CH_2)$	2854	N/A[c]	
	$\nu_{as}(CH_2)$	2924	N/A[c]	
CH_3-Si(111)				
	$\nu_s(CH_3)$	2910	N/A[c]	$\perp$
	$\delta_s(CH_3)$	1256.5	6	$\perp$
	$\rho(CH_3)$	752.5	15-17	$\parallel$
CD_3-Si(111)				
	$\nu_s(CD_3)$	2128	14	$\perp$
	$\delta_s(CD_3)$	979	4-5	$\perp$
	$\rho(CD_3)$	604	12-13	$\parallel$

a for resolution of 4 cm^{-1}, incident angle of 74°

b orientation with respect to surface plane: $\perp$ = normal to the surface, $\parallel$ = parallel to the surface

c not available — asymmetric and/or had contributions from adventitious hydrocarbon

5.4 Discussion

5.4.1 Methyl-Terminated Ge(111) Surfaces

Infrared absorption spectra of CH_3-Ge(111) provide structural evidence that well-ordered monolayers of methyl groups bonded normal to the surface can be produced through the bromination/alkylation method. The peak positions of the methyl vibrational modes are lower frequency for CH_3-Ge(111) than for CH_3-Si(111), as would be expected considering the larger mass of the Ge atoms compared to Si atoms. The absorption peaks of the Ge surface were less intense than those on the Si surface, which could indicate fewer oriented methyl groups, and hence lower quality grafted layer, than that of the analogous Si surface. However, the refractive index is not the same for the two semiconductors, so only Si was truly measured at the Brewster's angle with the transmission accessory available. Because the reported angle of incidence is really an average of values defined by the cone of the narrowing IR beam, no attempt was made to normalize the peak intensity to the electric field at the surface for a fixed angle of 74 °. The similar peak width of the umbrella modes, limited by the 4 cm^{-1} resolution, is a qualitative indication that the CH_3-Ge(111) is well ordered like the CH_3-Si(111) surface.

Many variations of the halogenation/alkylation method yield modified surfaces, as evidenced by the electrical characteristics and surface elemental analysis described in earlier chapters, however not all of those procedures would yield methyl monolayers of sufficient quality to be measured by IR absorption. Pre-treatment of samples with Superoxol etch before HF etching has a noticeable effect upon the final methyl monolayer.

The lack of clear IR absorption peaks for CH_3-Ge(111) prepared from methylation of the chloride surface was not expected. While it is possible that the hydrogen-terminated surface is not ideal for alkylation, the chlorine-terminated surface would be expected to be a good surface for the reaction because it is believed to be well-ordered and has been proven to react with Grignard reagents.[16,25–28] Although the chlorinated surface produced by etching was not found to be a good precursor surface for methylation itself, it was found to be adequate if it was subsequently exposed to Br_2, as seen in Figures 5.6 and 5.7. It can also be seen in Figure 5.6 that HBr-etched surfaces can be directly methylated to form well-ordered surfaces. Samples etched with HBr and HCl were both subjected to nearly identical handling conditions, so any artifact of contamination or moisture that is independent of the nature of the halogen surface should affect both surfaces. This indicates that it is possible to directly methylate a surface that has come from an aqueous environment, and that the Br_2 vapor and Schlenk vacuum are not strictly necessary. Surfaces which had only been etched with HF prior to exposure to Br_2 did not yield IR spectra with identifiable methyl modes, so there is no evidence that the brief exposure to Br_2 etched the Ge to cause a well-ordered surface. The IR results could be explained if the Cl-Ge(111) surface reacted less preferentially with the methylmagnesium reagent over any impurities than did the Br-Ge(111), for it cannot be determined from the XPS whether all of the C 1*s* component at 284.3 B. eV is due to a methyl group or to some larger hydrocarbon impurity. To say whether the Ge-Br bond is itself necessary, it would be necessary to chlorinate the etched surfaces with Cl_2 gas. Of the surfaces studied, every successfully methylated surface had been prepared from a brominated precursor surface.

5.4.2 Etched Surfaces

The elapsed time between removal of the sample from the etchant and completion of the spectrum collection (approximately 15 min) is significantly greater than the time that the etched sample is exposed to air during the methylation procedure (less than 10 s), so that the IR spectra do not necessarily represent the precursor surface of the alkylated surfaces. The ν(Ge-H) peak is at a higher frequency than would be expected (2040 cm^{-1} vs 1970 cm^{-1} for GeH or 2020 cm^{-1} for GeH_2), possibly because of partial oxidation of the surface.[18,29] Nevertheless, the apparent correlation between the presence of the absorption band at 560 cm^{-1} and the smaller ν(Ge-H) peak in the pre-treated HF-etched surface and the higher quality methyl monolayer produced from such a precursor surface indicates there is at least qualitative importance to the H-Ge(111) TIRAS results.

Addition of a hydrocarbon to the HF (aq) etchant was an attempt at slowing the rate of oxidation so that the HF-etched surface could be measured. If the hydrogen-terminated surfaces are sensitive to moisture and oxygen, the hydrocarbon contaminants could adhere to the wafer surface after the oxides are removed, forming a protective layer. That assumes the hydrocarbon layer does not interact with the hydrogen-terminated surface, which may not be valid.[18] The lack of a significant ν(Ge-H) peak in either spectrum in Figure 5.12 would indicate that either the hydrogen-terminated surface had already reacted with the hydrocarbons, or that there never was a ν(Ge-H) absorption band for this surface. The presence of the 560 cm^{-1} band in the spectrum that compares the sample to itself after 50 min (the upper spectrum of Figure 5.12) indicates that the decay of the chemical species responsible for that band absorption was slowed. The addition of hydrocarbons to the HF etchant was investigated because the NH_4Cl-HF mixed etch coated the sample with an organic contamination film, yet subsequent bromination and methylation steps produced the high-quality methyl-terminated surface as seen in Figure 5.8, indicating that organic contaminants did not necessarily interfere with the etching process.

Figure 5.11 shows ν(Ge-H) absorption bands for 12.0 M HF-etched surfaces, both pre-treated with the anisotropic etch and not pretreated. This is most likely due to surface roughening, which would negate the effects of the anisotropic etch. The total time required for the pre-treated sample to become hydrophobic in the 12.0 M HF(aq) was approximately 30 s, however the apparent transition from hydrophilic to hydrophobic was less than 5 s, which made it difficult to manually optimize the etching time. These doubts aside, both the presence of a peak at 560 cm^{-1} for the etched surface and the presence of distinct absorption bands on the methylated surface are associated with the use of the anisotropic etch. Prolonged HF-etchant exposure can lead to atomic surface roughening, so the HF-only methods of etching may yield surfaces that are too rough to allow for well-ordered methyl monolayers.[6,18]

5.4.3 Decyl-Terminated Ge(111) Surfaces

The reduction in $\nu(CH_3)$ mode absorption intensity seen in Figure 5.13 compared to Figure 5.14 indicates an anisotropic layer with the alkyl chains directed away from the surface, however the peak positions are are too high energy for crystalline alkanes, so there is some degree of disorder.[12,30] While monolayers with a more crystalline nature have been achieved on flat surfaces including Ge(100), the peak positions are in agreement with thiol- or alkane- derived monolayers on Ge(111).[15,30,31] The similarity between the spectra of the decyl layers prepared through the two different etching methods is compatible with the XPS data of alkylated surfaces, including methyl. If the etching method does not have a large impact upon the number of grafted alkyl groups per unit area and that any slight changes in chemical environment or bond orientation due to varying degrees of surface roughness would affect the carbon bonded to the top Ge, but would have less of an effect upon the hydrocarbon groups further from the surface.

5.5 Conclusion

Well-ordered CH_3-Ge(111) surfaces can be prepared via the two-step halogenation/methylation method if the appropriate etching method is employed. 6.0 M HCl or, if the surface is etched first with an HF/H_2O_2 anisotropic etchant, 6.0 M HF may be used to remove oxide prior to exposure of the surface to Br_2 vapor. Alternatively, the surface may be directly brominated with 6.0 M HBr. Exposure of the HCl-etched or HF-etched surface directly to CH_3MgX (X=Cl,Br,I,CH_3) results in a hydrophobic, oxidation resistant surface, but characteristic IR absorption peaks cannot be detected.

The methyl umbrella mode and methyl rocking mode are similar to what is observed with CH_3-Si(111), but at lower frequency. The umbrella mode absorption peak is dependent upon the wafer orientation with respect to the incident infrared beam, indicating the vibration mode is normal to the surface.

In contrast to what was observed with the CH_3-Ge(111) case, $C_{10}H_{21}$-Ge(111) surfaces prepared with or without the anisotropic etch prior to 6.0 M HF etch yielded nearly identical IR spectra. The packing density and degree of order in the hydrocarbon monolayer is not as sensitive to the initial surface quality as the more restricted methyl monolayer.

Bibliography

[1] Webb, L.; Rivillon, S.; Michalak, D.; Chabal, Y.; Lewis, N. *J. Phys. Chem. B* **2006**, *110*, 7349–7356.

[2] Yu, H.; Webb, L.; Heath, J.; Lewis, N. *Appl. Phys. Lett.* **2006**, *88*, 252111.

[3] Hunger, R.; Fritsche, R.; Jaeckel, B.; Jaegermann, W.; Webb, L.; Lewis, N. *Phys. Rev. B* **2005**, *72*, 045317.

[4] Rivillion, S.; Chabal, Y. *J. Phys. IV* **2006**, *132*, 195–198.

[5] Sharp, I.; Schoell, S.; Hoeb, M.; Brandt, M.; Stutzmann, M. *Appl. Phys. Lett.* **2008**, *92*, 223306.

[6] Choi, K.; Buriak, J. *Langmuir* **2000**, *16*, 7737–7741.

[7] Ardalan, P.; Sun, Y.; Pianetta, P.; Musgrave, C. B.; Bent, S. F. *Langmuir* **2010**, *26*, 8419–8429.

[8] `http://eom.umicore.com/en/materials/library/brochuresAndMarketingMaterial/GermaniumOpticsBrochure.pdf`.

[9] `http://www.harricksci.com/~harrcov7/silicon`.

[10] Greenler, R. *J. Chem. Phys.* **1966**, *44*, 310–315.

[11] Mielczarski, J.; Yoon, R. *J. Phys. Chem.* **1989**, *93*, 2034–2038.

[12] Hoffmann, H.; Mayer, U.; Krischanitz, A. *Langmuir* **1995**, *11*, 1304–1312.

[13] Brunner, H.; Mayer, U.; Hoffmann, H. *Appl. Spectr.* **1997**, *51*, 209–217.

[14] Chernyshova, I.; Rao, K. *J. Phys. Chem. B* **2001**, *105*, 810–820.

[15] Kosuri, M.; Cone, Q., R. Li; S.M., H.; Bunker, B.; Mayer, T. *Langmuir* **2004**, *20*, 835–840.

[16] Lu, Z. *Appl. Phys. Lett.* **1996**, *68*, 1996.

[17] Zahler, J.; Fontcuberta i Morral, A.; Griggs, M.; Atwater, H. A.; Chabal, Y. J. *Phys. Rev. B* **2007**, *75*, 035309.

[18] Rivillion, S.; Chabal, Y. J.; Amy, F.; Kahn, A. *Appl. Phys. Lett.* **2005**, *87*, 253101.

[19] Lauwaert, J.; De Baerdemaeker, J.; Dauwe, C.; Clauws, P. *J. Mater. Sci.: Mater. Electron.* **2007**, *18*, 793–797.

[20] Jobson, K.; Wells, J.-P.; Schropp, R.; Vinh, N.; Dijkhuis, J. *J. Appl. Phys.* **2008**, *103*, 013106.

[21] Ferguson, K., G.A.and Raghavachari; Michalak, D.; Chabal, Y. *J. Phys. Chem. C* **2008**, *112*, 1034–1039.

[22] Hellstrom, P.; Holmgren, A.; Oberg, S. *J. Phys. Chem. C* **2007**, *111*, 16920–16926.

[23] Linford, M.; Fenter, P.; Eisenberger, P.; Chidsey, C. *J. Am. Chem. Soc.* **1995**, *117*, 3145–3155.

[24] Scheres, L.; Giesbers, M.; Zuilhof, H. *Langmuir* **2009**, *26*, 4790–4795.

[25] Amick, J.; Cullen, G.; Gerlich, D. *J. Electrochem. Soc.* **1962**, *109*, 127–132.

[26] He, J.; Lu, Z.; Mitchell, S.; Wayner, D. *J. Am. Chem. Soc.* **1998**, *120*, 2660–2661.

[27] Cao, S.; Tang, J.-C.; Wang, L.; Zhu, P.; Shen, S. *Surf. Sci.* **2002**, *505*, 289–294.

[28] Wang, D.; Dai, H. *Appl. Phys. A* **2006**, *85*, 217–225.

[29] Maroun, F.; Ozanam, F.; Chazalviel, J.-N. *J. Phys. Chem. B* **1999**, *103*, 5280–5288.

[30] Porter, M.; Bright, T.; Allara, D.; Chidsey, C. *J. Am. Chem. Soc.* **1987**, *109*, 3559–3568.

[31] Ardalan, P.; Musgrave, C.; Bent, S. *Langmuir* **2009**, *25*, 2013–2025.

Appendix A

Python Script for Surface Conductance

Listing A.1: Surface Conductance to Surface Potential Script

```
#! /usr/bin/env python


# This will generate the conductance versus surface potential curves
# for undoped Germanium, 15 Ohm-cm n-Germanium, 4 k-cm FZ Si,
# or 70 Ohm-cm n-Si
# Requires python, numpy, and scipy, which can be obtained from
# http://www.scipy.org


from math import *
from numpy import *
import csv
import sys
```

```
#print sys.argv[1]


# set up the array of sp values
v = linspace( -60.,30.,900 )


while True:
    try:
        print "0 - Conductance Curve, 1 - Conversion to Potential"
        purp = int(raw_input('-->'))
        break
    except ValueError:
        print "Try again..."


while True:
    try:
        print "0 - Undoped Ge, 1 - 15 Ohm-cm n-Ge, 2 - 4k-cm FZ Si, 3 -
        dope = int(raw_input('-->'))
        break
    except ValueError:
        print "Try again..."


if dope <= 1:
```

```
# parameters for Ge
    kappa = 16
    e0 = 8.85e-014 # F/cm
    q = 1.60e-19 #C
    ni = 2.40e+13 #cm-3
    k = 8.61e-05 #eV/K
    L = 6.8e-05 #cm debye, intrinsic
    T = 300 # K
    mun = 3800 #
    mup = 1820 #
else:
# parameters for Si

    kappa = 11.9
    e0 = 8.85e-014 # F/cm
    q = 1.60e-19 #C
    ni = 1.45e+10 #cm-3
    k = 8.61e-05 #eV/K
    L = 2.4e-03 #cm debye, intrinsic
    T = 300 # K
    mun = 1500 # cm2/V-s
    mup = 450 #
```

```
    if dope == 0:
    # Ge-Intrinsic
    # gmind is for minority carriers under depletion/inversio
    # gmaja is for majority carriers under accumulation, etc.


        def gp(x):
            return exp(0.5*abs(x))-1

        def gn(x):
            return exp(-0.5*abs(x))-1

        gmind = 2*L*ni*gp(v)
        gmina = 2*L*ni*gn(v)

    # calling electrons majority, even for intrinsic

        gmaja = gmind
        gmajd = gmina
```

```
# These values use:
# nb = impurity concentration (Hall or fig.22 Ch1 Sze)

elif dope == 1:
# Ge-15 Ohm-cm
    nb = 1.0e+14
    pb = (ni**2)/nb
    ub = log(nb/ni)
    Le = L*(((2*ni)/(nb+pb))**0.5) #effective Debye length

elif dope == 2:
# Si-4 k-cm
    nb = 4.5e+11
    pb = (ni**2)/nb
    ub = log(nb/ni)
    Le = L*(((2*ni)/(nb+pb))**0.5)

elif dope == 3:
# Si-70 Ohm-cm
    nb = 6.6e+13
    pb = (ni**2)/nb
```

```
    ub = log(nb/ni)
    Le = L*(((2*ni)/(nb+pb))**0.5)


# now calculate for extrinsic
if dope == 1 or dope == 2 or dope == 3:
    def fuv1(ub,v1):
        return cosh(ub+v1)/cosh(ub)
    def fuv2(ub,v1):
        return 2.*fuv1(ub,v1)-2.*v1*tanh(ub)-2
    def fuv3(ub,v1):
        return fuv2(ub,v1)**0.5
# majority carriers, accumulation
    def integrand_maja(v1):
        return (exp(v1)-1.)/fuv3(abs(ub),v1)
# majority carriers, depletion
    def integrand_majd(v1):
        return (exp(-v1)-1.)/fuv3(-abs(ub),v1)
# minority carriers, accumulation
    def integrand_mina(v1):
        return exp(-2.*abs(ub))*(exp(-v1)-1.)/fuv3(abs(ub),v1)
# minority carriers, depletion
    def integrand_mind(v1):
```

```
        return exp(-2.*abs(ub))*(exp(v1)-1.)/fuv3(-abs(ub),v1)
# integration
    from scipy.integrate import quad


    def gna(ub,vs):
        return quad(integrand_maja,0.,abs(vs),args=())[0]
    def gnd(ub,vs):
        return quad(integrand_majd,0.,abs(vs),args=())[0]
    def gpa(ub,vs):
        return quad(integrand_mina,0.,abs(vs),args=())[0]
    def gpd(ub,vs):
        return quad(integrand_mind,0.,abs(vs),args=())[0]

    gmaja = zeros((900),dtype=float)
    gmina = zeros((900),dtype=float)
    gmind = zeros((900),dtype=float)
    gmajd = zeros((900),dtype=float)
    it=0
    while it < 900:
        gmaja[it] += Le*nb*gna(ub,abs(v[it]))
        gmina[it] += Le*nb*gpa(ub,abs(v[it]))
        gmajd[it] += Le*nb*gnd(ub,abs(v[it]))
```

```
        gmind[it] += Le*nb*gpd(ub,abs(v[it]))
        it = it + 1



# this is more generalized
# array 'sig' has two axes, 600 is for each surface potential
# 2 is for (x-sp,y-sc)
sig = zeros((900,2), dtype=float)
# only add to depleted/inverted
sig[0:599,1] += mun*gmajd[0:599]
sig[0:599,1] += mup*gmind[0:599]
# only add to accumulated
sig[600:899,1] += mun*gmaja[600:899]
sig[600:899,1] += mup*gmina[600:899]
# multiply by q and we are done
sig[:,1] *= q
sig[:,0] += v

if purp == 0:
    fest = csv.writer(open('/home/dk246/Thesis/SPmap_pub/curveout-dummy.
    print fest
```

```
    it=0
    while it < 899:
        fest.writerow([sig[it,0],sig[it,1]])
        it = it + 1
################################################################################

if purp == 1:

# find the minimum
    it = 0
    cmin = 1.0e-03 # an unlikely value
    while it < 899:
        if sig[it,1] < cmin:
            cmin = sig[it,1]
            pmin = sig[it,0]
        it = it + 1

# now the data actually gets read
# The file to read

    filein = '/home/dk246/Thesis/SPmap/SPmap_in/%s.csv' % (sys.argv[1])
    fileout = '/home/dk246/Thesis/SPmap/SPmap_out/%s.csv' % (sys.argv[1]
```

```
    f = open(filein,'r')
    af=f.readlines()
    l=0 # line number
    data_out = zeros((len(af),2), dtype=float)
    apot_old = -50. # so that we choose the correct arm of curve
#                     it needs to be changed for the oxide
    a_old = 1.0e-3
    while l < len(af): # len(af) is from readlines
        ax = af[l]
        it=0
        while it < 20:  # 20 is just a nice size
            it += 1
            if ax[it] == ',':
                break
        a = float(ax[0:it]) # a is the conductacnce
# the data is conductance change relative to minimum, but calculations a
        a = a + cmin
        b = float(ax[it+1:-2]) # b is the SRV
        it = 0
        ahold1 = 1.0e-03 # some unlikely residual
        ahold2 = 1.0e-03 # some unlikely residual
        apot_out = 0.
```

```
        while it < 899:
            adiff = a - sig[it,1]
            if abs(adiff) < abs(ahold1) and sig[it,0] < pmin:
                apot1 = sig[it,0]
                ahold1 = adiff
            elif abs(adiff) < abs(ahold2) and sig[it,0] > pmin:
                apot2 = sig[it,0]
                ahold2 = adiff
            it = it + 1

# two unambiguous cases
# conductance is decreasing, and old potential is closer to negative cho
        if a < a_old and abs(apot_old - apot1) < abs(apot_old - apot2):
            apot_out = apot1
            apot_old = apot1
            a_old = a
# conductance has increased, and old potential is closer to positive cho
        elif a >= a_old and abs(apot_old - apot1) >= abs(apot_old - apot
            apot_out = apot2
            apot_old = apot2
            a_old = a
# ambiguous cases
```

```
# the coductance has increased, but last potential is closer to negative
# choose negative potential, but store positive potential and don't over
# If it is not a jitter, the next one will be increased too
# and stored potential will be closer to positive choice next time
# If it is jitter, the next conductance will not be increased and will b
        elif a >= a_old and abs(apot_old - apot1) < abs(apot_old - apot2
            if abs(abs(apot_old - apot1) - abs(apot_old - apot2)) < 3.0:
                apot_out = apot2 # it is a toss-up, just proceed
                apot_old = apot2
            else:
                apot_out = apot1
                apot_old = apot2
# The conductance has decreased, but last potential is closer to poitive
# choose positive potential but store negative and don't overwrite condu
# If it is not jitter, next conductance will decrease too, and stored po
# will be closer to negative next time
# If it is jitter, next conductance will increase but stored potential w
# closer to negative, so it will go to case above for one value, then ge
        else:
            if abs(abs(apot_old - apot1) - abs(apot_old - apot2)) < 3.0:
                apot_out = apot1
                apot_old = apot1
```

```
            else:
                apot_out = apot2
                apot_old = apot1


# so that output is in volts
        apot_out *= k*T
        data_out[l,0] = apot_out
        data_out[l,1] = b
        l = l + 1
    it = 0
    f2 = csv.writer(open(fileout,’w’),delimiter=’ ’)
    while it < len(af):
        f2.writerow([data_out[it,0],data_out[it,1]])
        it = it + 1
```